Application of Artificial Intelligence in the Exploitation of Deflection Measurements for the Mechanical Characterization of Pavement Structures

Abdelgader Abdelmuhsen

COLLEGE ED MATHEMATIQUES
DOCTORAL STIC
PAYS DE LA LOIRE

Nantes Université

THÈSE DE DOCTORAT DE

Université Gustave Eiffel

LAMES
LABORATOIRE AUSCULTATION, MODÉLISATION, EXPÉRIMENTATION DES INFRASTRUCTURES DE TRANSPORT

NANTES UNIVERSITÉ

ÉCOLE DOCTORALE N° 641
Mathématiques et Sciences et Technologies de l'Information et de la Communication
Spécialité : *Informatique*

Par
Abdelgader ABDELMUHSEN

Application of Artificial Intelligence in the Exploitation of Deflection Measurements for the Mechanical Characterization of Pavement Structures

Thèse présentée et soutenue à l'université Gustave Eiffel - Nantes, le 30 septembre 2024
Unité de recherche : LAMES - MAST - Université Gustave Eiffel

Rapporteurs avant soutenance :

Prof. Khalil EL Khamlichi Drissi	Professeur des universités - Université Clermont Auvergne
Prof. Simona Fontul	Enseignant chercheur (Assistant Professor) - LNEC - Portugal

Composition du Jury :

Président :	Prof. Khalil EL Khamlichi Drissi - Professeur des universités - Université Clermont Auvergne
Examinateurs :	
Prof. Khalil EL Khamlichi Drissi	Professeur des universités - Université Clermont Auvergne
Prof. Simona Fontul	Enseignant chercheur (Assistant Professor) - LNEC - Portugal
Prof. Fekri Meftah	Professeur des universités - INSA Rennes
Prof. Yide Wang	Professeur des universités - Université de Nantes
Dr Amine Ihamouten	Dir. de thèse - IDTPE - HDR - Université Gustave Eiffel
Dr Franziska Schmidt	Co-dir. de thèse - IDTPE - HDR - Université Gustave Eiffel

Invité(s) :

Dr Jean-Michel Simonin : Chargé de recherche - Directeur de laboratoire (LAMES - MAST) - Université Gustave Eiffel

ACKNOWLEDGEMENT

In life's journey, we are often fortunate to meet mentors who illuminate our careers. This happened to me on April 1st, 2021, when I stepped into Nantes City for my master's internship at G. Eiffel University under **Dr. Jean-Michel Simonin**'s supervision. Mr. Simonin laid the foundation for my understanding of pavement engineering to inspire me to pursue this PhD. He instilled in me not only the technical expertise ("savoir-faire") but also the essential qualities and values of a competent researcher ("savoir-être"). Words are certainly inadequate to express my gratitude for his impact on my career.

Likewise, it is well known that the success of any PhD project requires exceptional leadership capable of unleashing the potential of the PhD candidate. This is exactly what my thesis directors, **Dr. Amine Ihamouten** and **Dr. Franziska Schmidt**, achieved with me. I believe France is fortunate to have them guiding the future of scientific exploration and shaping researchers like myself. Their dedication to pushing the boundaries of knowledge and fostering scientific development is invaluable. I'm so grateful for their time, efforts, and advice, which will be a driving force in my long-term career.

In parallel, I'm privileged to have the opportunity to present my thesis to such a distinguished jury, who are considered subject matter experts and international references in their respective fields. Thus, my sincere thanks go to **Dr. Khalil Drissi, Dr. Simona Fontul, Dr. Fekri Meftah, and Dr. Yide Wang**. Their participation as reporters and examiners to enrich my thesis is highly appreciated and admired.

Also, I'd like to extend my gratitude to **Dr. Dirk Jansen** and **Dr. Carl van Geem** for their active participation during my two years 'CSI' and for their constructive comments that played an instrumental role in enhancing my research orientation and prioritization.

From the technical side, my sincere appreciation goes to Mr. **Denis Lièvre** and Mr. **Murilo Freitas** for their constant availability, which was fundamental to the success of this project. Furthermore, I'd like to thank my esteemed colleagues at **LAMES**, especially at the Reseal building, for the unforgettable moments we shared, including our cherished coffee breaks. These moments will forever hold a special place in my memories and heart.

My gratitude goes as well to my Master's Professor, **Dr. Jean-Marie Bilbault**, who devoted his 40-year career helping students like myself achieve their professional aspirations.

Last but not least, I am grateful to the board of directors of **MAST** department and the **Conseil régional des Pays de la Loire**, for their financial and logistical support.

Ultimately, thank you to **everyone** who helped bring this project to fruition.

Acknowledgement

"Il n'y a qu'un bonheur dans la vie, c'est d'aimer et d'être aimé !"
"There is only one happiness in life, to love and be loved !" — George Sand.

To my parents: Mohamed and Amani

Perhaps, you're an ordinary couple in the eyes of this world, but you're the entire world in my eyes

To my sister and brothers: Douaa, Ahmed, Ayman

Indeed, each one of us lives now on a different continent! Distance may separate us physically, but the bond of our shared blood and souls will forever connect us

To my wife and my children: Hayat, Mrwan, Mutaz

You are the most precious gift God has ever given me. I hope to make you proud to call me your Papa

To my cousin: Amro

You've dropped off from the train of life too early (bro), I know you are resting at peace in paradise. I look forward to our reuniting to tell you how your advice has paid off

To my friend: Enad

Those who haven't experienced your friendship yet couldn't sense the true meaning of having a genuine friend to be count on

RÉSUMÉ EN FRANÇAIS

La détérioration progressive de l'état des chaussées routières nécessite une évaluation structurale rapide, efficace et automatisée afin d'estimer la durée de vie résiduelle de la chaussée. L'estimation précise du module d'élasticité des différentes couches de la chaussée (E_i) joue un rôle essentiel dans ce processus, permettant la conception de chaussées résilientes, l'optimisation des stratégies de maintenance et l'amélioration de la sécurité routière globale. Cependant, les méthodes et dispositifs conventionnels utilisés pour estimer E_i, tels que le Falling Weight Deflectometer (FWD), présentent plusieurs limitations en raison de contraintes opérationnelles et de sécurité lors des mesures à l'échelle du réseau.

Pour surmonter ces obstacles, les dispositifs de Traffic Speed Deflectometer (TSD) sont proposés comme des solutions innovantes pour l'évaluation continue de la capacité portante des chaussées, éliminant ainsi le besoin de contrôle de la circulation. en effet, TSD fonctionne à la vitesse normale de circulation jusqu'à 80 km/h, et repose sur la mesure de la vitesse de déflexion verticale (D_V) de la chaussée au lieu de la déflexion elle-même. Les mesures continues du TSD fournissent des données beaucoup plus adaptées que le FWD, ce qui permet une planification de la maintenance plus précise et efficace. Par contre, le traitement efficace de la quantité importante de données qu'il génère présente de défi. Cela pourrait cependant être surmonté en utilisant des techniques spécialisées, telles que l'apprentissage automatique (ML).

Ainsi, cette thèse présente un modèle et une méthodologie efficaces basés sur la combinaison (ML+TSD) pour l'estimation de E_i. Cette approche novatrice utilise des mesures de pente de déflexion D_S par TSD, plutôt que sur la méthode classique de déflexion. Le modèle développé dans le cadre de cette recherche repose sur des données issues de logiciels (Alizé-LCPC) reconnus par les praticiens et d'un simulateur extérieur expérimental, garantissant ainsi leur conformité aux conditions du monde réel. De plus, pour valider leur performance, un processus de validation paramétrique avancé a été exécuté de manière méticuleuse.

Ce modèle relève non seulement les défis liés à l'estimation précise de E_i, mais il mène également une analyse de sensibilité quantitative rigoureuse. Cette analyse examine systématiquement les impacts de quatre défis majeurs: la complexité des données TSD en haute dimension, l'influence du bruit de mesure, les variations de température, et Les incertitudes de E_i des autres couches des chaussées.

Abstract in English

The progressive deterioration of road pavement structural health necessitates fast, efficient, and automated structural assessment to evaluate the residual life of the pavement. The accurate estimation of the pavement elastic modulus (E_i) plays a pivotal role in this process, also serving as a fundamental factor for designing resilient pavements and optimizing maintenance. Strategies and improving overall road safety.

However, conventional methods and devices that are used to estimate E_i, such as the Falling Weight Deflectometer (FWD), have several limitations due to operational and security constraints when measuring at the network level. These limitations stem from the need for traffic control during measurement data collection.

To tackle these obstacles, the Traffic Speed Deflectometer has emerged as an innovative solution for continuous assessment of pavement bearing capacity, as it eliminates the need for traffic control. TSD runs at an average traffic speed of up to (80 km/h). The continuous measurements of TSD ensure much more adequate data than traditional point measurements, which allows for more accurate and cost-effective maintenance planning. TSD's principle of operation is based on measuring the vertical deflection velocity (D_V) of the pavement instead of the deflection itself. Although the TSD concept holds considerable potential for pavement analysis, effectively processing the substantial data it generates presents another challenge. However, these challenges can be overcome by employing specialized techniques, such as Machine Learning (ML), that excel in learning complex data patterns while offering the prospect of developing a generalized approach.

Thus, this thesis presents an efficient and effective ML-based model and methodology for estimating E_i. This novel approach utilizes deflection slope D_S measurements instead of the conventional deflection measurement method. The model developed in this research has been built upon data derived from industry-approved software (Alizé-LCPC) and an experimental outdoor simulator, ensuring their alignment with real-world conditions. Furthermore, an advanced parametric validation process was implemented to validate their performance. With this model analysis and quantitative sensitivity analysis to investigate and quantify the adverse impacts of some challenges spanning the high-dimensional TSD data, the influence of TSD measurement noise, temperature variations, and the uncertainties associated with E_i values.

Thus, the ultimate aim is to underscore this thesis's primary objective: having the potential to make valuable contributions to the field of pavement mechanics engineering.

Table of Contents

List of acronyms

AI	Artificial Intelligence
ANN	Artificial Neural Networks
AWGN	Additive White Gaussian Noise
CNN-CDM	Convolutional Neural Networks for Condition Distress Monitoring
DL	Deep Learning
DT	Destructive Testings
ERF	European Union Road Federation
FCN	Fully Convolutional Network
FEM	Finite Element Method
FWD	Falling Weight Deflectometer
GPR	Ground Penetrating Radar
HMA	Hot Mix Asphalt
ML	Machine Learning
NDT	Non Destructive Testings
PCA	Principal Component Analysis
PCC	Portland Cement Concrete
PCI	Pavement Condition Index
PMS	Pavements Management System
RF	Random Forest
SHM	Structural Health Monitoring
SVM	Support Vector Machine
SVC	Support Vector Classification
SNR	Signal-to-Noise Ratio
SVR	Support Vector Regression
SSD	Single Shot MultiBox Detector
Raptor	Rapid Speed Testors
TSDDs	Traffic Speed Deflectometer Devices
TSD	Traffic Speed Deflectometer
UAV	Unmanned Aerial Vehicle
YOLO	You Only Look Once

MATHEMATICAL NOTATIONS

Support Vector Machines (SVMs)

$\boldsymbol{\epsilon}$	A margin parameter that controls the width of the $\boldsymbol{\epsilon}$-insensitive tube
$\boldsymbol{\gamma}$	The kernel parameter that controls the shape of the decision boundary
$K(\mathbf{x}_i, \mathbf{x}_j)$	The radial basis function kernel (RBF)
$\mathbf{C}$	The regularization parameter controlling the margin and error
$\text{sign}(\mathbf{w}^T\mathbf{x} + b)$	The decision boundary in classification tasks
$\mathbf{w}^T\mathbf{x} + b$	The hyperplane that best fits the data in regression tasks
$\boldsymbol{\xi}_i$ $\boldsymbol{\xi}'_i$	Slack variables, allowing for errors within and outside the margin

TSD

D_V	Deflection Velocity
D_S	Deflection Velocity Slope
V_v	measured Vertical deflection Velocity
V_h	Instantaneous TSD speed
V	Moving speed of TSD

Pavement mechanical properties

E_i	Modulus of elasticity of layer i
M_R	Subgrade Resilient Modulus
h	Layer Thickness
ν	Poisson's ratio
Θ °C	Temperature

Raptor

d_i^M	Distance measurement from laser i to a random evaluation point M on the surface
d_{i-1}^M	Distance measurement from laser $i-1$ to the same point M on the surface
$\Delta\theta_{i\to i-1}$	Change in sensor beam angle between consecutive detections
$\Delta h_{i\to i-1}$	Change in sensor beam height between consecutive detections

List of Figures

List of Tables

Chapter 1

General introduction

1.1 Research global context

In 2019, France allocated 438.2 billion euros to transportation, constituting 18.1% of the national Gross Domestic Product (GDP), according to a statistical study by the French Ministry of Ecological Transition [1]. 72% of these expenses are allocated to road transportation, recognizing the contribution of a well-structured road infrastructure network in socio-economic development. The importance of such networks for efficient goods distribution, mobility, and regional accessibility has been underscored [2]. The impact of poorly developed road systems on economic growth and individuals' quality of life is considerable [3]. Consequently, there is a growing emphasis on enhancing the efficiency, safety, and security of transportation infrastructure, aligning with the strategic goals outlined in the European Union's transportation policy framework [4].

Recent data, sourced from the European Union Road Federation (ERF), underscores the immense importance of the health of the infrastructure. The European road network is extensive, covering approximately 5 million kilometers, and a substantial segment, roughly 1 million kilometers, lies within the boundaries of France. The estimated value of this extensive road network surpasses a staggering 8,000 billion euros, highlighting its pivotal position as the circulatory system of transportation. It is responsible for facilitating the movement of goods and passengers, serving as the backbone of logistics and supply chain systems [5].

According to ERF, roads are entrusted with the transportation of a major portion of freight, accounting for 50% of the total volume, and they also enable the travel of 70% of passengers, surpassing all other modes of transportation combined. Furthermore, it's worth noting that the road infrastructure sector provides gainful employment to over 10 million individuals throughout the European Union [5]. This underscores the sector's vital role in facilitating economic activity and offering employment opportunities. In the context of pavement durability, ERF highlights the accelerating rate at which road conditions deteriorate over time due to the traffic load and climate conditions. This acceleration underscores the importance of regular and proactive maintenance to ensure the longevity and efficiency of pavement structures. Recent research insights further stress the significance of

proactive maintenance, even when roads appear in good visual condition. This underscores the necessity for comprehensive maintenance strategies that encompass various treatments to address minor deterioration, extend the lifespan of pavements, and proactively prevent potential failures [6].
In the pursuit of advancing proactive maintenance through Structural Health Monitoring (SHM), the integration of network-level structural assessment, specifically in terms of bearing capacity evaluation, into the Pavement Management System (PMS) emerges as a strategic approach. This integration empowers transportation authorities with data-driven insights to prioritize maintenance tasks efficiently, thus extending the lifespan of the road network while optimizing maintenance costs [7].

1.2 Research gap and problematic statement

To fulfill the strategic aim of integrating the structural assessment into the PMS's network level, it is essential to estimate accurately the fundamental mechanical properties that quantify the material stiffness or rigidity. One of the critical primary factor that describes how a material deforms when subjected to an applied load is the elastic modulus E_i per layer i. This parameter is central in characterizing the pavement's load-bearing capacity and remaining service life within the framework of stress-strain analysis during pavement assessment. In essence, precise E_i estimation is essential, not just for designing durable and resilient roads but also for advancing proactive maintenance practice, optimizing budget allocation, and improving overall road safety [8, 9].
However, in the quest to estimate the modulus of elasticity per each layer E_i, traditional laboratory testing methods have shown limitations. These procedures are often punctual and destructive, making them complex and resource-intensive. Highway agencies have turned to Non-Destructive Techniques (NDT) to overcome these challenges as a more efficient means of determining E_i. Among these techniques, the Falling Weight Deflectometer (FWD) has become a popular choice in the industry for its ability to provide valuable data. Nevertheless, FWD has operational constraints that require careful consideration. One known drawback of the FWD is its stationary nature. This characteristic increases costs and time demands, especially when conducting network-wide assessments [10]. Furthermore, FWD testing necessitates traffic management to ensure safety during the procedures. This requirement can introduce challenges in maintaining smooth traffic flow and raise concerns regarding workplace safety. As a result, the existing back-calculation methods, which rely on multilayer elastic theory and static loading characteristics derived from FWD data, underscore the need for alternative models [11, 12].
In response to these challenges, innovative solutions have emerged in recent years to fa-

cilitate continuous bearing capacity assessment. A standout among these solutions is the Traffic Speed Deflectometer (TSD). TSD has gained prominence due to its capacity to provide ongoing measurements across vast distances at speeds exceeding 80 km/h. This capability enables rapid and extensive surveys to assess pavement conditions at a network level. An additional advantage of TSD is that it eliminates the need for traffic control or lane closures during testing, thereby minimizing FWD disruptions to traffic flow. However, the main issue with TSD persists in the interpretation of the measurements, particularly in the estimation of elastic modulus using TSD measurements [13, 14, 15].

In the broader context: Over the years, various methods have been developed to calculate pavement moduli using FWD deflection basin data, including the database search method, regression equations method, optimization techniques, genetic algorithms, and others [16, 17]. These methods primarily deal with static deflection data, distinct from the dynamic data obtained from TSD. The objective is to determine a structural layer moduli set that optimally matches the measured and theoretical static deflection basins. However, these methods often necessitate predefined mechanical properties for different layers. When such properties are unknown, reliance on initial assumed values can result in non-uniqueness and reduced accuracy [18, 19]. To address this challenge, the prevailing solution today involves transforming TSD measurements into FWD data and incorporating the transformed TSD-FWD data into FWD-based back-calculation softwares. This is achieved by numerically integrating the deflection slope [20].

Given challenges in converting TSD measurements into FWD data for pavement modulus estimation, this impractical solution motivates the current research. Specifically:

— First, there is a distinction in loading configurations, where FWD utilizes a single plate, whereas TSD employs twin tires. This variance in the arrangement of loading elements contributes to disparities in the measured deflection responses. Second, differences in loading mechanisms further compound the issue. FWD applies an impulse load to the pavement surface, while TSD utilizes a dynamic or moving load. These distinct loading mechanisms generate different stress distributions on the pavement structure, leading to varying deflection patterns. Additionally, a fundamental difference lies in the measurement principles of the two devices. FWD directly measures pavement deflection, whereas TSD captures deflection slope. The challenge arises when attempting to correlate these disparate measurements. The transformation from deflection slope to deflection involves numerical integration, introducing complexities. This process results in information loss and is highly sensitive to the chosen integration method. Consequently, different integration methods can yield divergent results for the same measurement. Notably, there is currently no universally accepted integration method applicable to all operators [11, 20, 21].

— The second motivation arises from the increasing use of TSD and network-level deflection testing, which generates substantial amounts of data. Traditional methods struggle to handle this data effectively. However, there are still challenges in estimating the pavement mechanical behaviour from TSD data [21, 22, 23]. Therefore, this research aims to develop new methodologies to address these challenges and contribute to the improvement of pavement modulus calculation techniques.

1.3 Thesis objectives and hypothesis

This thesis aims to develop a Machine learning based intelligent framework that integrates data science techniques and pavement modeling to interpret data from simulating pavement deflection behavior under Traffic Speed Deflectometer (TSD) network-level measurement.

The primary objective is to address existing knowledge gaps and make a contribution to the pavement engineering field by proposing an innovative methodology and computational tools for directly estimating pavement mechanical properties, specifically the pavement elastic modulus E_i, from TSD deflection slope data D_S instead of conventional deflection data. The model developed in this research has been built upon data derived from industry-approved software and an experimental outdoor simulator, ensuring their alignment with real-world conditions.

The hypothesis of integrating ML into pavement condition assessment could offer numerous advantages over the traditional methods. Notably, the robust learning algorithms empower the system to extract patterns and specific features within extensive datasets related to pavement conditions. ML models excel in accuracy and computational efficiency performance compared to conventional methods. This is applicable even when dealing with vast datasets encompassing hundreds of thousands of kilometers of assessed roads. Furthermore, what truly sets ML models apart is their remarkable capacity for generalization, resulting in superior performance even when dealing with new and noisy data, surpassing the capabilities of conventional methods [24, 25, 26].

Based on the preceding argument, the research questions are formulated as follows: The research endeavors to address a set of crucial questions arising from the outlined argument. The primary objective is to investigate the potential impact of machine learning (ML) on pavement structural assessment. This exploration centers on understanding how ML can offer versatile solutions to challenges in mechanical and physical modeling, signal processing, and other relevant applications. The aim is to surpass conventional approaches in addressing these challenges, thereby enhancing the efficacy of pavement structural assessment.

In parallel, the investigation extends to the integration of ML with TSD. This concept aims to strengthen the analysis of extensive datasets related to pavement structural assessment. Specifically, the research delves into how the fusion of ML and TSD data, denoted as inverse model integration, improves overall efficiency and influences the estimation of the modulus E_i.Through these inquiries, the research aims to contribute valuable insights to advancing pavement structural assessment methodologies.

1.4 Thesis scope and framework

The primary motivation behind this doctoral research stems from the pressing need for improved assessment techniques for the structural health of deteriorating road pavements. There is a compelling desire to develop a novel model that addresses the limitations mentioned earlier and offers enhanced capabilities and solutions. This research aims to bridge existing gaps in knowledge and contribute to the state of the art, particularly in the advancement of methodologies for precise estimations of pavement modulus E_i. To address these issues, two primary challenges have been identified:

1. The first challenge is related to the current E_i estimation method via TSD: It stems from the discrepancies encountered when converting TSD measurements into FWD. The differences in measurement principles (TSD: Deflection slope, FWD: Deflection), loading configuration (TSD: Dynamic, FWD: Impulse), and mechanisms between FWD and TSD present some barriers when applying traditional FWD back-calculation techniques to TSD data [11, 27].
2. The second challenge is associated with the increasing adoption of TSD and the expansion of network-level deflection testing. This has led to the generation of vast amounts of data that conventional methods struggle to process effectively [23, 28].

To this end, following the identification and definition of the primary challenges, research questions, hypotheses, and objectives, the upcoming section will elucidate the methodology and scope of the framework in each chapter of the thesis.

1.5 Structure and outline of the thesis

1.5.1 Chapter I: General introduction

The general introductory chapter of the thesis serves as a foundational overview for the research. It identifies and emphasizes the gaps and challenges inherent in conventional deflection measurement devices and methods of interpreting measurements. This underscores the importance of addressing these identified shortcomings within the context of

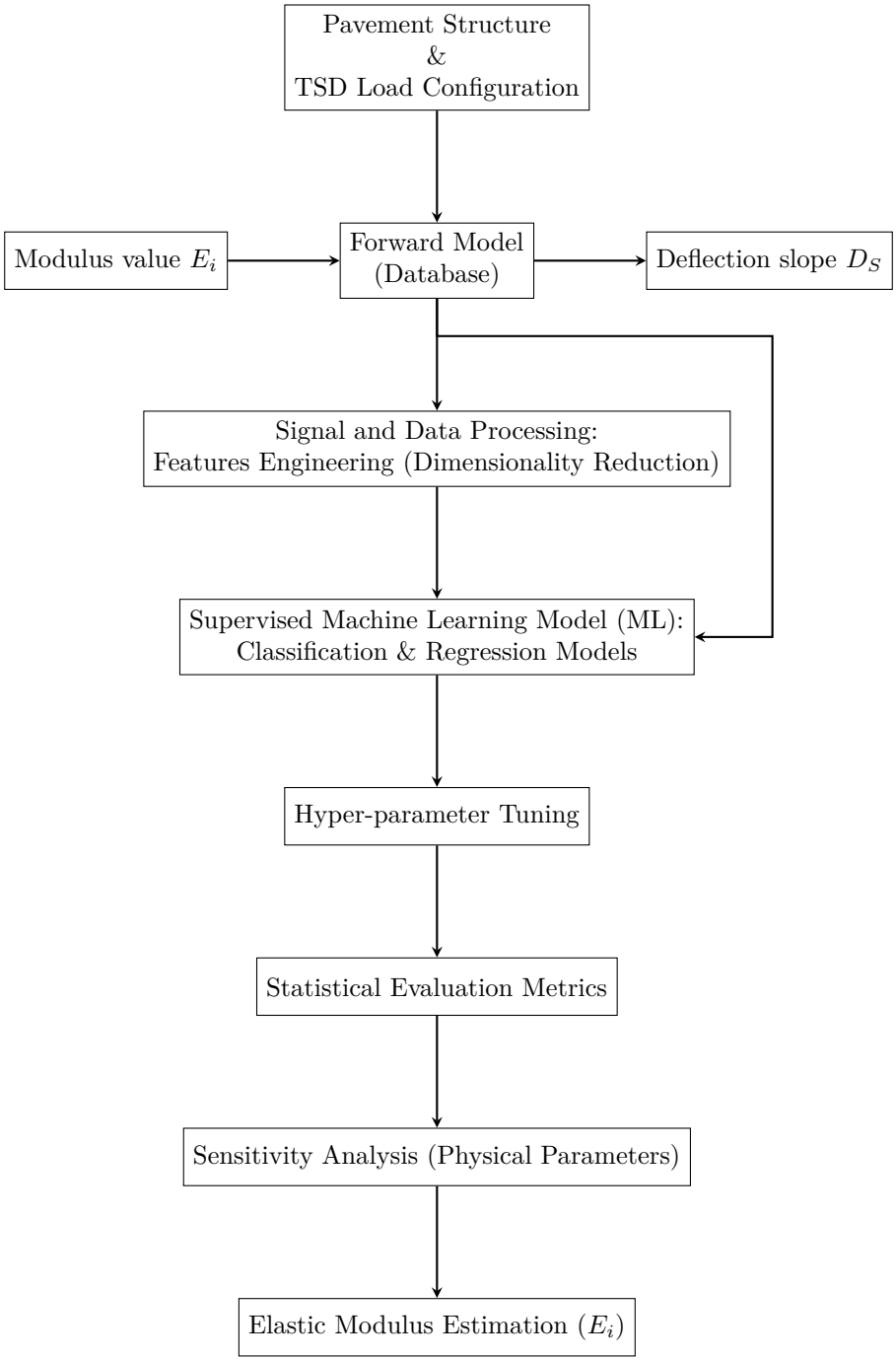

Figure 1.1 – Research framework and methodology for E_i estimation via TSD data

pavement network-level structural assessment. In addition to this contextualization, the introduction articulates the research objectives and elucidates the motivation behind the study. It establishes a feasibility framework for automating TSD data with ML model. This segment is pivotal in shaping the research question, formulating hypotheses, and outlining the consistent methodology and framework of the model that is to be applied

throughout the study delineated in Figure 1.1.

1.5.2 Chapter II: The state of the art

The State-of-the-Art chapter conducts a bibliographic analysis of pavement mechanics and engineering, identifying research gaps and introducing a supervised learning-based ML framework. Split into two sections, the first explores road pavement engineering, covering composition, mechanical behaviors, deflection analysis models, and device limitations. It emphasizes parameters influencing pavement-bearing capacity, especially network-level measurements within PMS. The second section explores ML's relevance to Structural Health Monitoring, focusing on advanced supervised learning algorithms for classification and regression tasks, with justifications for their selection. This chapter addresses the research question: What are the critical gaps and limitations in existing pavement mechanics engineering literature, and why can ML effectively address these challenges, particularly in the context of Structural Health Monitoring (SHM)?

1.5.3 Chapter III: Forward Model: Numerical validation

This chapter presents a methodology for modeling numerically TSD simulated measurement to construct a forward model database. This database adheres to the French standard (NF P98-086/2019) [29, 30] and encompasses various pavement structure scenarios of partially or entirely damaged pavement layers. The novel approach presented in this research directly utilizes the deflection slope D_S instead of the deflection to estimate E_i, eliminating information loss and potential biases due to numerical integration in deriving deflection values from deflection slope [31]. After completing these processes, the final database comprises two critical sets of parameters: D_S, functioning as the input (feature), and E_i values, serving as output labels. The central research question is: "How will the pavement deflection behavior under TSD be simulated and validated numerically?

1.5.4 Chapter IV: Inverse problem: Numerical validation

Following the construction of the forward model, this chapter is principally dedicated to the estimation of E_i, with a specific emphasis on the Subgrade Resilient Modulus (M_R), recognized as a pivotal indicator of the inherent stiffness in the soil or aggregate materials forming the foundational layers of pavement systems [32]. The estimation of numerical M_R utilizes Support Vector Machine (SVM) methodology [33]. This process encompasses both classification and regression [34, 35, 36]. To ensure the accuracy of the estimated modulus, a validation process is conducted involving comprehensive statistical analysis, hyperparameter tuning, and evaluation metrics [37]. In the final segment of this chapter,

a thorough sensitivity analysis is undertaken to explore the impact of various factors on the accuracy of the estimation process, including temperature variation and measurement noise. To this end, the central research question to be addressed in this chapter is: "From a numerical standpoint, how does the effectiveness of employing ML in the exploitation of TSD data provide more reliable results than traditional methods ?"

1.5.5 Chapter V: Experimental validation

This chapter is dedicated to the experimental validation of the developed numerical model, utilizing a dataset derived from bearing capacity tests conducted within the I-Street project framework [38]. These tests took place at the fatigue carousel of the University Gustave Eiffel (formerly IFSTTAR) over four months. Pavement instrumentation included strain gauges, temperature sensors, and a geophone. A notable challenge in this experimentation was the limited availability of labeled structured data, even internationally. To address this limitation, data augmentation was implemented, explicitly simulating Geophone measurements to construct a hybrid database (synthetic and experimental), resulting in an augmented dataset with high-dimensional data. Following this, a comprehensive evaluation was conducted to optimize the model's performance and validate its efficiency. This evaluation included advanced validation techniques, sensitivity analysis, and parametric estimation. For this purpose, two distinct types of databases are introduced: one employing global and local approaches. The global approach dataset has dimensions allocated for all the features extracted from the deflection slope D_S. In contrast, the local approach dataset is obtained after applying PCA, resulting in lower dimensions of features represented by two principal components PCs derived from the deflection slope D_S. The overarching research question addressed in this chapter is how to experimentally validate the numerical approach developed in the previous chapter and assess the performance of the inverse model in global and local applications.

1.5.6 Chapter VI: General conclusion

In the conclusion of the thesis, an overall summary and synthesis of the research findings will be presented. This includes a brief recapitulation of the key contributions and outcomes derived from the investigation into the methodology for precise E_i estimation using the ML model. The implications of the study's results on the broader field of pavement engineering will be discussed, emphasizing the advancements made in understanding and optimizing the estimation process. Furthermore, the limitations and challenges encountered during the research will be acknowledged. Recommendations for future research endeavors and potential enhancements to the proposed methodology will be outlined, fostering avenues for continued exploration and refinement in the field.

Chapter 2

The State of the Art

2.1 Introduction

In the context of the transportation sector, road pavements are indispensable elements of infrastructure that facilitate safe and efficient traffic flow. Pavement infrastructure has long been recognized as a vital part of the road system, and rehabilitating it is becoming a complex and costly challenge. This is especially true now, as many pavement networks are approaching the end of their usable life. Most countries face financial constraints for rehabilitation [2, 39, 40].

To making decisions about rehabilitating pavements lies in the Pavement Management System (PMS), which provides condition scores for each pavement segment in the system [41]. In the past, PMSs mainly focused on functional assessments like ride quality and distress tests, leading to concepts like Serviceability Rating and Present Serviceability Index [42]. However, as technology advanced, pavement engineers began using distress indicators (like cracking and rutting) and roughness measurements (specifically the International Roughness Index or IRI) to decide how to manage pavements. While distress and roughness are vital indicators, an equally important factor for making smart pavement investment decisions is structural adequacy [43].

Currently, there's a gap in research regarding structural assessments, particularly in the context of routine network level PMS activities. Some countries have started considering structural adequacy by incorporating deflection testing [9, 28, 44].

Therefore, this research aims to fill these gaps by contributing to enhancing the measurement interpretation methodology of structural adequacy, with a particular focus on the bearing capacity assessment highlighted green section in Table 2.1.

In pavement load-bearing capacity assessment, traditional methods such as Falling Weight Deflectometer (FWD) are still widely used by two-thirds of agencies for backcalculating the pavement elastic modulus (E_i) according to Flintsch [45].

However, traditional deflection devices face challenges in addressing the expansive scale of road networks, thereby limiting their ability to make network-level predictions. This limitation has implications for road safety and maintenance [11, 46, 47].

To address these operational challenges, TSD has been introduced as an alternative so-

lution that measures deflection slope instead of deflection [48]. For interpretation purposes, TSD deflection slope D_S data is transferred to FWD deflection data to estimate E_i. However, challenges arise in this data-transferring process due to differences in loading configuration between TSD and FWD, making standard FWD back-calculation tools not directly applicable to TSD [11]. This necessitates innovative approaches for accurate load-bearing capacity assessment methods. Conversely, recent research studies showed the advancements that have been achieved by incorporating ML into the SHM domain [49].
Thus, to overcome the challenges of the growing demand for accurate performance predictions from the TSD data, this thesis's overall objective is to propose an efficient and effective ML-based procedure and methodology for the estimation of E_i. This novel approach utilizes D_S measurements instead of the conventional deflection measurement method; the state-of-the-art chapter lays the foundation for the subsequent chapters by providing an analysis of the current literature and research gaps relevant to the pavement structural assessment research.
The chapter is structured into two primary subsections. The first subsection focuses on pavement mechanics, encompassing the layers and materials that constitute road pavements, mechanical behavior, and modeling. It also addresses the interpretation of deflection measurement and the inherent limitations of NDT-bearing capacity measurement and assessment devices. Furthermore, it investigates the influential parameters affecting the structural assessment of pavement-bearing capacity, considering measurements at the network level within the context of the PMS. The second section delves into the essential concepts of ML used in the context of this research, in addition to an overview of its application in the SHM field. Specifically, it focuses on the supervised learning techniques and the choice justifications. Considering the expansive nature of pavement assessment, The components highlighted in green Figure 2.1 and Table 2.1 signify the aspects that will be specifically investigated in this research endeavor.

Table 2.1 – PIARC Typical pavement condition indicators and indices.

Evaluation	**Function**	**Charateristics**	**Indicator**
Functional	Serviceability	Roughness	International Roughness Index Present Serviceability index (PSI) Quarter-car index (QI)
	Safety	Texture	Macro-texture Micro-texture
		Skid resistance	Skid R. Coff Int'l friction index (IFI)
		Mechanical properties	Deflections
Structural	Bearing Capacity	Pavement distress	Cracking Surface defects Profile deformation, rutting

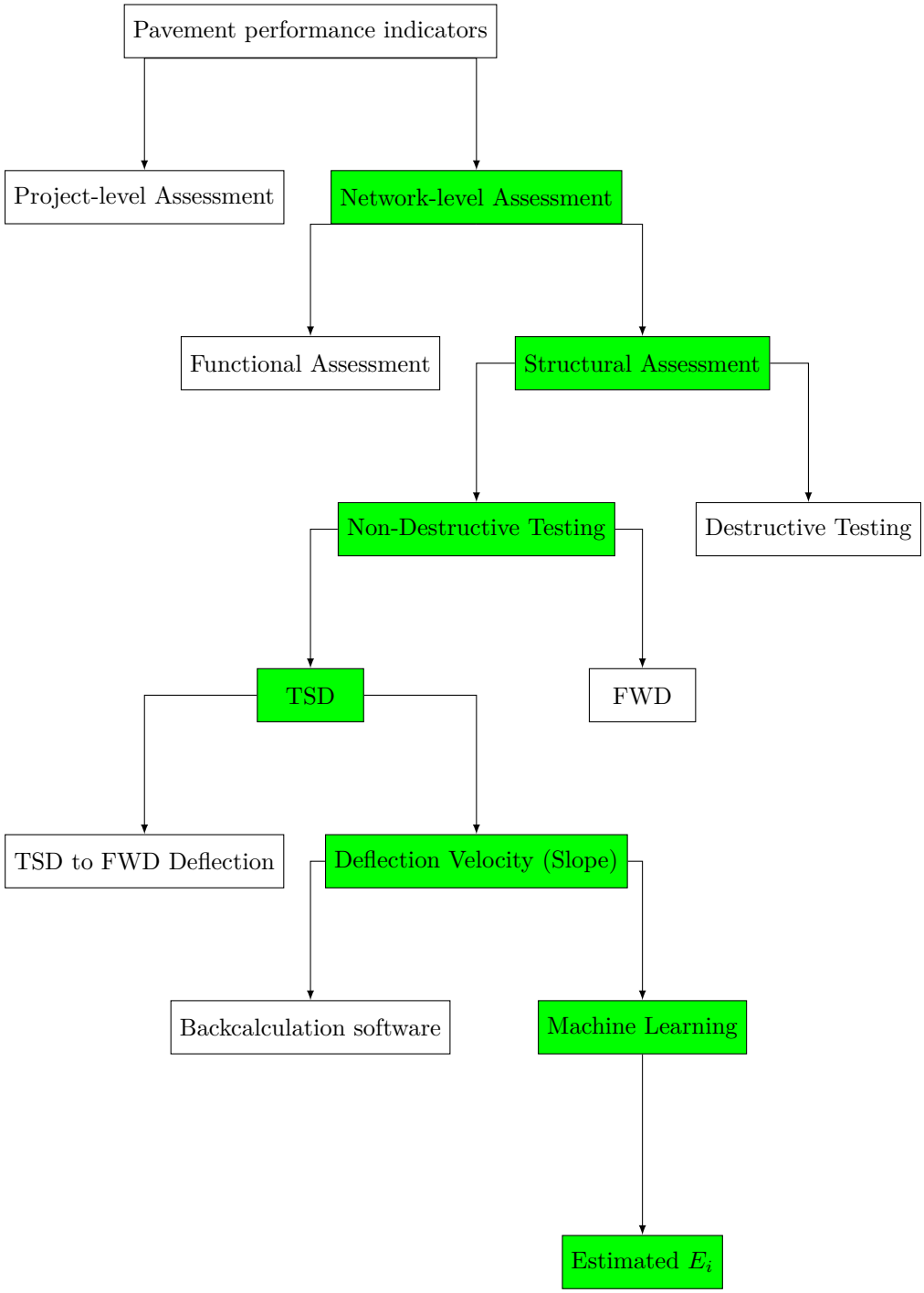

Figure 2.1 – The state-of-the-art framework of the thesis, certain areas of study highlighted in Green

2.2 Pavement in general

Overall, a pavement structure can be defined as a composite arrangement consisting of multiple layers with different materials and thicknesses. Its primary contribution is to effectively distribute the weight of traffic and minimize its impact on the soil bearing capacity, all while providing a cost-effective, long-lasting surface and prioritizing the safety and comfort of road users [30, 50].
A properly designed pavement structure involved in providing a dependable and durable transportation infrastructure that maintains performance and structural integrity over time. However, as time passes, the properties of pavement materials change due to the combined effects of traffic, weather conditions, and the natural aging process [51]. These changes lead to the development of distress and fatigue issues within the pavement structure, which, in turn, affect the pavement's ability to function optimally [52, 53].
In the following subsections, a brief overview of the pavement material and its mechanical behavior most relevant deterioration mechanisms specific to each of these factors is briefly presented herein.

2.2.1 Pavement material

The structure of a road pavement typically comprises several layers, each composed of various materials. For instance, the surface course is generally made of asphalt or concrete, providing a skid-resistant and durable riding surface with good compressive strength and resistance to deterioration and damage. The granular base, composed of materials like crushed stone, acts as a transition layer, offering structural stability and load distribution. The subbase, often made of granular materials, supports upper layers and helps manage moisture. The subgrade, the natural ground or compacted soil beneath the pavement, must possess sufficient bearing capacity to resist deformation under loads. When bedrock is available, it serves as a high bearing capacity stable foundation [30, 50, 54, 39].
However, in pavement engineering, the mechanistic approach uses stress-strain models to characterize these pavement materials' mechanical properties effectively. These materials are typically categorized into three primary classes based on their stress-strain relationships and performance under various loading conditions [55, 56, 57].

— Bituminous materials: These materials are often used in asphalt pavements and characterized by the visco-elastic behavior [58, 59]. This means factors like temperature and loading time influence their stress response. Bituminous materials become softer and more deformable at higher temperatures and low-frequency solicitations, which impacts their stiffness. In colder conditions, they become stiffer.

— Concrete and Cement-bound layers: These are typically characterized by linear-elastic behavior [60]. This means their deformation is proportional to the applied load within their elastic limit. They return to their original shape when the load is removed.

— Soils and Granular Materials: These exhibit non-linear behavior [61]. Their stiffness depends on the stress state they experience, and their behavior varies based on factors like the material type (whether cohesive or granular). They are also sensitive to seasonal variations. The stiffness could vary with moisture content in cohesive soils, such as clay.

Thus, the distinct characteristics of materials are pivotal in pavement engineering, shaping road surface design, construction, and overall performance.

2.2.2 Pavement design and deterioration mechanisms

The primary sources of stress and strain within a pavement are traffic and temperature variations [51]. Due to environmental interactions and normal aging, road pavements are continuously exposed to mechanical, thermal, physical, and chemical forces. These factors combine collectively, resulting in mechanical stress within the pavement structure. The specifics of this stress depend on the properties of individual layers, including materials and thickness, and the degree of bonding at their interfaces [62].

1. Surface: time-induced deterioration: As recognized, the surface course is one such layer typically made of materials like asphalt or concrete, which must provide a skid-resistant and durable riding surface with good compressive strength and resistance to deterioration and damage. However, when it comes to the time-induced pavement deterioration on the surface, it represents a gradual process primarily caused by alterations in the molecular structure of bitumen. These alterations give rise to various issues, including aging, hardening, raveling, and chemical changes. Bitumen undergoes increased stiffness, loses its elastic recovery capacity, and weakens the bond between aggregates and bitumen. These transformations result in the loss of aggregates on the pavement surface, known as raveling or fretting. In some instances, the aging and raveling process may advance to cracking, characterized by top-down cracking, refer to Figure 4.6, which originates at the pavement's top surface and extends downward. This form of cracking facilitates water infiltration, contributing to the deterioration of the unbound layers beneath the pavement surface [63, 64].
2. Structure: traffic-induced stress: For the pavement structure, the mechanical approach uses stress-strain models to characterize these pavement materials' mechanical properties effectively. However, the stress induced by traffic primarily occurs

when vehicles traverse the road, subjecting them to repeated loading cycles over their lifetime. This leads to horizontal and vertical cyclic stresses within the structure, as illustrated in Figure 4.6. Although the stress associated with each loading cycle may be relatively small, accumulating these cycles can lead to strain buildup and irreversible damage. When the layers are strongly bonded, the structure behaves like a monolithic beam [64, 65]. The repeated horizontal tensile stress at the bottom of each layer, as illustrated in Figure 4.6, can induce micro-damage and contribute to the propagation of cracks within the structure, a phenomenon known as **fatigue**. Hence, the structure design holds paramount importance in mitigating fatigue-related concerns. Conversely, repeated vertical compressive forces in Figure 4.6 may result in permanent deformations, commonly called rutting [52, 53].

To this end, the interplay of traffic and temperature-induced stress, along with time-induced deterioration in bitumen structure, is meaningful pavement evaluation. Adopting a mechanistic approach in pavement engineering enhances material characterization, enabling accurate prediction of behavior under diverse loading conditions.
Expanding on the preceding discussion, the upcoming section establishes the framework for modeling the mechanical behavior of pavements, with a specific emphasis on the linear elastic model adopted within this thesis.

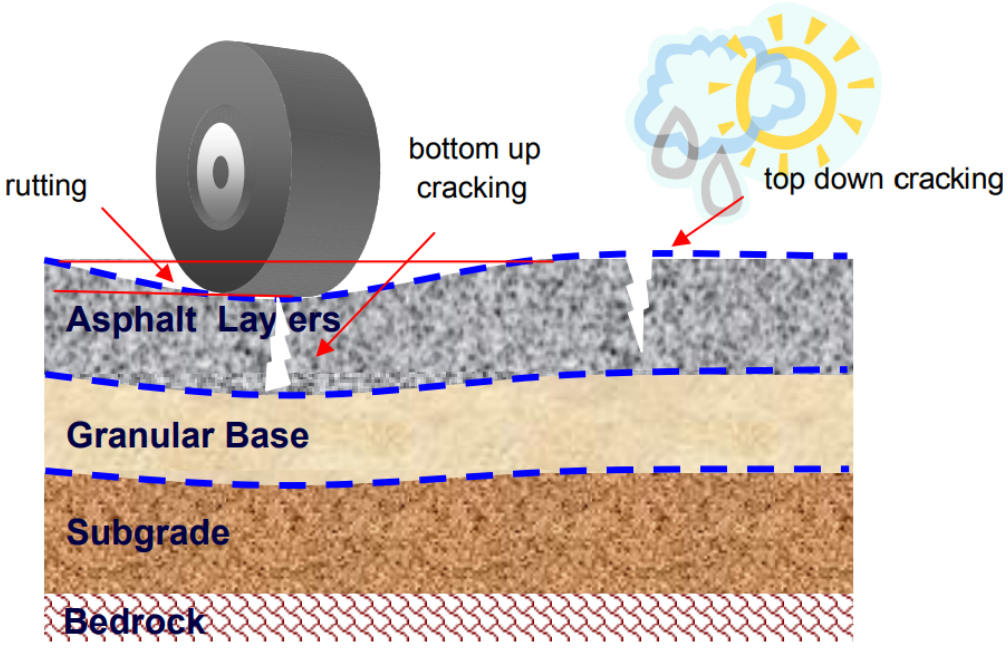

Figure 2.2 – The principal mechanisms of flexible pavement deterioration [66].

2.2.3 Pavements mechanical behavior modeling

For analyzing and designing pavement roadways, conventional analytical models have been the primary approach for an extended period. However, contemporary methods such as Finite Element Methods (FEM) have emerged as prominent alternatives. FEM is renowned for its ability to integrate non-linear behaviors and handle intricate geometries, albeit with a trade-off between calculation time and accuracy [67]. Moreover, numerous pavement models have been proposed over the years to calculate the behavior of pavement structures, including the Boussinesq model (1885) [68], Westergaard model (1926) [69], Hogg model (1938) [70], Burmister model (1943) [71], Jeuffroy model (1955) [72].
Boussinesq (Boussinesq, 1885) [68] was a pioneer in proposing a set of equations for determining the response of a semi-infinite, homogeneous, isotropic, linear elastic medium to a static point load. This response encompassed parameters such as strain, stress, and deflections. However, road pavements are composed of multiple layers, each with distinct mechanical properties [55, 62, 73].
A more accurate theoretical framework was introduced by Burmister (Burmister, 1943) [71] for two-layered elastic systems, subsequently extending to systems with three or more (n) layers. This model has become widely adopted in mechanical pavement design methodologies. It operates under several assumptions as shown in Figure 2.3:

- The pavement is treated as a multi-layered medium, with each layer being homogeneous, isotropic, and linearly elastic, characterized by its modulus of elasticity (E_i) and Poisson's ratio (ν_i).
- Each layer possesses a finite thickness (h_i) and extends infinitely in the horizontal direction, with the bottom layer extending infinitely downward.
- It is a 2D asymmetric model, and the load is described as a constant vertical pressure applied over a circular area. Loads are uniformly distributed over a circular area with a radius (a), and the effects of multiple loads can be aggregated (superposition effect).
- Interfaces are classified as either fully bonded (with both layers exhibiting the same displacement at the interfaces) or frictionless (where the displacement of one layer is independent of the other).

Various software tools have been developed using the Burmister model. However, this thesis predominantly employs Alizé-LCPC for several reasons; it serves as the primary software utilized for pavement design in France, offering widespread industry recognition [74]. Additionally, Alizé-LCPC incorporates a comprehensive library of standardized materials as outlined by French guidelines for pavement design, explicitly conforming to the Standard NF P98-086 [29]. Moreover, owing to its industrial endorsement and reputation for simplicity in calculations, this section on pavement mechanics has established a foun-

dational understanding of pavement structure and mechanical behavior. It has delineated the modeling approach and justified the selection of Alizé-LCPC for the numerical study dedicated to estimating E_i.
Subsequently, the following sections will highlight the research gaps related to pavement performance model indicators. The objective is to reveal limitations in conventional Pavement Structural Assessment devices and methods. Moreover, the section will examine the measurement interpretation limitations of the proposed alternative methods, seeking to mitigate drawbacks inherent in traditional approaches.

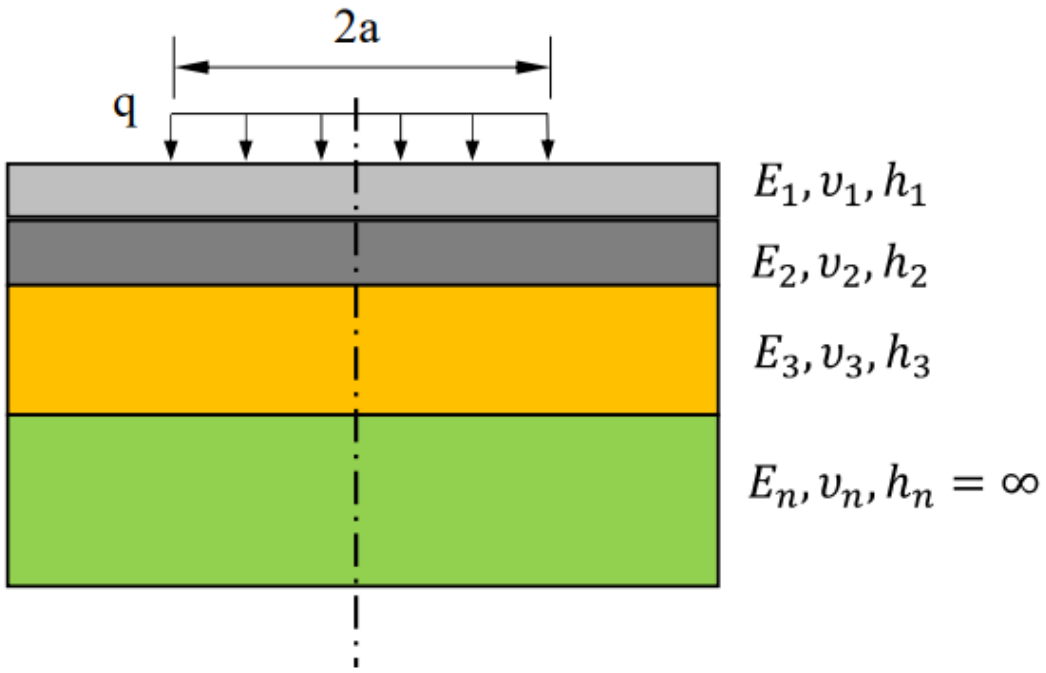

Figure 2.3 – Burmister multilayer elastic model [75].

2.3 Bearing capacity assessment: Deflection concept

The evolution of pavement structural assessment techniques has been propelled by the necessity for precise and efficient methods to evaluate the condition and performance of roadways. An array of destructive and non-destructive technologies has emerged to offer valuable insights into the structural integrity of pavements. However, as detailed in Table 2.1 and Figure 2.1, this thesis focuses on assessing mechanical properties reliant on deflection measurements, particularly for estimating the pavement elastic modulus E_i. Before delving into this approach, what is the concept of pavement deflection.
Deflection, as depicted in Figure 2.4, refers to the vertical displacements or deformations on the pavement surface when subjected to applied loads. The resultant maximum surface deflection, or an array of surface deflections, constitutes a deflection basin [46].
Deflection measurement serves a critical mission in evaluating existing pavements' ability to withstand future traffic loads effectively. A strong correlation exists between pavement deflections, indicating structural adequacy, and the pavement's capacity to bear traffic loads at specific service levels [76]. Moreover, the analysis of the entire deflection basin, as depicted in Figure 2.4, is essential for extracting deflection basin parameters. These parameters have consideration in pavement design procedures and performance analysis, aiding in the estimation of remaining service life or load-carrying capacity [40].
The subsequent chapter will provide an overview of some of the deflection basin parameters commonly utilized in the industry. Additionally, various other parameters have been introduced by Simonin in the thesis of [77].

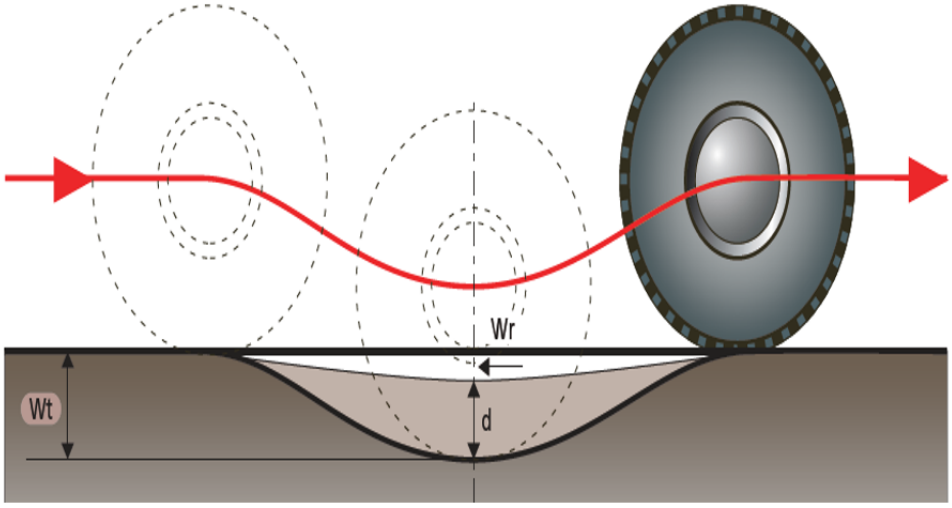

Figure 2.4 – Pavement deflection basin [78].

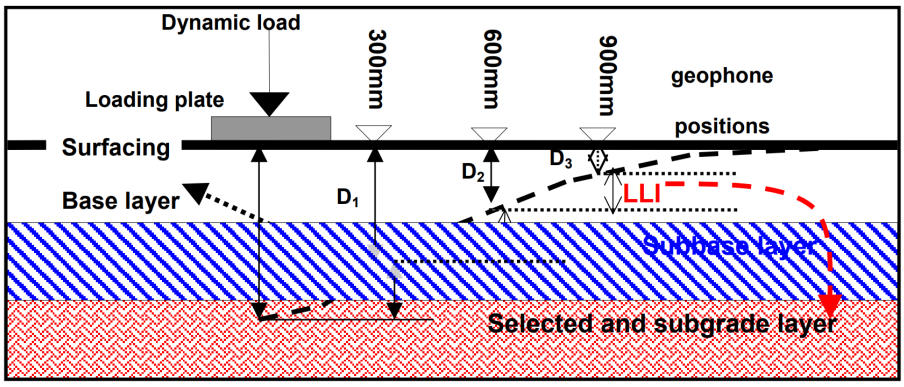

Figure 2.5 – Deflection bowl main parameters [79].

2.3.1 Deflection measurement interpertation

Calculation of Deflection Bowl Indices has emerged as one of the most reliable approaches for evaluating the structural capacity of flexible pavements. While initially developed for structural assessment using the FWD, they have found practical applicability in the context of the other devices. Deflection basin parameters presented in Figure 2.5 and Table 2.2 introduce valuable insights into the pavement's structural capacity and demonstrate an ability to identify sections with different conditions, such as sound, fair, or weak [79].

Where D_x: x represents the deflection distance in (mm) from the loading point.

BLI: Base Layer Index (also known as Surface Curvature Index, SCI):

$$SCI = D_0 - D_{300}$$

MLI: Middle Layer Index (also known as Base Damage Index, BDI):

$$BDI = D_{300} - D_{600}$$

LLI: Lower Layer Index (also known as Base Curvature Index, BCI):

$$BCI = D_{600} - D_{900}$$

However, It is argued that relying on these correlations for determining remaining lives in the structural analysis of flexible pavements during rehabilitation design could oversimplify the complex structural response and result in embarrassing inaccuracies. Instead, a more fundamental approach is recommended, steering away from remaining life calculations. The recommended application involves using these correlations to enhance the condition and behavior state of pavement layers [79]. Nevertheless, the efficiency of deflection mea-

surement is contingent upon the characteristics and capabilities of the devices utilized for this purpose. Thus, a comparative analysis of various deflection measurement devices will be presented in the subsequent section, elucidating their operational methodologies and associated limitations.

Table 2.2 – Structural condition rating criteria for various pavement types [79].

Structural	Pavement condition	D0 (μm)	BLI (μm)	MLI (μm)	LLI (μm)
Granular base	Sound	<500	<200	<100	<50
	Warning	500–750	200–400	100–200	50–100
	Severe	>750	>400	>200	>100
Cementitious base	Sound	<200	<100	<50	<40
	Warning	200–400	100–300	50–100	40–80
	Severe	>400	>300	>100	>80
Bituminous base	Sound	<400	<200	<100	<50
	Warning	400–600	200–400	100–150	50–80
	Severe	>600	>400	>150	>80

2.3.2 Traditional deflection measurement devices

Traditional deflection devices are used extensively in assessing pavement structural conditions. These devices measure the deflection of pavements under load, offering valuable insights into their response to various loading conditions. However, it's necessary to grasp the limitations of these traditional deflection devices to ensure accurate and reliable pavement evaluations. Thus, this section delves into some examples of conventional deflection devices, highlighting their advantages and their operational limitations presented in Table 2.3. The comparative table outlines the features of four traditional pavement deflection measurement devices Figure 2.6: Benkelman Beam, FWD, Deflectograph, Curviameter. Each device has strengths and limitations, making it suitable for specific pavement investigations. To overcome the limitations of traditional deflection devices, researchers have explored alternative approaches that capitalize on modern technologies to enhance the accuracy and efficiency of pavement assessment while offering a promising advancement for the field.

A : Benkelman beam (Static nature)

B : FWD (Impulse-Stationary nature)

C : Deflectograph (Slow-move nature)

D : Curvimètre (Constant-move nature)

Figure 2.6 – Traditional deflection measurement devices [77].

Table 2.3 – Comparison of traditional pavement's deflection measurement devices [77, 80, 81].

Device	**Principle of Operation**	**Advantages**	**Limitations**
Benkelman Beam	Operates on lever arm principle, applying a known load to measure the deflection. It is cost-effective for investment	Provides single-point measurement.	Limitation in capturing overall deflection behavior. It is time-consuming and less accurate compared to automated devices.
Falling Weight Deflectometer (FWD)	Applies a load pulse to replicate the effects of vehicle wheel load. It involves dropping a substantial weight onto a circular load plate. The deformation of the pavement surface is then measured using Geophones sensors	Permits adjustments to the load level, allowing for controlled variations in the applied force. It provides measurements at specific locations to ensure precise data collection and offer accurate measurement.	Measurement rate is slow and low, mainly because it involves a stop-and-go process that can lead to traffic disruptions; it is not practical at the PMS Network level.
Deflectograph	Comprises a truck that maintains a constant speed, applying the wheel load to the pavement, and a measurement beam equipped with a rotary coder to conduct two vertical displacement measurements within the wheel paths. The process is automated, with the beam being advanced for measurements	With successive versions, it has shown improved accuracy. It provides measurements at short, regular intervals. Additionally, some versions of it are equipped with an inclinometer to measure the radius of curvature, adding valuable information to the assessment process.	Very slow-moving nature (8 km/h); old versions cannot measure the entire deflection basin. Lower measurement rate compared to curviameter. The measured Deflection is subjected to bias.
Curviameter	Uses a geophone to measure the velocity of vertical displacement of pavement under the passage of the truck's rear axle. The deflection was obtained by integrating geophone measurement.	Have continuous measurements along the pavement section. Provides insights into pavement performance.	Requires precise calibration of geophones and maintaining a constant speed (18 km/h) during measurements. Also, it tends to underestimate the deflection values relatively, but less than the deflectograph level.

2.3.3 Traffic-Speed Deflection Devices (TSDDs)

TSDDs have emerged as a mobile and efficient alternative to traditional devices in assessing pavement structures. The demand for such devices was driven by the need to enhance safety and minimize traffic disruptions, particularly on heavily trafficked highways [82]. TSDDs can collect data at traffic speeds, efficiently surveying a large number of kilometers in a single operation. This capability makes TSDDs suitable for assessing the PMS network-level [45].
The dense dataset obtained by TSDDs, with measurement spacing often less than 10 m, enables the identification of weak zones within the pavement structure, allowing for the implementation of specific corrective decisions before undertaking extensive rehabilitation efforts. By addressing these issues proactively, transportation agencies can optimize their maintenance strategies and allocate resources more effectively [83].
In the following Table 2.4, an overall literature review will be undertaken to analyze the two central TSDDs Figure 2.7, available in the field of pavement evaluation: the Traffic Speed Deflectometer (TSD) and the Rapid Pavement Tester (Raptor) [84].
The features, capabilities, and applications of these devices in assessing pavement conditions and structural performance will be thoroughly examined. This analysis will provide valuable insights to inform the selection and implementation of TSDD technologies.
It is important to highlight that while both TSD and Raptor are components of the TSDD family, this research primarily focuses on the TSD. The decision to emphasize TSD over Raptor is based on the operational history of TSD, which has been utilized for many years and is supported by existing research and literature. In contrast, Raptor was still in the trial phase at the outset of this thesis.

Figure 2.7 – TSDDs, with TSD on the left-hand side & Raptor on the right-one [85].

Table 2.4 – Comparison between TSD and Raptor [20, 13, 22, 48, 86, 87, 88].

Aspect	Traffic Speed Deflectometer (TSD)	Rapid Pavement Tester (Raptor)
Principle of Operation	Measures deflection velocity of a loaded pavement at survey speeds up to 96 km/h. Utilizes Doppler lasers for in-motion measurements. Integrates deflection velocity to calculate deflection profiles.	In-motion measurement of pavement deflections using a rear-mounted sensor beam with laser-based line profilers. Individual lasers measure self-distance to the pavement surface. Forms a 3D scan of road surface during advancement.
Data Collection Speed	Survey speeds up to 96 km/h. High sampling rate of 250 kHz.	In-motion data collection during normal traffic speeds up to 96 km/h.
Device Design	Articulated truck with adjustable rear-axle load. Equipped with a servo-hydraulic beam and Doppler lasers.	Semi-trailer truck with rear-mounted independent single-wheel suspension systems. Sensor beam with laser-based line profilers.
Manufacturer/Diffusion	Greenwood Engineering with +21 diffused devices.	Developed in collaboration between Dynatest and the Technical University of Denmark (DTU) and then bought by Ramboll, with two diffused prototypes so far.
Calibration	Requires thorough calibration to eliminate systematic biases. Calibration addresses factors like laser orientation bias, driving speed dependency, and beam biases.	Demonstrates sound capabilities for road surface data collection. Thorough calibration to eliminate limitations related to high-sensitivity lasers, introducing noise and erratic behavior.
Deflection Calculation	Integrates deflection velocity over time. Applies the Area Under The Curve using Piecewise Cubic Hermite Interpolating Polynomial approach (AUTC-PCHIP) for calculating deflection basins.	Measures individual laser distances, providing a 3D road surface scan. Patch-matching techniques identify pavement surface points for deflection calculation.
Limitations	Influenced by factors like TSD speed variations, noise, and pavement roughness. Numerical integration challenges in deriving deflection profiles. Correlation with FWD measurements requires accounting for load configuration differences. Lack of back-calculation software for determining layer moduli directly.	Sound capabilities but influenced by limitations related to high-sensitivity lasers introducing noise. Overlooks surface displacements along the y-axis. The untapped potential of patch-matching techniques to identify lateral displacements. **More information about the Raptor in the chapter: Appendix**

2.3.4 The Traffic Speed Deflectometer (TSD)

TSD is a specialized vehicle developed by Greenwood Engineering and designed for the assessment of pavement bearing capacity by quantifying the deflection velocity of a loaded pavement [48] .

TSD data are collected at survey speeds of up to 96 km/h, utilizing a high sampling rate +250 kHz in more recent devices. The vehicle features an articulated truck with an adjustable rear-axle load, which can range from 60 to 130 kN, achieved using sealed lead loads. To hold the Doppler laser sensors, the TSD is equipped with a servo-hydraulic beam as shown in Figure 2.8, ensuring accurate and stable measurements during the assessment process [13].

In previous iterations of the TSD, six and Doppler lasers were utilized to capture the deflection velocity measuring in the longitudinal centreline between the rear twin wheels with lasers behind and in front of the load axle as shown in Figure 2.8, in addition to an reference laser , positioned 3,500 mm in front of the rear axle, aiming to measure an undeflected portion of the pavement for calibration purposes (hypothesis deflection =0 at this point) [89].

However, the most recent iteration introduced in 2021 as shown in Figure 2.8 has incorporated twelve Doppler lasers, providing an enhanced deflection measurement capability [22].

As per Greenwood, the TSD accurately assesses the structural integrity of runways, taxiways, and aprons. This advanced technology enables an overall evaluation, offering a full picture of the runway condition to facilitate informed maintenance decisions, ensuring safety and durability with minimal lane closure. [48].

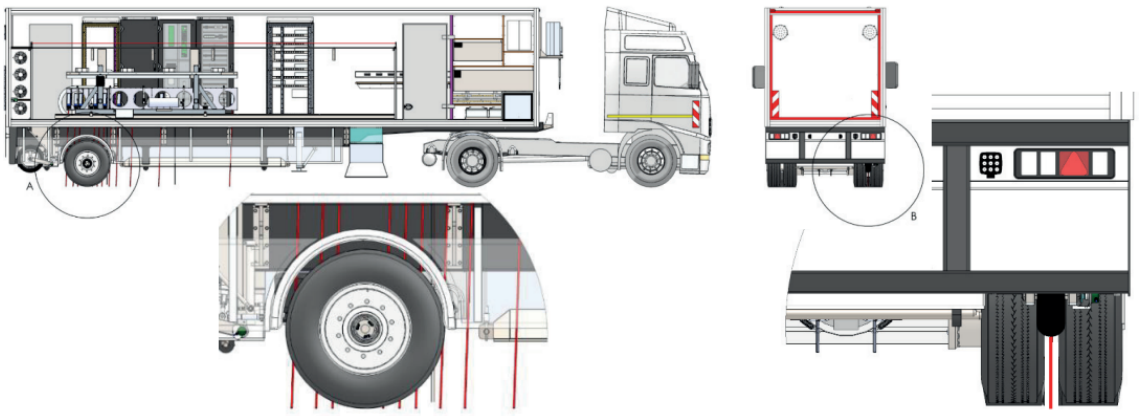

Figure 2.8 – Greenwood Engineering's TSD [48].

2.3.5 Preliminary analysis for TSD Operation

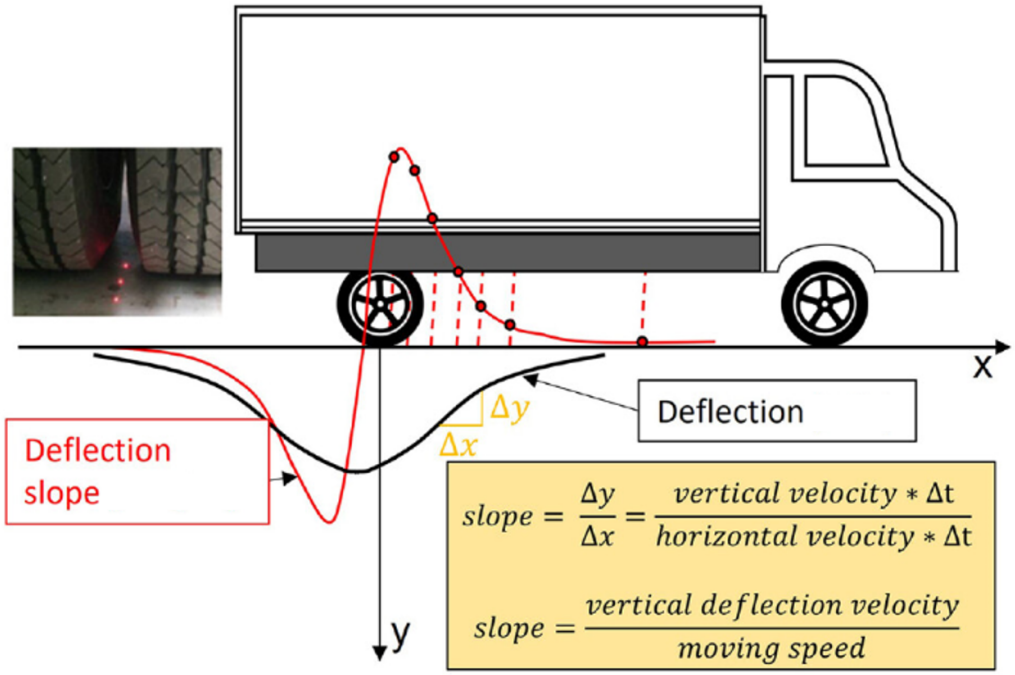

Figure 2.9 – TSD operation analysis [15]

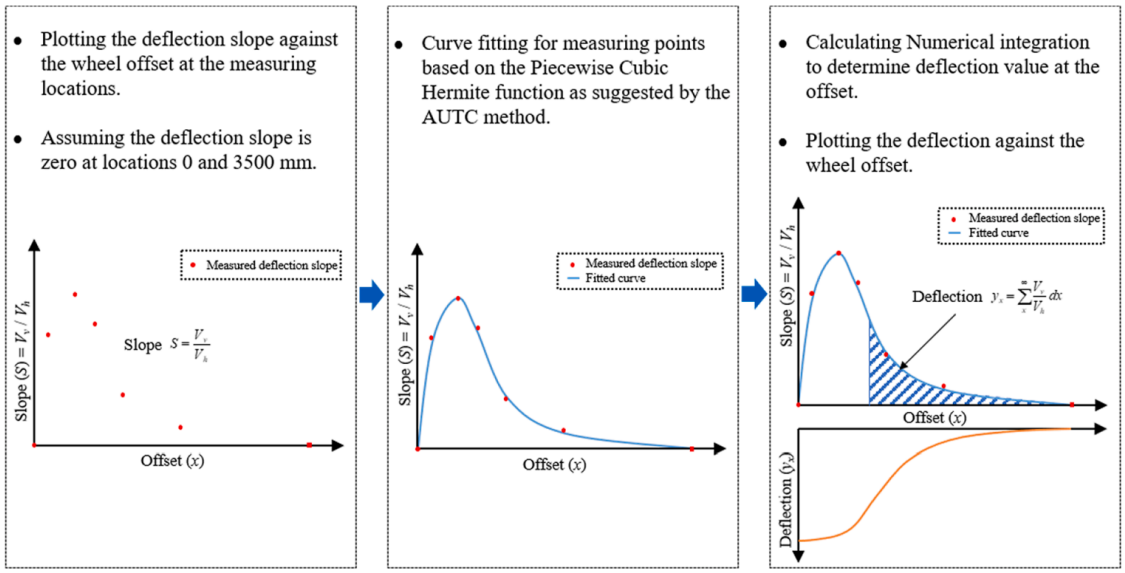

Figure 2.10 – The mechanism for calculating pavement deflection under TSD [20]

The calibration of the TSD is a fundamental process, ensuring the precision and dependability of its measurements. This process involves a systematic approach encompassing load configuration, sensor alignment, and meticulous data synchronization. The method commences by mounting the Doppler laser sensors at a 2-degree angle to accu-

rately record D_V from the pavement surface, primarily along the mid-line of the rear right dual tires Figure 2.9. The measurements include the vertical deflection velocity V_v of the road surface under the load and the response's horizontal TSD speed V_h. The relationship between V_h and V_v is direct and interrelated, thus requiring the division of V_v by the instantaneous V_h to remove this dependence and obtain deflection slope S_D. This thorough calibration process ensures the reliability of the TSD's measurements, providing a solid foundation for its operation. Then, as shown in Figure 2.10 this S_D is subsequently used for numerical integration to calculate the deflection [20]. The technique predominantly revolves around calculating the area under the fitting curve by numerically integrating the plot from the deflection basin's edge towards the loading center, thus earning it the name "AUTC" or "Area Under The Curve" method [90].
However, these methods have several limitations that warrant criticism. Firstly, they artificially assume that the deflection slope equals zero at the position of the reference sensor and the loading point. Additionally, to date, there are no unified standard integration methods to calculate deflection, and each method results in information loss during integration and potential biases introduced by different integration techniques. While these assumptions have been made to simplify calculations, the primary question arises regarding the impact of these hypotheses on the accuracy of deflection measurements. In Chapter 3, a quantitative analysis has been conducted to elucidate the uncertainty resulting from these assumptions on the deflection slope curve.

2.3.6 TSD systematic bias elimination

Several factors, including variations in TSD speed, noise, and pavement roughness, influenced the measurements obtained from TSD. Thus, a thorough calibration procedure is essential for consistent and precise deflection measurements using the TSD [45, 91]. It involves addressing the sources of systematic errors, commonly called biases, which can affect the accuracy of the measurements. The fundamental biases that require correction are as follows :

- Laser Doppler Sensor Orientation Bias: to accurately measure the vertical deflection speed of the road surface beneath the load, the Doppler laser is positioned at a nominal 2-degree angle. This positioning allows for measuring both the vertical deflection speed and the horizontal speed of the response, which is directly related to the sensor's horizontal speed (driving speed) [31].
- Driving Speed Dependency: to remove the bias associated with the speed dependency of the measurements, a correction is applied by dividing the vertical deflection speed (V_v) by the instantaneous measured velocity (V_h). This division allows for calculating the deflection slope, the main parameter in the TSD measurements [14].

— Servo-hydraulic Beam Bias: Eliminating beam bias involves precise alignment and installation of instruments like inclinometers, gyroscopes, and accelerometers. Additionally, a climate controller maintains a controlled temperature to control thermal bending [20].
— Reference Sensor Bias Mitigation: to address bias related to the reference sensor, it is assumed that the velocity slope and deflection at the reference sensor's measuring point are negligible. This assumption allows appropriate corrections to be applied to the measurement data from the reference sensor [14].
— Variation in Dynamic Load Bias Reduction: Fluctuations in dynamic loads induced by pavement roughness during measurements can introduce bias (noise) [92]. A rolling average technique is employed to mitigate this, where measurements are averaged over a certain distance (10m). This averaging process effectively reduces the impact of dynamic load variations on the deflection measurements [45].

By mplementing these calibration procedures and eliminating systematic biases, the TSD system can consistently deliver precise and reliable deflection measurement data [91]. The upcoming section will explore current direct and indirect methods used and their limitations to advance the understanding of modulus backcalculation from TSD measurement data.

2.4 Backcalculation of layer moduli from TSD data

The backcalculation of pavement E_i from non-destructive deflection measurements has become a pivotal focus in recent pavement research. This surge in interest is driven by the necessity to adopt mechanistic design and analysis methods alongside the widespread utilization of nondestructive testing devices like the FWD and TSD.
While FWD is widely used for this purpose; challenges arise when applying backcalculation techniques to data obtained from TSD. Differences in loading configuration and mechanism between FWD and TSD necessitate tailored approaches for TSD data compatibility with back-calculation techniques [45].
In response to this challenge, researchers have developed numerous pavement structural models and computerized procedures aimed at enabling backcalculation using TSD data. Table 2.5, [93, 21] has thoroughly explored and investigated these methods.

— 3D-Move and ANN Integration [94, 95].
— Velocity Method [96].
— Deflection Method [96].
— Viscoelastic Back-calculation Algorithm [97].

— FEM + Constrained Extended Kalman filter(CEKF) [98].

Table 2.5 summarizes five prominent backcalculation methods, detailing their features, advantages, and limitations.

In evaluating these methodologies, several vital considerations emerge. Firstly, accuracy stands out as paramount. The precision of a method in estimating E_i values directly impacts its efficacy in pavement analysis and design. Secondly, computational is indispensable, especially for large-scale applications. Methods demanding excessive computational resources may face challenges in widespread implementation. Lastly, the applicability of a method at the network level is essential for its practicality in real-world pavement management systems covering extensive road networks.

Thus, the analysis of various methodologies for backcalculating pavement layer moduli reveals nuanced differences in their approaches and capabilities. For instance, the 3D-Move and ANN Integration method combines TSD and FWD data with an ANN model. While practical, its accuracy is limited, particularly with data beyond its established database, and it struggles to capture the intricate viscoelastic characteristics of pavement materials. Conversely, the Velocity Model method adopts a meticulous approach by considering TSD loading characteristics and pavement material viscoelastic behavior. However, its reliance on manual iteration renders it time-consuming, limiting its applicability in large-scale network management scenarios.

In contrast, the Deflection Model provides a more straightforward yet practical solution. However, it overlooks dynamic pavement responses under moving loads and fails to account for the viscoelastic nature of asphalt layers, compromising its accuracy.

The Hysteretic Damping Model offers an approximation of asphalt rheology but requires substantial computational resources. Although it partially accounts for viscoelastic behavior, it only calculates a constant asphalt modulus at specific TSD loading conditions, neglecting the master curve. Lastly, the FEM + CEKF method incorporates tire-pavement contact stress. Still, it disregards asphalt's viscoelastic nature under moving loads and lacks maturity for widespread field use.

Overall, each method exhibits unique strengths and weaknesses, underscoring the complexity of backcalculation methodologies. While some prioritize accuracy over computational efficiency, others prioritize practicality at the expense of precision. Addressing these disparities and developing a more comprehensive approach is pivotal for advancing pavement engineering practices.

A critical research gap exists for creating a more generalizable approach capable of overcoming these limitations. Machine Learning (ML) presents a promising avenue due to its ability to learn complex patterns from data. By incorporating TSD measurements and potentially other relevant data sources, ML models could achieve a more accurate and

efficient method for directly backcalculating E_i values from TSD data while considering different mechanical behavior. The following section will introduce the theory and application of machine learning.

Table 2.5 – The available E_i back-calculation methods from TSD data [21].

TSD Back-calculation Method	**Summary**	**Advantages**	**Limitations**
ANN model [95]	In this method, a database of TSD and FWD deflection bowls was developed utilizing the 3D-Move program. Then, the ANN model is used as a regression technique to convert the TSD deflections to FWD deflections. Finally, the back-calculation can be performed using the available back-calculation tools for FWD data.	Use the available tools for FWD data to back-calculate TSD data.	The 3D-Move cannot accurately simulate FWD deflection bowls, adversely affecting the conversion tool's validity. Using a regression-based conversion tool influences the accuracy of back-calculation results for TSD data outside the utilized database. This method cannot back-calculate the viscoelastic characteristics of the pavement layer.
Velocity Model [96]	The 3D-Move determines the asphalt concrete's master curve and the unbound layer moduli through manual iteration matching computed and measured TSD deflection velocities.	The method accurately considers TSD loading and viscoelastic characterization of the asphalt layer. It can derive the entire asphalt master curve from TSD data.	The manual iteration and calculation time required in 3D-Move analysis limits its practical applicability in network-level pavement management systems.
Limited data Deflection Model [96]	A back-calculation Excel-based worksheet that was created that uses TSD computed deflections and linear elastic analysis modified to match the TSD loading configuration.	It is simple to use with limited quantity TSD data.	While using a limited amount of simplified data can expedite the analysis, it comes at the cost of accuracy. Also, the Excel-based analysis isn't suited for capturing real-world pavement responses under moving loads. Additionally, this method fails to capture the viscoelastic properties (i.e., how the material behaves under stress and strain over time) of the asphalt concrete (AC) layer.
Hysteretic Damping Model [97]	Using a hysteretic damping model to approximate asphalt rheology, the model employs measured TSD slopes to derive viscoelastic asphalt's layer characteristics.	The method considers viscoelastic characterization of the asphalt layer using a simplified approach.	it is quite challenging to forecast the whole asphalt master curve with this method. Instead, the technique calculates a constant value for the asphalt modulus corresponding to the TSD loading condition. In its current version, the back-calculation approach is too computationally costly for large-scale usage in typical PMS applications.
FEM [98]	The model employs measured TSD data (either deflection slopes or calculated deflections from the algorithm) to generate pavement layer moduli using the 2.5D FEM technique as forwarding analysis and an improved iteration process with CEKF.	The used model considers actual tire-pavement contact stress, modulus nonlinearity, and interface discontinuity.	The constitutive models of pavement materials in 2.5D FEM are elastic materials, which cannot account for the actual response of TSD moving load on a viscoelastic asphalt layer. The created tool is not yet ready for actual use in the field.

2.5 Pavement structure conclusion

The purpose of this bibliographic section is to conduct a foundational analysis of the current state of pavement mechanics. This includes identifying research gaps, critically evaluating the limitations of existing methods, and providing well-founded justifications for the chosen approaches.

The section began by exploring fundamental concepts such as pavement material composition, thermo-mechanical behavior, design mechanisms, and deterioration processes. The discussion then progressed to assess pavement bearing capacity through deflection measurement and interpretation. Traditional methods were evaluated, leading to a detailed examination of Traffic-Speed Deflection Devices (TSDDs), particularly the Traffic Speed Deflectometer (TSD). Operational considerations for TSDs and systematic bias elimination were also explored for reliable data collection.

A central theme revolved around back calculating layer moduli from TSD data. We presented and analyzed various methodologies, acknowledging their strengths and limitations. Despite this advancements, a critical research gap remains: while the backcalculation of pavement layer moduli from deflection measurements provides valuable data for mechanistic design and analysis, the outcomes often differ among analysts due to varying assumptions and inputs in each procedure. This variability raises concerns, as road authorities may lack confidence in using the backcalculated moduli for pavement evaluation or design without knowing the associated error size. To address this issue, there is a need for a more robust and generalizable approach.

Machine Learning (ML) emerges as a potential solution to address the shortcomings of existing methods. ML algorithms excel in learning complex patterns within datasets, offering the prospect of developing a generalized approach for E_i estimation from TSD data. By training on diverse datasets, ML models can adapt to various loading configurations and overcome the limitations of traditional techniques. The exploration of ML in the upcoming section as an alternative approach signifies an essential step towards bridging this research gap and advancing pavement mechanics. Future research endeavors should focus on harnessing the capabilities of ML to develop robust and versatile methodologies capable of enhancing the precision and efficiency of pavement E_i estimation from TSD data.

2.6 Machine Learning: Bibliographic analysis

2.6.1 Introduction

ML is an essential aspect of AI that mimics computers and can enhance task performance without explicit programming. By employing sophisticated algorithms and statistical models, machines can learn from data, adapt to new information, and make well-informed decisions. A notable characteristic of ML is its ability to automatically identify patterns and relationships within data, granting computers the capability to comprehend complex information and make accurate decisions independently. This paradigm shift from traditional rule-based programming to data-driven learning has brought about a profound transformation in various industries, rendering ML indispensable for tackling intricate problems and extracting valuable insights from vast datasets [99].
Given the growing demand for accurate performance predictions, integrating ML into pavement condition assessment offers numerous advantages. Notably, the robust learning algorithms empower the system to extract patterns and specific features within extensive datasets related to pavement conditions. Compared to traditional methods, ML models excel in terms of accuracy and computational efficiency performance. This is applicable even when dealing with vast datasets encompassing hundreds of thousands of kilometers of assessed roads. Furthermore, what truly sets ML models apart is their remarkable capacity for generalization, resulting in superior performance even when dealing with new and noisy data, surpassing the capabilities of conventional methods [100].
This section delves into a comprehensive review of cutting-edge research in the realm of applying various ML techniques to assess pavement conditions. It begins by examining the current state of data collection methods and technologies in this field, focusing on pavement condition indices and presenting the utilization of ML techniques in pavement monitoring and distress detection. The section also offers an in-depth discussion on evaluating and comparing these techniques. Finally, it provides a concise summary of the findings derived from this extensive review.

2.6.2 Machine Learning categories

ML encompasses several categorizations based on data labeling: supervised, unsupervised, and reinforcement learning. As depicted in Figure 2.11, each has its models. Supervised learning involves estimating an unknown mapping between known input and output samples, where the output is labeled, for tasks such as classification and regression. In contrast, unsupervised learning relies solely on input samples without labeled outputs and is used for clustering and probability density function estimation tasks. Semi-supervised learning combines aspects of both supervised and unsupervised learning, where some data

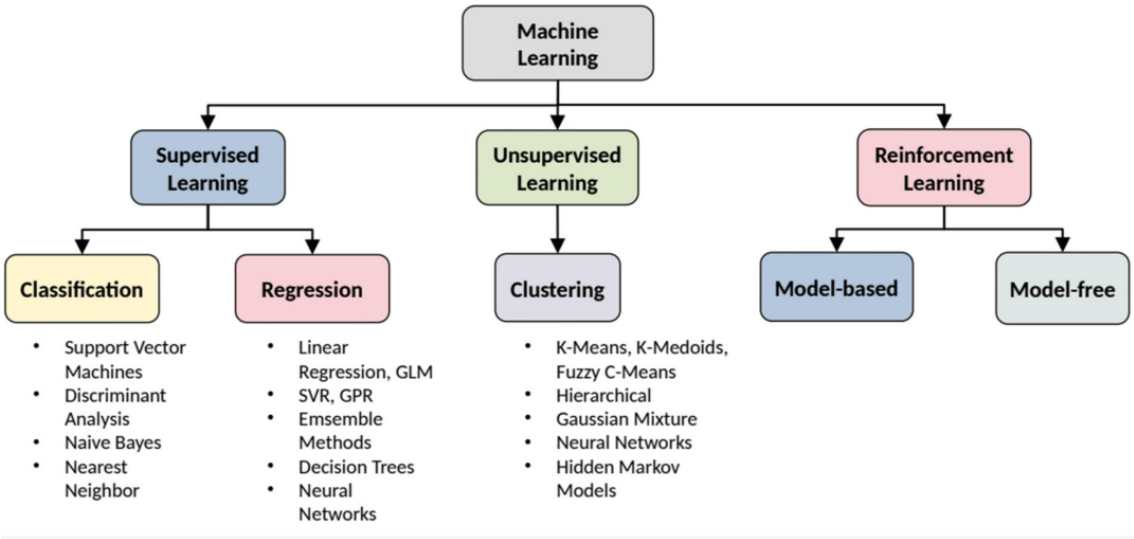

Figure 2.11 – Machine learning models [101].

is partially labeled, and the labeled portion is used to infer the unlabeled part [99, 100]. Reinforcement learning, distinct from supervised and unsupervised learning, operates within a dynamic environment. Its objective is to identify the optimal action sequence that maximizes long-term rewards. The agent or algorithm engages with and learns from the environment through exploration and interaction to formulate an effective policy. Reinforcement learning can be categorized into two primary groups: Model-based reinforcement learning and Model-free reinforcement learning [99].

However, due to the type of data and the required application, the preference for supervised machine learning models in estimating pavement elastic modulus E_i in this thesis is supported by key factors: Supervised learning relies on labeled training data, essential for accurate elastic modulus estimation E_i. This approach establishes correlations between input features (deflection slope) D_S and the target variable E_i. The strength of supervised ML lies in achieving high accuracy and precision, identifying subtle patterns in pavement E_i estimation. Also, historical measurement data enhances the model's ability to generalize predictions. While recognizing the merits of other learning methods, the specific demands and availability of labeled data make supervised learning the apt choice for this thesis. The upcoming section provides a broader context on applied supervised learning categories and algorithms.

2.6.3 Supervised Machine Learning

Supervised ML is a robust method where the algorithm learns from labeled data consisting of input features and corresponding output labels. The goal is to train the algorithm to make precise predictions for new, unseen data [101]. Supervised modeling can be divided

into two sub-areas: regression and classification. Regression models analyze relationships between variables to predict continuous outcomes, like forecasting maximum temperatures in weather prediction. On the other hand, classification assigns discrete class labels to observations as prediction outcomes [102]. In the research conducted by Sebastian Raschka [103], the critical steps involved in the supervised ML process are outlined, as also shown in the below flow chart in Figure 2.12. The stages from raw data collection to the final model selection and evaluation for regression and classification tasks are covered.

— Raw Data Collection: gather the dataset containing input features and their corresponding target labels for training the supervised learning model.
— Preprocessing: clean and prepare the data by handling missing values, dealing with outliers, and standardizing or normalizing the features to ensure consistent scaling.
— Feature Selection: identify the most relevant and informative features from the dataset, either manually or using automated techniques, to reduce dimensionality and improve model performance.
— Training and Testing: split the dataset into training and separate testing sets. Train the supervised learning algorithm on the training set to learn patterns and relationships between features and target labels. Test the model's performance on the testing set to evaluate its generalization ability.
— Performance Metrics: choose appropriate evaluation metrics based on the problem type (regression or classification) to measure the model's performance. For regression tasks, metrics like Mean Squared Error (MSE) or Root Mean Squared Error (RMSE) are commonly used, while for classification tasks, metrics like accuracy, precision, recall, and F1-score are used as seen in Table 2.6.
— Cross-Validation: employ cross-validation techniques (e.g., k-fold) to validate the model's performance on different subsets of the data. This helps to assess the model's ability to generalize to unseen data and reduces the risk of overfitting.
— Model Selection: select the appropriate supervised learning algorithm based on the nature of the problem (regression or classification). Standard algorithms include decision trees, random forests, support vector machines, and neural networks.
— Hyperparameter Optimization: Fine-tune the model by adjusting hyperparameters, such as learning rate, regularization strength, or the number of hidden layers, via techniques like grid or random search to find the optimal combination.
— Post-Processing Validation: Perform additional validation steps, such as analyzing model outputs and assessing any specific requirements of the problem domain, to ensure the model's results are meaningful and valuable.

These steps in supervised ML are designed to develop a robust model to make precise predictions/estimations [103].

Table 2.6 – Calculation of evaluation metrics

Metric	Formula	Description
Precision	$\frac{TP}{TP+FP}$	Proportion of correctly identified positive cases
Recall	$\frac{TP}{TP+FN}$	Proportion of actual positive cases identified correctly
DSC (F1 score)	$\frac{2\times TP}{2\times TP+FP+FN}$	Harmonic mean of precision and recall
IoU score	$\frac{TP}{TP+FP+FN}$	Measure of overlap between predicted and ground truth masks

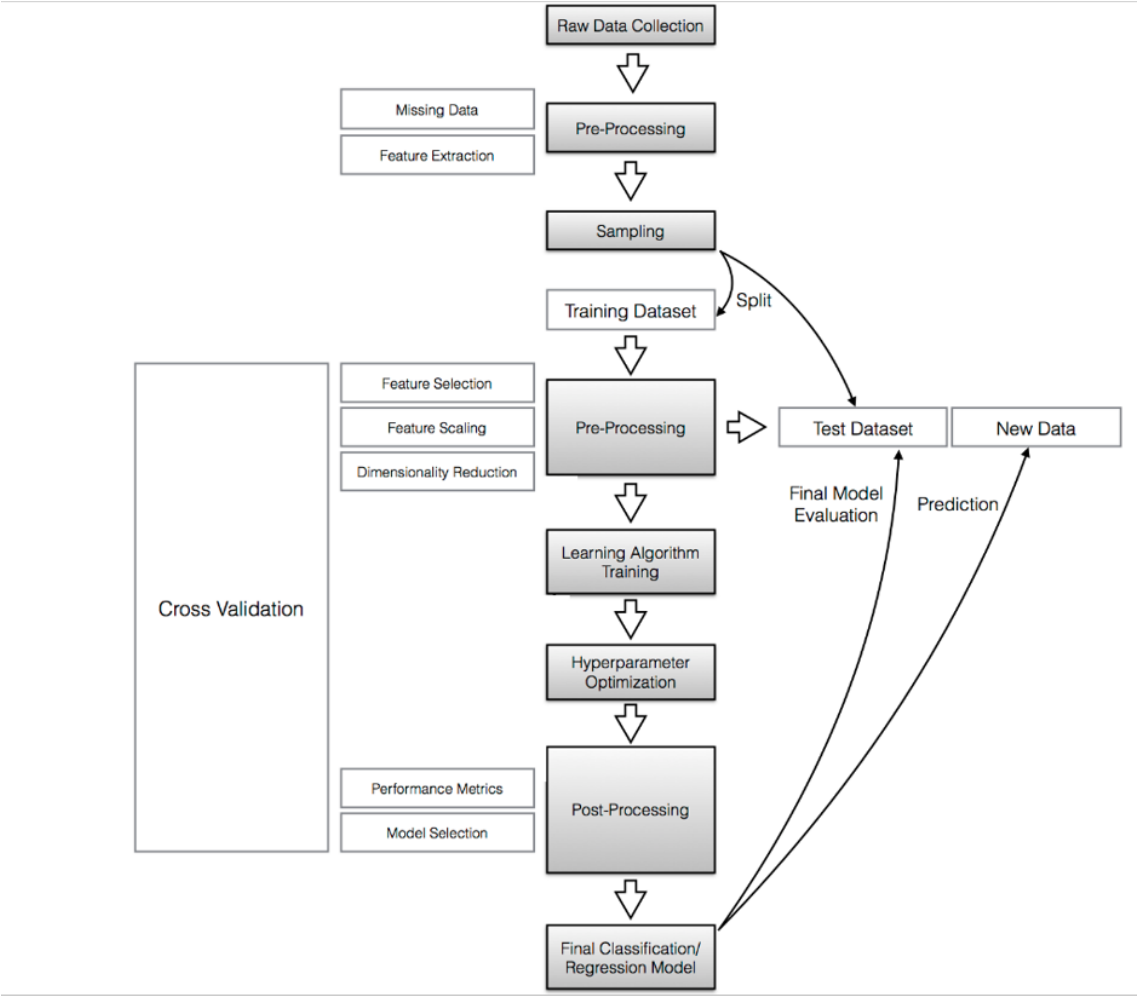

Figure 2.12 – Supervised learning workflow diagram [103].

2.7 Supervised ML models: Classification & Regression

Given the specific application of this research thesis and the inherent data structure, with input features acting as independent variables and output labels serving as dependent variables, the thesis primarily focuses on supervised machine learning. His choice is deliberate, as supervised learning aligns well with the nature of the problem encountered in this research. In this context, the main objectives of utilizing supervised machine learning involve predicting continuous values (regression) and categorizing data (classification). The following provides an overview of the introduced concepts and models [99, 104, 105, 106]:
As shown in Table 2.7 and Table 2.8, which summarize some of the supervised learning classification and regression algorithms by introducing their operational principles and optimal use cases. Factors such as data characteristics, interpretability, and the applicability of nonlinear data are considered.
Additionally, Table 2.9 concisely compares the trade-off characteristics of machine learning algorithms, delineating variations in prediction and training speeds, memory usage, and tuning requirements and providing a brief assessment of each algorithm's suitability for specific problem types. This reference is instrumental for practitioners aiming to balance computational considerations and algorithmic performance, aiding in selecting an appropriate model for their tasks.
It worth mentioning that, throughout this research, various supervised ML models underwent testing and cross-validation. While most provided approximate results, Support Vector Machine (SVM) has outperforming in both regression and classification.
This success can be attributed to its adeptness at learning from the data, facilitated by hyperparameter optimization. Also, SVM proves to be a versatile choice for both regression and classification tasks, aligning perfectly with the dual objectives of estimating and classifying pavement elastic modulus. Its adaptability across varying data sizes is commendable, making it particularly suitable for datasets with limited or noisy information [33, 34, 107]. Moreover, SVM's inherent capability to handle high-dimensional and nonlinearly separable data is pivotal, ensuring its efficacy in capturing the intricate patterns inherent in pavement characteristics. When compared to alternative algorithms like Random Forest (RF) and Artificial Neural Networks (ANN), SVM exhibits a slight performance advantage in this research dataset, as detailed in Chapters 4 and 5.
Consequently, it has been chosen as an exemplary model in this research. However, it's worth noting that alternative algorithms could potentially replace it, contingent upon the dataset's structure, type, and specific objectives. The overarching aim is to present a comprehensive methodology for utilizing supervised machine learning, irrespective of the chosen algorithms, recognizing their potential variance based on the dataset at hand.
To this end, the subsequent section will examine SVM theory.

Table 2.7 – Most common classical supervised learning classification algorithms [99, 104, 105, 106].

Algorithm	**How it Works**	**Best Used**
Logistic Regression	fits a model that can predict the probability of a binary response. Because of its simplicity, logistic regression is commonly used as a starting point for binary classification problems.	When a single, linear boundary can separate data.
K-nearest neighbor (kNN)	Categorizes objects based on the classes of their nearest neighbors in the data set. KNN predictions assume that objects near each other are similar. Distance metrics, such as Euclidean, city block, cosine, and Chebychev, are used to find the nearest neighbor.	When a simple algorithm to establish benchmark learning rules is required.
Support Vector Machine (SVM)	Classifies data by finding the decision boundary (hyperplane) that separates all data points of the class from those of the other classes. The best hyperplane has the largest margin between the two classes when the data is separable. A loss function penalizes points on the hyperplane's wrong side if the data is not linearly separable. SVMs sometimes use a kernel transform to transform nonlinearly separable data into higher dimensions where a linear decision boundary can be found.	For high-dimensional, nonlinearly separable data. A simple, easy-to-interpret, and accurate classifier is required.
Neural Networks	Inspired by the human brain, a neural network consists of highly connected networks of neurons that relate the inputs to the desired outputs. The network is trained by iteratively modifying the connections' strengths to map the given inputs to the correct response.	For modeling highly nonlinear systems, the goal is to update the model regularly.
Naïve Bayes	Assumes that the presence of a particular feature in a class is unrelated to the presence of any other feature. It classifies new data based on the highest probability of belonging to a particular class.	For a small data set, a classifier that is easy to interpret is needed.
Discriminant Analysis	Classifies data by finding linear combinations of features. The discriminant analysis assumes that different classes generate data based on Gaussian distributions. Training a discriminant analysis model involves finding the parameters for a Gaussian distribution for each class. The distribution parameters are used to calculate boundaries, which can be linear or quadratic functions. These boundaries are used to determine the class of new data.	When a simple model that is easy to interpret is needed, memory usage during training is a concern.
Decision Tree	Predicts responses to data by following the tree's decisions from the root (beginning) down to a leaf node. A tree consists of branching conditions where the value of a predictor is compared to a trained weight. The training process determines the number of branches and the weight values. Additional modification or pruning may be used to simplify the model.	When an algorithm that is easy to interpret and fast to fit is a requirement.
Ensemble Methods (Bagged and Boosted Trees)	Several "weaker" decision trees are combined into a "stronger" ensemble. A bagged decision tree consists of trees trained independently on data bootstrapped from the input data. Boosting involves creating a strong learner by iteratively adding "weak" learners and adjusting each weak learner's weight to focus on misclassified examples.	When predictors are categorical (discrete) or behave nonlinearly, the time needed to train a model is less of a concern.

Table 2.8 – Most common supervised learning regression algorithms [99, 104, 105, 106].

Regression Algorithm	**How it Works**	**Best Used**
Linear Regression	It is a statistical modeling technique used to describe a continuous response variable as a linear function of one or more predictor variables. Because linear regression models are simple to interpret and easy to train, they are often the first model to be fitted to a new data set.	When an algorithm that is easy to interpret and fast to fit is needed.
Nonlinear Regression	It is a statistical modeling technique that helps describe nonlinear relationships in data. Nonlinear regression models are generally assumed to be parametric, where the model is described as a nonlinear equation.	When data has strong nonlinear trends and cannot be easily transformed into a linear space.
Gaussian Process Regression Model	GPR models are nonparametric models that are used to predict the value of a continuous response variable. They are widely used in spatial analysis for interpolation in the presence of uncertainty. GPR is also referred to as Kriging.	For interpolating spatial data.
SVM Regression	Similar to SVM classification algorithms but modified to predict a continuous response. Instead of finding a hyperplane that separates data, SVM regression algorithms find a model that deviates from the measured data by a predefined value no greater than a small amount, with parameter values that are as small as possible (to minimize sensitivity to error).	For high-dimensional data (where there will be a large number of predictor variables).
Generalized Linear Models	It is a special case of nonlinear models that uses linear methods. It involves fitting a linear combination of the inputs to a nonlinear function (the link function) of the outputs.	When the response variables have nonnormal distributions, such as a response variable that is always expected to be positive.
Regression Trees	Similar to decision trees for classification, but modified to predict continuous responses.	When predictors are categorical (discrete) or behave nonlinearly.

Table 2.9 – Trade-off characteristics of some ML algorithms. [99, 104, 105, 106].

Type of Algorithm	**Prediction Speed**	**Training Speed**	**Memory Usage**	**Required Tuning**	**General Assessment**
Logistic Regression	Slow	Slow	Medium	Some	Suitable for many binary problems
Decision Trees	Fast	Fast	Small	Some	Good generalist but prone to overfitting
SVM	Fast	Fast	Medium	some	Suitable for many linear and nonlinear problems and handles high-dimensional data well
Nearest Neighbor	Moderate	Minimal	Medium	Minimal	Lower accuracy, but easy to use and interpret
Naïve Bayes	Fast	Fast	Medium	Some	Widely used for text, including spam filtering
Ensembles	Moderate	Slow	Varies	Some	High accuracy and good performance for small to medium-sized data sets
Neural Network	Moderate	Slow	Medium to Large	Lots	Popular for classification, compression, recognition, and forecasting

2.8 Support Vector Machine (SVM)

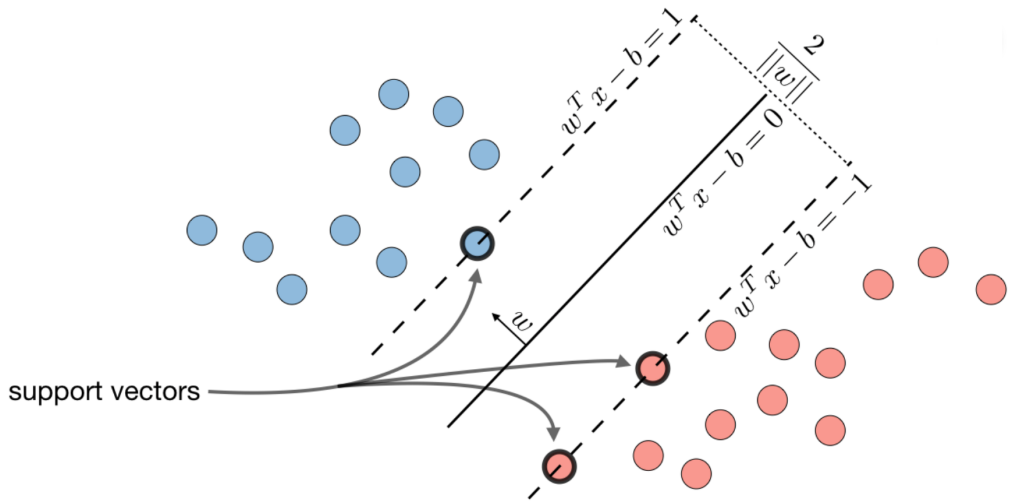

Figure 2.13 – Support Vector Machine (SVM) [106].

SVM is a popular ML method used for classification and regression. Vladimir Vapnik introduced it to solve pattern recognition problems [36]. It Uses support vectors, which are the data points closest to the decision boundary Figure 2.13. As detailed in the subsequent sections, SVM can effectively tackle regression and classification tasks by utilizing the Support Vector Classification (SVC) algorithm for classification and Support Vector Regression (SVR) for regression.

2.8.0.1 SVM for regression and classification

SVM can be used for regression and classification tasks. In classification, the goal is to find a hyperplane that best separates the input data into different classes. In regression, the goal is to find a hyperplane that best fits the data. In both cases, SVM achieves this by finding a decision boundary that maximizes the margin between the classes or best fits the data. The decision boundary is defined as a hyperplane in the feature space of the input data. The hyperplane is defined by a weight vector $\mathbf{w}$ and bias term b.
In a classification task, the decision boundary is given by [33, 34, 107]:

$$f(\mathbf{x}) = \text{sign}(\mathbf{w}^T\mathbf{x} + b) \tag{2.1}$$

Here, $\mathbf{x}$ is the input data, and the sign function returns either +1 or -1, depending on which side of the decision boundary $\mathbf{x}$ lies.
In a regression task, the hyperplane that best fits the data is given by:

$$f(\mathbf{x}) = \mathbf{w}^T\mathbf{x} + b \tag{2.2}$$

Here, $\mathbf{x}$ is the input data, and the predicted output is a continuous value.
In both cases, the SVM algorithm finds the optimal values for $\mathbf{w}$ and b by solving the optimization problem. The optimization problem for classification is expressed as:

$$\text{minimize} \quad \frac{1}{2}||\mathbf{w}||^2 \text{ subject to} \qquad y_i(\mathbf{w}^T\mathbf{x}_i + b) \geq 1 - \xi_i, \quad \xi_i \geq 0$$

where y_i is the class label of the i-th training example, $\mathbf{x}_i$ is the corresponding feature vector, and ξ_i is a slack variable that allows for some misclassifications.
The optimization problem for regression is similar, but the constraints are different:

$$\text{minimize} \quad \frac{1}{2}||\mathbf{w}||^2 \text{ subject to} \qquad |y_i - (\mathbf{w}^T\mathbf{x}_i + b)| \leq \epsilon$$

where y_i is the target output value for the i-th training example, $\mathbf{x}_i$ is the corresponding feature vector, and ϵ is a margin parameter that controls the width of the ϵ-insensitive tube.

2.8.0.2 SVM Hyperparameters Tuning

SVM has several hyperparameters that can be tuned to optimize performance. The two most essential hyperparameters are the regularization and kernel parameters C & γ, respectively.
C is the regularization parameter that controls the trade-off between maximizing the margin and minimizing the classification or regression error. A more considerable value of C results in a narrower margin and better fitting to the training data.
γ is the kernel parameter that controls the shape of the decision boundary. The kernel function maps the input data to a high-dimensional feature space. The most commonly used kernel functions are the linear kernel, polynomial kernel, Radial Basis Function (RBF) kernel and sigmoid kernel.
RBF kernel is a mathematical technique used to approximate a non-linear function called the Gaussian kernel. It is defined as [37, 106, 35]:

$$K(\mathbf{x}_i, \mathbf{x}_j) = \exp(-\gamma||\mathbf{x}_i - \mathbf{x}_j||^2) \tag{2.3}$$

Here, the parameter γ is a positive scalar that determines the scale of the kernel function. RBF works by transforming the input vectors $\mathbf{x}_i$ into a multi-dimensional space represented by F (the z-space) through a mapping function $\Phi : X \to F$. The equation then defines the final approximation function:

$$f(\mathbf{x}) = \sum_{i=1}^{l} (\alpha_i^* - \alpha_i) K(\mathbf{x}_i, \mathbf{x}_j) \tag{2.4}$$

where K is the kernel function and $\mathbf{x}_i$ and $\mathbf{x}_j$ are the input feature vectors. The function combines the kernel function with the inner product of two input vectors to produce an output that approximates the non-linear function Figure 2.14.
The RBF kernel maps the input data into a high-dimensional feature space, where the decision boundary is non-linear. The feature space has infinite dimensions, making it possible to separate the input data that is not linearly separable in the original input space. The RBF kernel has a local nature, which means it assigns higher weights to the data points close to the decision boundary.

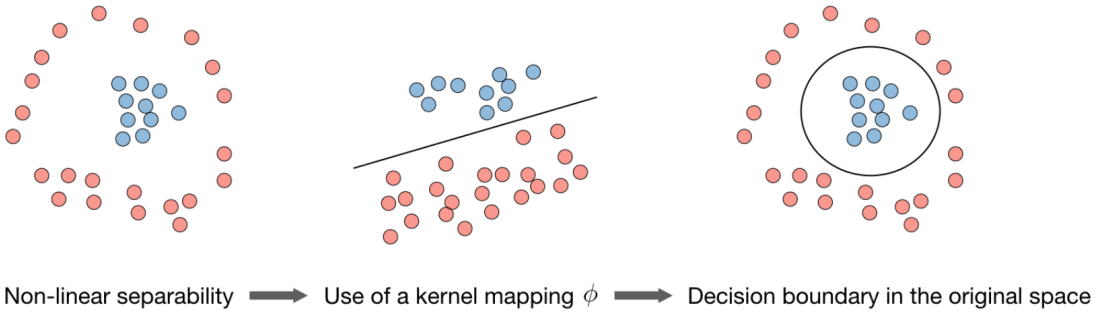

Figure 2.14 – Mechanism of the RBF Gaussian Kernel [106].

2.8.0.3 The optimization problem for SVM

The optimization problem for SVM with soft margin and slack variables is given by [108, 109]:

$$\min_{\mathbf{w},\boldsymbol{\xi},\boldsymbol{\xi}^*} \quad \frac{1}{2}\|\mathbf{w}\|^2 + C\sum_{i=1}^{n}(\xi_i + \xi_i^*) \tag{2.5}$$

$$\begin{aligned} \text{subject to} \quad & y_i - f(\mathbf{x}_i, \mathbf{w}) \leq \epsilon + \xi_i \\ & f(\mathbf{x}_i, \mathbf{w}) - y_i \leq \epsilon + \xi_i' \\ & \xi_i, \xi_i' \geq 0 \quad \text{for all } i \end{aligned}$$

Where ξ_i and ξ_i' are slack variables that allow for errors within and outside the margin, respectively. The performance of the regression model is evaluated based on the approximation error, which tolerates errors within the ϵ-insensitivity zone, and the linear loss function can be introduced to penalize errors outside the ϵ-insensitivity zone Figure 2.15. Overall, SVM offers a powerful tool for supervised learning tasks, providing efficient and accurate classifications and regression based on the learned patterns and data [36].

To this end, This research adopts Support Vector Machines (SVM) for estimating pavement elastic modulus due to SVM's suitability for both regression and classification tasks, robust performance across various data sizes, adept handling of high-dimensional and nonlinearly separable data. However, It's important to recognize that alternative algorithms may have the potential to substitute it, depending on the dataset's structure, type, and specific goals. The main objective is to provide a methodology for employing supervised machine learning, regardless of the algorithms selected, while acknowledging their potential differences based on the dataset used. The forthcoming section will explore several instances of machine learning applied to structural health monitoring (SHM).

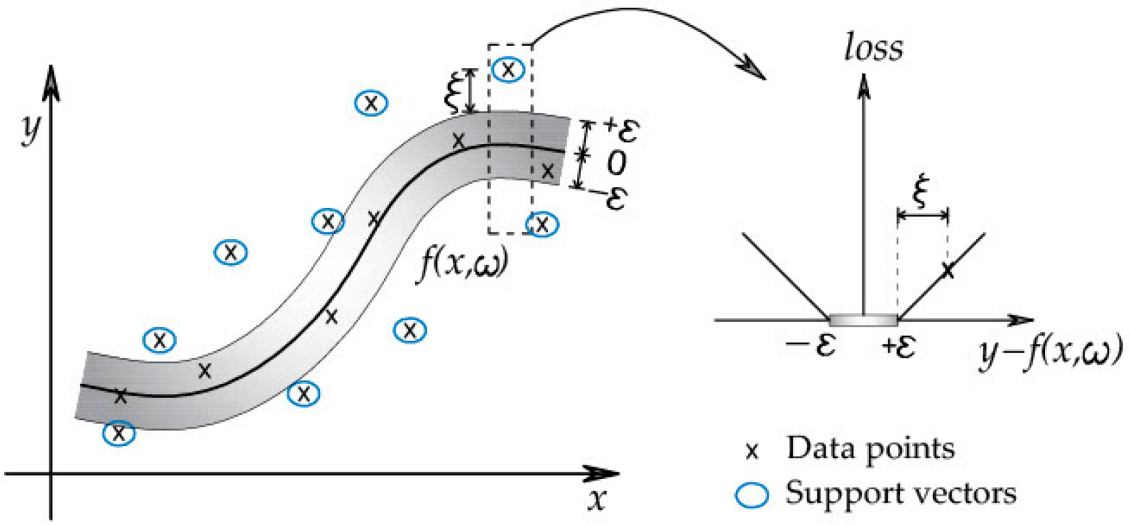

Figure 2.15 – The errors within and outside the margin for nonlinear SVM [109].

2.9 ML application in SHM

Machine Learning (ML) is rapidly transforming how we monitor and assess the health of critical infrastructure like pavements. This review section has highlighted the versatility and effectiveness of ML techniques in addressing various challenges within Pavement Structure Health Monitoring (SHM). However, the applications of ML extend far beyond this specific domain.
In the domain of Pavement Structure Health Monitoring (SHM), the application of machine learning (ML) methods has become indispensable, addressing various challenges [25]. The selection of ML algorithms depends on problem complexity, data size, computational resources, and model intricacy [110].

Table 2.10 – Examples of ML application in SHM

Algorithm	Application	Reference
SVMs	Pavement distress and cracks detection,	[34]
ANN	Detecting potholes	[111]
RF	Distress categorization	[112]
SVM, ANN, and RF	Estimating Pavement Condition Index (PCI)	[113]
CNNs	Image Classification, crack classification	[114]
CNN-CDM	Crack detection	[115]
CNNs	Multi-class: Pavement defect analysis	[116, 117]
YOLO, Faster R-CNN	Real-time crack and pothole detection	[118, 119]
ResNet-based U-Net	Semantic segmentation, crack segmentation	[120, 121]
DeepCrack, PCSN	Semantic segmentation	[122]

As depicted in Table 2.10, classical ML models, such as Support Vector Machines (SVMs) [34], have extensive applications in pavement distress detection. SVMs excel in recognizing intricate patterns, making them suitable for tasks like identifying pavement cracks through meticulous image analysis and pattern recognition. Their versatility is evident in studies detecting multiple distress types [35].
Another well-known model in this domain is Artificial Neural Networks (ANN) [111]. ANN introduces sophistication, particularly when combined with SVMs. In a notable application, the collaboration of ANN with SVM (ANN-SVM) proved effective in detecting potholes [107]. This approach enhances distress identification complexity, allowing for effective handling of intricate tasks.
Additionally, Random Forests (RF) [112] excel in estimating the probability of pixels belonging to specific distress categories [123]. For instance, the "CrackForest" model, built by [124], leverages Random Structured Forests (RSF) for enhanced overall accuracy.
Furthermore, for pavement condition assessment involving various defects and data sources, a combination of SVM, ANN, and RF is often employed. This collaborative approach is deployed to estimate the Pavement Condition Index (PCI) while considering an array of pavement defects or analyzing Unmanned Aerial Vehicle (UAV) images [113]. This methodology underscores the adaptability and resilience of classical ML models when dealing with complex assessment tasks.
In the context of computer vision; the choice between classical Machine Learning (ML) models and Deep Learning (DL) models (specifically Artificial Neural Network-based ones) is often guided by experimentation and empirical application. Additionally, in certain scenarios, a hybrid approach combining DL for feature extraction and ML for further analysis proves advantageous [125]. This collaboration between techniques could enhance the accuracy and efficiency of pavement management practices, particularly in applications such as Image Classification [126], Object Detection [127], and Semantic Segmentation [128].
For instance, in binary classification, researchers have utilized Convolutional Neural Networks (CNNs) to classify images captured by smartphones as containing cracks or being crack-free, as demonstrated in [114]. Similarly, studies such as [115] have developed crack detection models based on CNN-CDM (Color Image Demosaicking), showcasing improved accuracy. Additionally, pre-trained models are utilized in binary classification scenarios, yielding promising results.
Moreover, In multi-class classification scenarios, CNNs have been employed for practical pavement defect analysis, as seen in studies like [116, 117]. These studies compare various models and highlight the effectiveness of certain lightweight CNN architectures.
Furthermore, object detection models such as YOLO (You Only Look Once) and Faster R-CNN have a recognized contribution in real-time crack and pothole detection [118, 119].

These models integrate region proposal algorithms for pre-processing and achieve enhanced accuracy in identifying distresses on pavements.
Additionally, in semantic segmentation, CrackU-net [120], ResNet-based U-Net [121], and innovative approaches like combining U-Net with YOLO [129] are employed. These methods demonstrate superior performance in accurately segmenting various crack types and determining severity, contributing to the development of new pavement indices like PASER [129].
Other segmentation models, such as DeepCrack and PCSN, showcase the continual exploration of novel architectures for improved semantic segmentation [122].
To this end, this section provides an overview of the transformative role of ML in Pavement Structure Health Monitoring (SHM). ML techniques have been instrumental in addressing various challenges encountered in pavement distress detection, classification, and overall condition assessment.
A takeaway from the review of Machine Learning (ML) applications highlights a versatile toolkit for various infrastructure health monitoring tasks. From detecting anomalies in bridges and buildings to predicting maintenance needs in pipelines and power grids, ML algorithms excel at analyzing large amounts of sensor data. They can extract subtle patterns and proactively identify potential problems before they escalate [100, 99, 25, 118, 119].
Looking towards the future, the rapid advancement of ML holds immense promise for even more groundbreaking applications in infrastructure health monitoring. These advancements have the potential to revolutionize infrastructure management practices. By proactively monitoring and safeguarding infrastructure assets, ML could reduce maintenance costs, enhance safety protocols, and extend the lifespan of the built environment. This translates to a more sustainable and reliable infrastructure system overall.

2.10 Machine Learning (ML) conclusion

The backcalculation of pavement layer moduli from deflection measurements has become a focal point in recent pavement mechanics research, particularly with the emergence of nondestructive testing devices like the Traffic Speed Deflectometer (TSD). Various pavement structural models and computerized procedures have been developed to aid the TSD backcalculation process. However, outcomes often vary among methods due to differences in underlying assumptions, raising concerns for road authorities regarding the confidence in utilizing TSD backcalculated moduli. There is a pressing need for a more robust and generalizable approach, such as Machine learning (ML), to address this issue.
ML models exhibit remarkable generalization capabilities, and their Integrating into pavement condition assessment offers significant advantages in accurate performance predic-

tions.
ML's robust learning algorithms excel in extracting patterns and specific features from extensive pavement condition datasets, outperforming traditional methods in accuracy and computational efficiency, even with vast datasets covering extensive road networks.
However, the success of ML in infrastructure health monitoring depends on several factors, including the choice of algorithm, data characteristics, and desired outcomes. In this research, supervised machine learning was chosen due to its suitability for having label data aligned with the specific application context and data structure.
While various supervised ML models were tested, and Support Vector Machine (SVM) has been selected as an example supervised model, as it demonstrated a slight superior performance in regression and classification tasks, and exhibiting adaptability across the specific data sizes and types within this reserch.
However, it's essential to acknowledge that alternative algorithms such as (ANN, RF,...) could potentially replace SVM based on dataset characteristics and research objectives. The overarching aim remains to present a methodology for utilizing supervised machine learning, recognizing potential variances based on specific datasets regardless of the used model.
Overall, as discussed at the end of the section, ML presents a powerful toolkit for infrastructure health monitoring, enabling proactive analysis of vast datasets, identification of subtle patterns, and prediction of potential issues, ultimately improving infrastructure management and enhancing safety while extending asset lifespans. The upcoming section will delve into various instances where machine learning is applied to structural health monitoring, expanding the scope of ML's impact beyond pavements and broader infrastructure domains. The upcoming chapter aims to establish a robust numerical TSD forward model and a synthetic database with a novel approach that directly employs deflection slope (D_S) to estimate M_R.

Chapter 3

Forward Model: Numerical Validation

3.1 Introduction

The Subgrade Resilient Modulus M_R, commonly known as the soil layer E_4, is a critical parameter that indicates the stiffness of soil or aggregate materials for the foundation of pavement systems. Evaluating the overall bearing capacity of the structure [130].
Despite the advancements in backcalculation models utilizing new deflection measurement technologies, particularly TSD data, a critical research gap still there [11, 131].
To contribute in addressing this gap, this research thesis introduces an innovative inverse model aimed at accurately estimating M_R by leveraging TSD data through ML Models.
However, the particular objective of this section is to establish a forward model that forms the foundation for implementing this inverse model for accurately estimating M_R [132]. It adopts the Burmister elastic linear isotropic approach with infinite in-plane layers as the analytical model [71].
The forward model developed in this section facilitates the creation of a controlled synthetic database via simulating the TSD deflection slope D_S instead of the deflection, eliminating the need for numerical integration to obtain TSD deflection [133].
The methodology applied in this chapter is illustrated in the framework diagram Figure 3.1. The effective development of this forward model requires two predefined fundamental groups of parameters: TSD load configuration and pavement structure properties per layer. These parameters serve as inputs for Alizé software to simulate pavement deflection behavior under TSD. This study has considered various physical hypotheses and parameters influencing measurements, explicitly focusing on the impact of factors such as measurement noise. The simulation, in turn, serves as the foundation for the creation of a structured and controlled database comprising two critical sets of parameters: D_S, functioning as the independent variable, and M_R values, serving as the dependent variable or label, as illustrated in Figure 3.1.

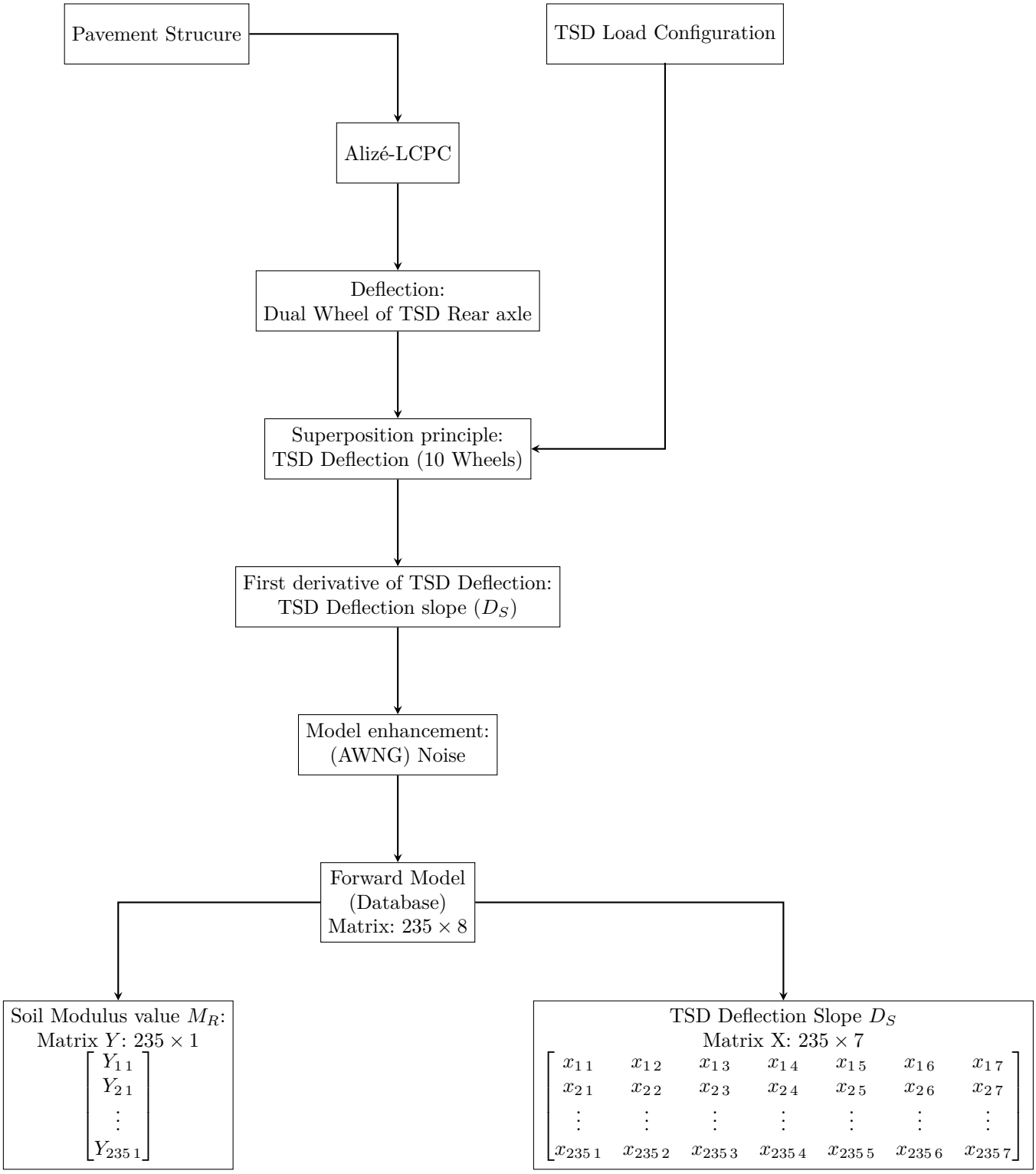

Figure 3.1 – Numerical forward model framework

3.2 The significance of (D_S) and (M_R)

The forward model employed in this research is based on two main parameters: deflection slope (D_S) and subgrade resilient modulus (M_R). The choice of these parameters is grounded for the reasons discussed below:

1. Deflection slope (D_S): The selection of deflection slope (D_S) in this forward model is a response to various challenges inherent in the computation of TSD deflection. These challenges primarily arise from the complexities associated with the TSD deflection calculation process, which involves integrating the deflection velocity. The choice of the integration method highly influences the outcome of this integration [20]. Additionally, the conventional approach to TSD deflection calculation introduces hypotheses to simplify the calibration and computation processes. However, these assumptions impact the final assessment of pavement bearing capacity [91]. In light of these challenges, this thesis advocates for an alternative methodology. Instead of relying on conventional deflection, the thesis proposes directly utilizing the TSD deflection slope (D_S) to estimate pavement elastic modulus. This methodological shift is designed to address and mitigate the inherent uncertainties associated with deflection calculations.

2. Significance of Soil Elastic Modulus (M_R) Estimation: As delineated in the literature, the French design method is an approach to the design of pavements. It encompasses three critical input parameters: subgrade bearing capacity, pavement materials, and traffic [29, 30]. Subgrade bearing capacity, quantified by its modulus value M_R. Estimating soil M_R is indispensable as it characterizes subgrade soil stiffness and resilience. M_R reveals how soil reacts to loads and distributes stresses, directly impacting pavement support and preventing deformation or failure [61, 132].
   Based on the argument presented above, the thesis places a priority emphasis on the estimation of the subgrade resilient modulus (M_R). To this end, the forthcoming section will discuss the principle hypotheses, parameters, and models used to construct the forward model database via Alizé software.
   The following section will delve into a detailed examination of the primary parameters essential for developing a numerical forward model to analyze pavement deflection behavior under TSD.

3.3 Numerical forward model construction

This section discusses developing a numerical forward model for analyzing pavement deflection behavior under TSD.
The construction of a synthetic database utilizing this forward model necessitates the predefined specification of two primary parameters: the pavement structure and the TSD load configuration. The characteristics of the predefined pavement structure are presented in Table 3.1.
Firstly, the case under investigation is derived from The French Catalogue of Structure, which provides a structured framework for defining and characterizing pavement structures based on factors such as traffic class and platform bearing capacity. Secondly, the forward model is based on the Burmister multi-layer Elastic pavement model, implemented in Alizé software. This model considers pavements as layered systems with homogeneous, isotropic, linear elastic layers. It uses a 2D asymmetric model to simulate loads applied over a circular area, applying the superposition principle for multiple wheel loads. Additionally, temperature corrections are implemented to simplify the calculation process from the influence of temperature on pavement behavior, especially in bituminous materials. Furthermore, the interface between pavement layers is categorized as fully bonded, allowing the model to quantify the impact of the interface on the deflection basin. Lastly, material fatigue is considered in the model, characterized by the gradual deterioration of soil resilience due to repeated loading and stresses. This phenomenon influences the long-term performance of pavement structures and is simulated using a progressive soil fatigue value [29, 30, 71, 134].

Table 3.1 – Characteristics of the pavement structure used to derive the forward model

Layer (i)	Thickness (m)	Material	E_i (MPa)	ν	Interface	°C
1	0.06	HMA	7000	0.35	(1) bound	15
2	0.09	BC-g2	9300	0.35	(1) bonded	15
3	0.09	BC-g2	9300	0.35	(1) bonded	15
4	∞	M_R	**16-250**	**0.35**	(1) **bonded**	**15**

In scientific terminology from [134], HMA denotes a Hot Mix Asphalt. Similarly,

$BC-g2$ represents grade 2 aggregate bituminous concrete, while M_R refers to soil subgrade Modulus.
Table 3.1 shows that M_R exhibits a variable modulus ranging from 16 to 250 MPa, implying gradual soil quality range. Layers 2 and 3, composed of 'BC-g2' materials, share similar characteristics in terms of thickness, modulus, Poisson's ratio, and bonding conditions, highlighting consistency that contributes to the overall integrity of the pavement structure. All layers interfaces are categorized as 'bonded,' emphasizing their interconnections and role as a composite structure, and temperature is corrected to 15 (°C) for all bituminous layers for calculation simplicity.
After introducing the first part of the forward model, the discussion now shifts to the upcoming part of the TSD load configuration for the Synthetic Database: Model, Process, and Analysis.

3.4 Synthetic Database: Model, Process and Analysis

In this section, a synthetic database will be constructed, serving as the central input data frame for soil modulus estimation in Chapter IV. To efficiently achieve and validate this objective, a structured approach involving three major steps will be undertaken.
The first step, the modeling phase, involves simulating pavement mechanical behavior under TSD using predefined parameters input into Alizé. Next, the data processing phase includes introducing additive noise to replicate real-world measurement noise and analyzing its effects on the data. Finally, the analysis phase involves physical and statistical analysis of two critical parameters within the final database: M_R (dependent variable) and D_S (independent variable). These analyses are pivotal for constructing the numerical forward model, which is essential in the estimation process in Chapter IV.

3.4.1 Modeling phase: Pavement's mechanical behavior under TSD

To simulate the pavement behavior under the TSD system, a load superposition principle simulation was applied [135]. The use of the superposition principle is justified as it aligns with the deflection behavior hypothesis assumed in this study, which is Burmister's elastic linear isotropic approach [71]. In principle, the TSD system consists of ten wheels as illustrated in Figure (3.2 a), therefore, the simulation involves summing (super-positioning) the deflection under each TSD wheel to calculate the deflection under the entire TSD instead of the rear axle. as the results in Figure 3.2 b shows that focusing solely on the rear axle load in TSD deflection measurement while neglecting other loads would lead to an underestimation of the deflection velocity measurement. Therefore, adopting the approach of summing the deflection from each TSD wheel (superposition)

yields more accurate results.
Furthermore; it is worth noting that the simulation of D_S is carried out at average 1 cm intervals for each 4m offset, as referred to in Figure 3.2 b. This measurement averaging hypothesis is based on the findings of [45, 28] to mainly balance between the accuracy and the bias as longer intervals may miss structural variations.
Once the deflection behavior of the entire TSD is simulated as shown in Figure (3.2 b), D_S is then calculated by taking the first-order partial derivative of the superpositioned deflection. D_S curves are shown in Figure (3.2 b) where TSD load configuration and coordinates have to be defined as discussed in Chapter II along with the position of seven laser Doppler sensors Sn_1 to Sn_7 relative to the TSD wheel loads.
For TSD deflection calculation, AUTC methods rely on fitting D_S curves and integrating them to determine the absolute deflection profile. However, to simplify the calibration and calculation process of TSD, a value of zero was artificially assigned to the loading center and reference sensor position Sn_8 (as depicted in Figure (3.2 b)). This hypothesis's impact on TSD measurement uncertainty caused by Sn_8 is illustrated in Figure (3.2 b), where the difference between the green curve ($Sn_8 = 0$) and black curves ($Sn_8 \neq 0$) is evident. Therefore, assuming zero deflection velocity measurement at the loading point and the reference sensor introduces uncertainty in TSD measurements, requiring careful consideration for accurate interpretation.

3.4.2 TSD repeatability analysis

Repeatability, an indispensable process of any NDT method, including TSDs, refers to the consistency of measurements obtained under identical test conditions.
The primary objective of this part is to analyze the repeatability across a range of deflection measurement levels and their corresponding standard deviations. This analysis aims to investigate the level of the standard error associated with measurements to define a minimum signal-to-noise ratio that establishes a noise threshold. This will allow for the analysis of the impact of this minimum noise level on measurement and estimation accuracy while developing the forward and inverse models.
As shown in Figure 3.3 about the standard error of deflection for the TSD, the analysis employs repeated measurements from the US, UK, and Australia, in addition to tests conducted in Greenwood's laboratory [23, 28, 31, 45, 91, 136].
Greenwood's laser Doppler velocimeter exhibits a minimum noise level of 5.5 µm, which remains constant regardless of the measurement level.
The results indicate average standard errors ranging from 20 to 38 µm, suggesting that repeatability tests provide a reliable means for estimating standard errors. Furthermore, the study supports Flentch's [45] observation that the standard error scales inversely with

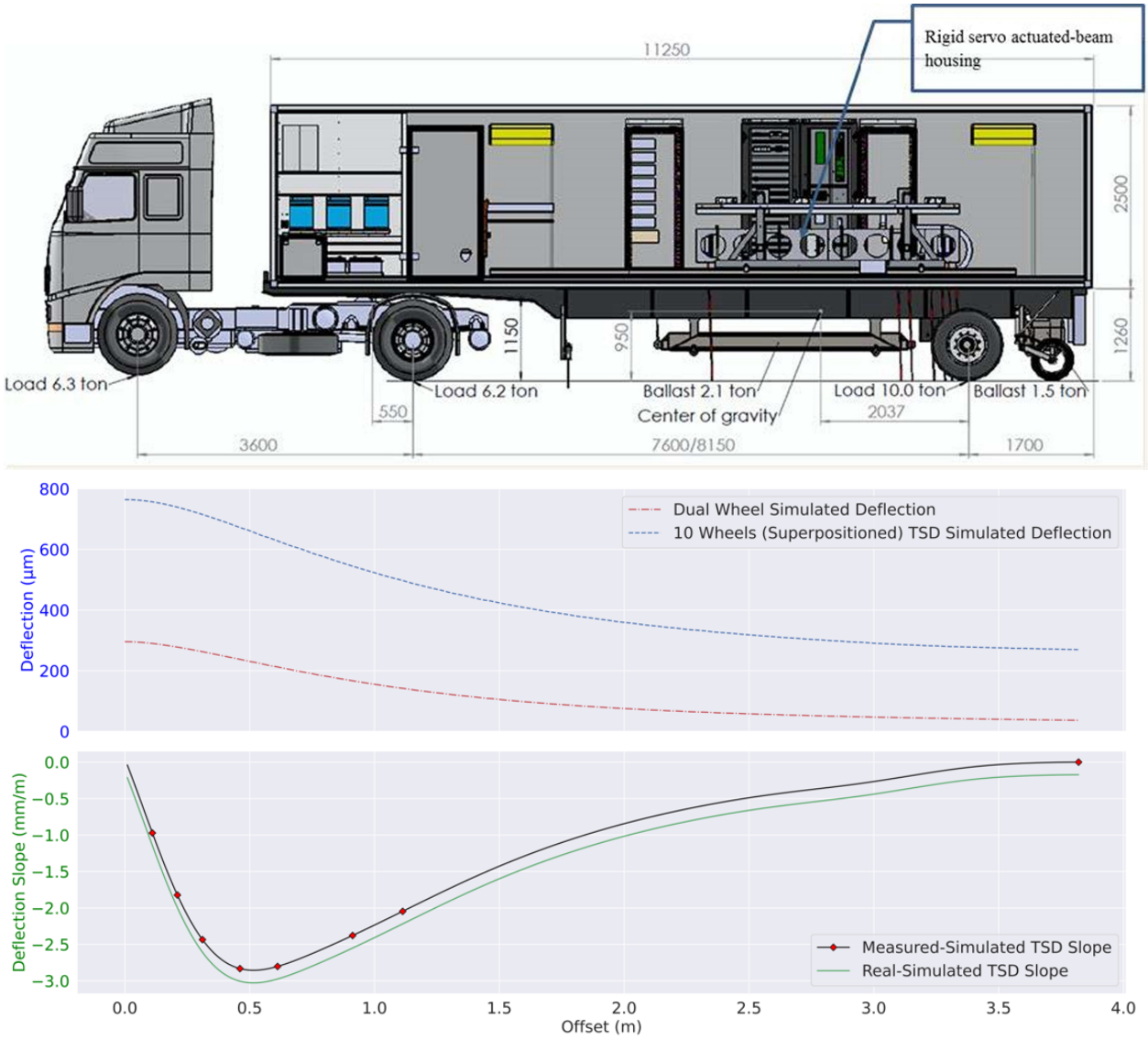

Figure 3.2 – TSD Numerical Model: a) Top: TSD load configuration [20] and b) Down: Numerical simulation of the pavement mechanical behavior under the TSD.

the square root of the number of averaged measurements. Measurements averaged over 1 meter had a standard error approximately three times larger. In contrast, those averaged over 100 meters had a standard error three times smaller (Following the statistical principle where, as measurements are averaged, the standard deviation decreases proportionally to the square root of the number of measurements being averaged).
However, this research utilizes Greenwood's reported repeatability level as a reference point. Greenwood's data is a benchmark for the minimum measurable noise level and its influence on modulus value estimation. The goal is to establish the impact of increasing measurement error on the signal-to-noise ratio (SNR) in (dB).

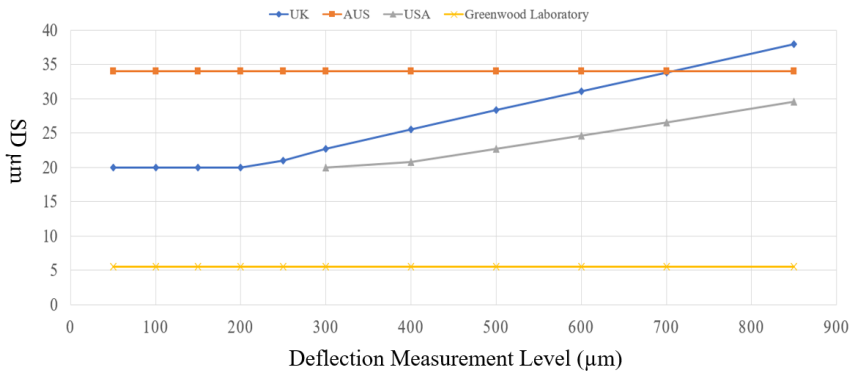

Figure 3.3 – TSD repeatability test analysis

The SNR (dB) is determined by the equation:

$$\text{SNR} = 10\log_{10}(\text{SD})^2 \tag{3.1}$$

where SD represents the standard deviation, typically measured in micrometers (µm). Given Greenwood's laser Doppler velocimeter has a minimum noise level of 5.5 µm, we can compute the SNR as follows:

$$20 \cdot \log_{10}(5.5) \approx 20 \cdot 0.740 \approx 14.80 \approx 15\ dB$$

This analysis provides valuable insights into the baseline noise level present within the sensor measurements. Based on this, the impact of noise can be effectively simulated using Additive White Gaussian Noise (AWGN) signals, a critical aspect to be explored further in the subsequent section.

3.4.3 Processing phase: Additive noise effect

The processing phase of the numerical TSD forward model employed in this research incorporates the introduction of noise as a vital component.
Specifically, Additive White Gaussian Noise (AWGN) has been injected into the simulated TSD pavement deflection behavior to [23, 137]:

1. Realistic representation: The inclusion of noise aligns the numerical model with real-world scenarios' complex and dynamic nature, providing a more accurate representation of TSD measurement conditions.

2. ML Robustness assessment: The deliberate introduction of AWGN allows for an evaluation of the ML method's robustness. This assessment considers the impact of noise on the accuracy and reliability of ML-based estimations.

3. Enhanced understanding: The incorporation of noise contributes to a deeper under-

standing of how the numerical model performs in the presence of external factors, offering insights into its behavior under varying conditions.
To fulfill the above objectives, an AWGN with a Signal-to-Noise Ratio (SNR) of 15 dB was introduced to modulate with TSD simulated measurements during this Processing and Optimization phase. The choice of the noise rate is based on the TSD as mentioned earlier bibliographic repeatability analysis.
The generic representation of AWGN as a signal, and the injection mechanism is given by [138]:

$$r(x) = s(x) + w(x) \tag{3.2}$$

r(x) represents the noised TSD signal with the addition of the deflection slope TSD signal $s(x)$ and the Additive White Gaussian Noise (AWGN) $w(x)$. This noise follows a Gaussian distribution and is characterized by having a mean (average) value of zero and a constant variance. Mathematically, it is expressed as

$$w(x) \sim \mathcal{N}(0, \sigma^2)$$

Where $\mathcal{N}(0, \sigma^2)$ represents the probability density function (PDF) for Gaussian distribution with a mean (μ) of zero and a standard deviation (σ) determining the spread of the distribution.
Thus, as data prepossessing and optimization step. Subsequently, Figure 3.4 illustrates the impact of this noise on three distinct classes, showcasing both noiseless and noised scenarios. These classes correspond to different deflection slope D_S (100, 150, and 200) MPa, each aligned with corresponding subgrade resilient modulus M_R values and positions spanning from Sn_1 to Sn_7. Following the introduction of noise, the forward model has acquired quasi-realistic attributes for the estimation process. Consequently, the results regarding the influence of this noise on the ML model for the modulus estimation will be detailed in Chapter IV of this study.
The upcoming subsection represents the exploratory data analysis of the two components of the forward model, aiming for a statistical interpretation and investigation of physical phenomena.

3.4.4 Analysis Phase: Exploratory Data Analysis (EDA)

This section encompasses an Analysis Phase focusing on Exploratory Data Analysis (EDA). EDA offers several benefits to the simulated TSD numerical forward model database, including understanding dataset characteristics, assessing data quality, identifying inherent patterns, and selecting relevant features. It serves as a fundamental initial step in the data analysis process [139].

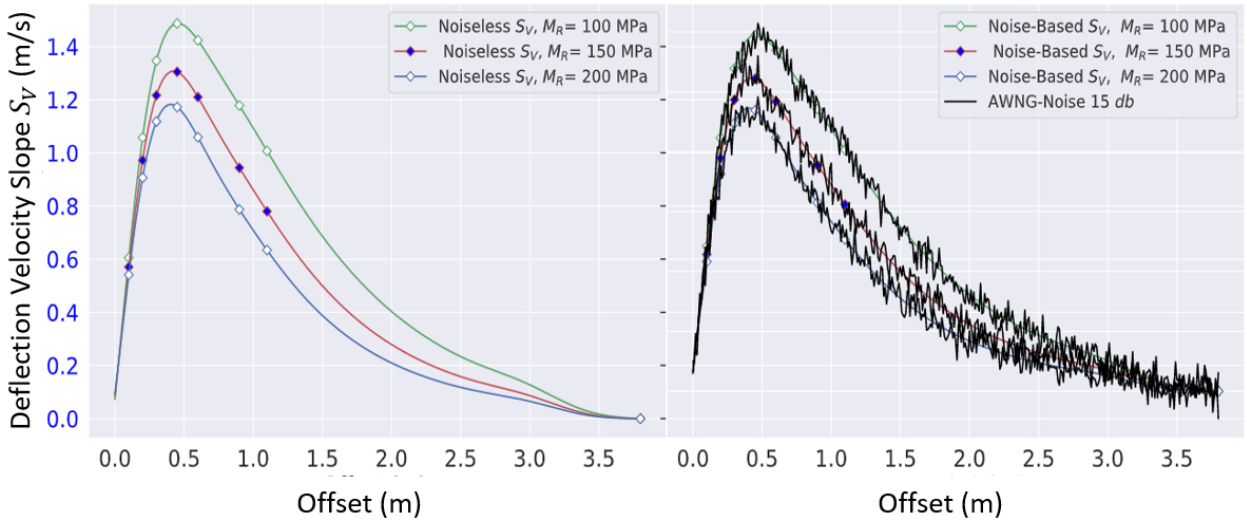

Figure 3.4 – Percentage distribution of M_R classes

In the upcoming subsections, a statistical and physical analysis of the database elements will occur. The dependent variable (referred to as the "label"), M_R data, will be investigated alongside the independent variable D_S (referred to as the "feature") obtained from seven TSD Laser Doppler sensors denoted as $S1$ to $S7$. This analysis will lay the groundwork for subsequent estimation procedures via ML in Chapter IV.

3.4.4.1 Analysis phase: Soil M_R data analysis

Table 3.2 – Classification of soil M_R

M_R Value (MPa)	(16 - 49)	(50 - 79)	(80 - 119)	(120 - 199)	(200 - 250)
Instances per Class	35	30	40	80	50

— The database used in this forward model contains 235 instances, as depicted in Table 3.2 and Figure 3.5. Each instance represents a unique scenario or condition and covers a wide range of M_R values, from 16 MPa to 250 MPa. This diversity in the dataset reflects its inclusion of various simulated soil conditions. Table 3.2 categorizes these soil conditions into five classes based on M_R modulus values.
The range of 16-49 MPa, indicates severely damaged soil platforms with compromised structural integrity, suggesting substantial deformation and diminished load-bearing capacity. The soil is classified as damaged in the 50-79 MPa range, representing notable impairment and potential structural challenges with reduced

resilience. The soil is considered semi-damaged for the 80-119 MPa range, implying moderate damage and compromised but not severely impaired structural resilience. The 120-199 MPa range denotes semi-sound soil platforms with moderate structural soundness, indicating satisfactory load-bearing capability with room for improvement. Soil platforms with modulus values exceeding 200-250 MPa are classified as sound, representing optimal soil conditions with structural integrity, ensuring high load-bearing capacity and minimal deformation. This qualitative classification will be the Representative reference for the ML model in Chapter V, as it provides a nuanced understanding of the physical characteristics of the soil, allowing for informed assessments of its suitability for supporting pavement structures.

— From Figure 3.5, it observed that the mean and median values are close at around 133 MPa. This instance indicates that the dataset's M_R values are distributed relatively evenly around the central tendency, with a few extreme values. This uniform distribution around the central tendency is advantageous for examining the influence of noise, especially in the form of clusters of outliers.

— The standard deviation from Figure 3.5 is approximately 67.98 MPa indicates major variability in soil M_R values. This variability reflects real-world soil conditions, which can differ widely from one site to another. To this end, after performing exploratory data analysis on the resilient modulus M_R, the subsequent sequence will transition to the second forward model component, namely the deflection velocity.

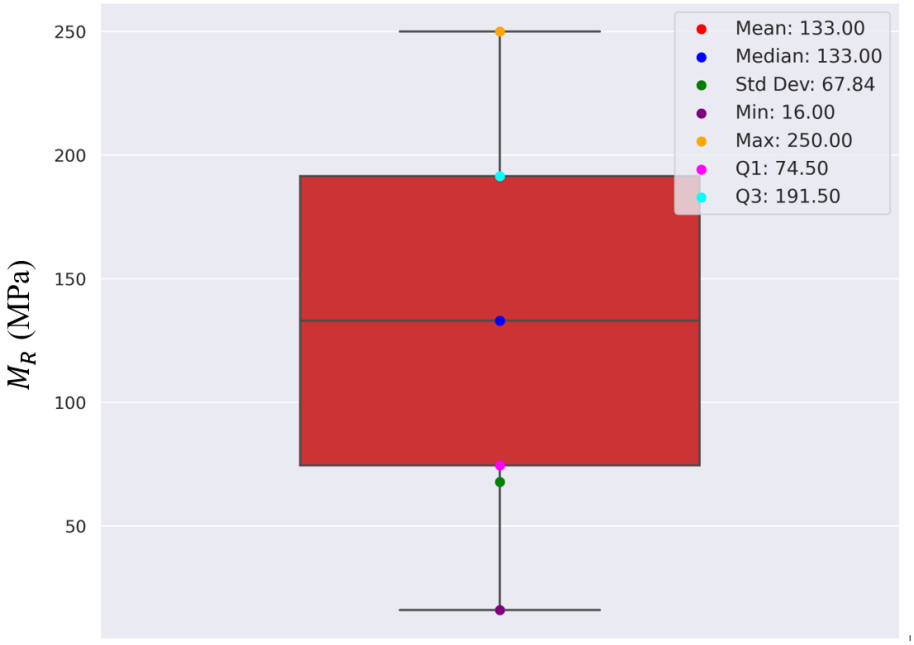

Figure 3.5 – M_R EDA

3.4.4.2 Analysis Phase: D_S Exploratory Data Analysis (EDA)

An EDA of D_S was conducted during this analysis phase. The unique insights derived from this analysis, which result from statistical and physical examinations, are summarized. These insights, derived from the data presented in Figures 3.6 and 3.7, provide a detailed understanding of the characteristics of the input features Sn_1 to Sn_7.

— Figure 3.6 presents a box-and-whisker plot to depict the trend in the D_S dataset. This non-parametric approach is particularly adept at capturing the central tendency and spread of the data, especially when normality assumptions are not met (the distribution of non-Gaussian data). The plot reveals a gradual increase in the D_S mean value as one moves away from the loading point, eventually reaching a peak value, followed by a decrease towards the reference sensor. This observed trend closely resembles the deflection slope curve in Figure (3.2 b), where D_S exhibits an almost zero value at both the loading point and the reference sensor. However, this pattern differs from the deflection slope curve in the same figure, where the maximum value is registered near the loading point. It is worth noting that the deflection is not solely affected by the TSD load's position; the sensor's location also has an influence.

— Figure 3.7 reveals a distinct progressive pattern in Deflection slope D_S from seven sensors Sn_1 to Sn_7. Each sensor's 25th and 75th percentile deflection values represent the data's lower (Q1) and upper (Q3) quarterlies. Calculating the interquartile range (IQR), Q3 - Q1, reveals the data's variability. Larger IQR values indicate greater variability. From analyzing the results, $S1$ exhibits the lowest IQR variation, and $S7$ displays the highest IQR variability.

This pattern signifies that when estimating M_R, the deflection slope near the loading point maintains a higher level of consistency but becomes progressively variable as one moves away from the loading point. In this context, it shows that the behavior of M_R is notably sensitive to sensors positioned downstream Sn_6 and Sn_7 in comparison to those located nearby Sn_1 and Sn_2.

Thus the placement of sensors exerts a substantial influence on the assessment of pavement deflection behavior under TSD, with specific sensors proving more effective in capturing deflection behavior, depending on their precise location and the E_i to be estimated.

— These findings validate the results of prior bibliographic studies [79] presented in Chapter II, where the benchmarking of flexible pavement structural condition was conducted using deflection bowl parameters (BLI, LLI, MLI). These parameters are meaningful in pavement structure analysis, aiding in identifying sections with varied structural capacity and behavior through a simplified approach. However,

the question remains regarding the negligible loss in accuracy associated with using these simplified methods, a topic that will be addressed in Chapter IV.
To this end, the upcoming section will explore the sensitivity analysis of the impact of temperature and noise on the soil modulus estimation model, providing deeper insights into the model's accuracy and reliability.

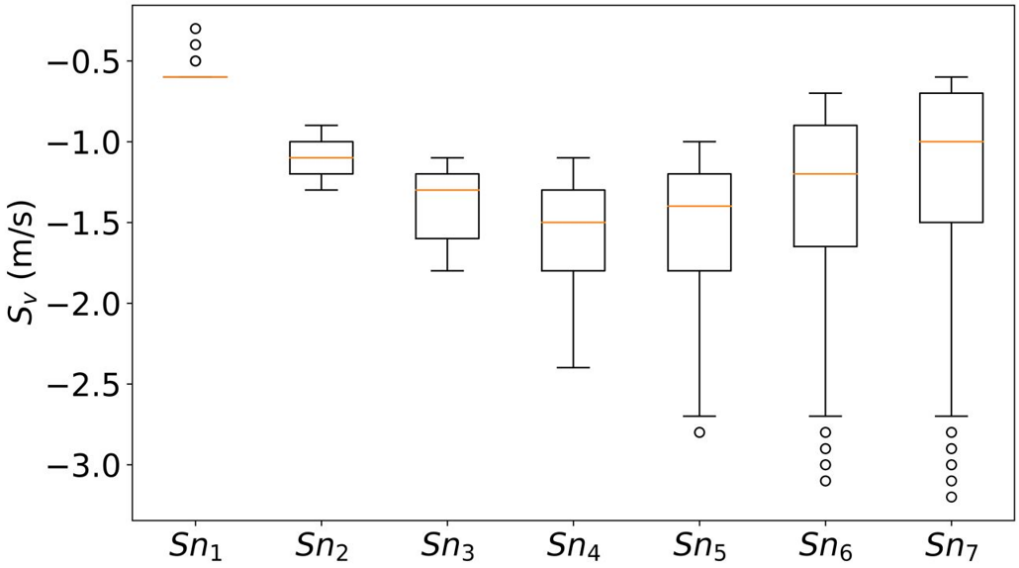

Figure 3.6 – Characteristics of the input features Sn_1 to Sn_7

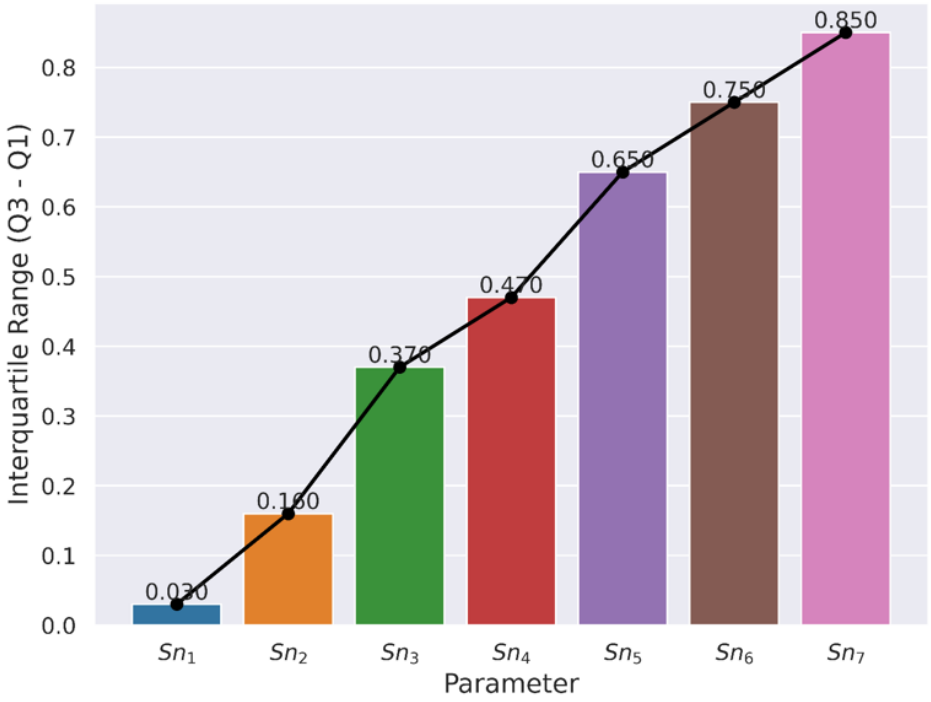

Figure 3.7 – Interquartile range (IQR) of the input features Sn_1 to Sn_7

3.5 Thermo-mechanical behavior of bituminous materials

3.5.1 Temperature sensitivity analysis

This section delves into the influence of temperature variations on measuring the TSD (Traffic Speed Deflection) deflection slope basin under bituminous pavement structures because temperature fluctuations substantially impact pavement performance. These variations directly influence distress development and the potential for structural failure [140, 62]. Consequently, they play a central role in determining the long-term maintenance needs of pavement structures.
However, temperature fluctuations also introduce uncertainties in the stiffness of pavement layers, which are quantified by the elastic modulus (E_i). These uncertainties result in variability in the calculated deflection slope (D_S).
Therefore, this section aims to quantify how these uncertainties, stemming from temperature fluctuations and measurement noise, collectively influence D_S calculations. This assessment is particularly crucial in scenarios where the soil modulus (M_R) is assumed to be known and unaffected by temperature impacts.
To achieve this objective, the research analysis in the case study is structured around three main sub-objectives:

1. Assessing temperature impact on pavement mechanical behavior: This objective involves observing the influence of changes in the E_i of individual layers translated by the simulated D_S. By gaining insights into how temperature variations in specific pavement layers affect the overall D_S calculation, the aim is to identify potential preliminary underestimations of the soil modulus.
2. Identifying Influential elements of pavement properties: The focus here is on identifying the layer E_i with the most marked impact on accurately estimating the soil modulus (M_R). This step is principal for pinpointing key contributors to variations in D_S and refining soil modulus estimation techniques.
3. Assessing Combined Effects: This objective examines how random simulated measurement noise and temperature uncertainty in E_i values might affect D_S calculation. By understanding the cumulative impact of these factors on estimation reliability, the goal is to enhance the robustness of M_R estimation.

3.5.2 Temperature dataset

The pavement structure under investigation is outlined in Table 3.3, offering an overall insight into its layered composition, thickness, bituminous material properties, and thermal characteristics.

Furthermore, Table 3.4 delves into the temperature profiles utilized in the study, elucidating the corresponding variations in the elasticity modulus (E_i) across different layers (E_1, E_2, E_3) composed of bituminous material. Notably, the modulus of the underlying material (M_R) is presumed to be temperature-independent.

Table 3.3 – Characteristics of the pavement structure used to derive the forward model

Layer (i)	Thickness (m)	Material	E_i (MPa)	ν	Interface	°C
1	0.06	HMA	7000	0.35	(1) bound	5-25
2	0.09	BC-g2	9300	0.35	(1) bonded	5-20
3	0.09	BC-g2	9300	0.35	(1) bonded	5-20
4	∞	M_R	**125**	**0.35**	(1) **bonded**	**15**

Table 3.4 – Material properties at vertical temperature profile

Temp-Profil Θ °C			E_i			M_R
L_1	L_2	L_3	E_1	E_2	E_3	125
5	5	5	11405	15090	15090	125
10	5	5	9310	15090	15090	125
15	10	10	7000	11880	11880	125
20	15	15	4690	9300	9300	125
25	20	20	3245	6120	6120	125

3.5.3 Correlation Analysis: Temperature Θ °C to modulus E_i

The relationship between temperature and modulus of elasticity (E_i) for each pavement layer, as illustrated in Table 2, presents the main insights for pavement engineering.

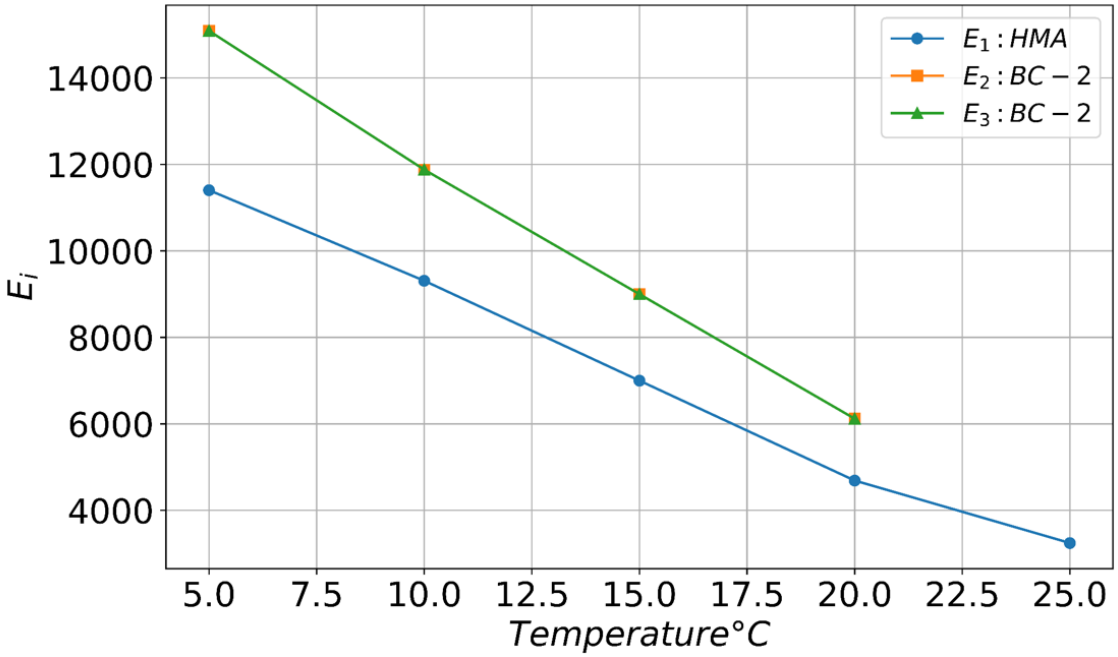

Figure 3.8 – Temperature influence on surface modulus E_1

Table 3.5 – Temperature sensitivity analysis for layer 1 (HMA)

Θ (°C)	**15°C: Reference E_1 (MPa)**	E_1 **(MPa)**	Δ **(MPa)**	Δ **% Change**
5	7000	11405	4405	63%
10	7000	9310	2310	33%
15	7000	7000	0	0%
20	7000	4690	2310	-33%
25	7000	3245	3755	-54 %

— Quantitative observations data in Figure 3.8 and Table 3.5, reveal a negative correlation between temperature and Young's modulus (E_1) for layer 1 (HMA) within the 5°C to 25°C range. This relationship indicates that as the temperature rises, the stiffness of the bituminous materials decreases.

Specifically, at reference 15°C, E_1 is measured at 7000 MPa. When the temperature

Table 3.6 – Temperature sensitivity analysis for layers 2 & 3 (BC-g2) - 5°C to 20°C

Θ (°C)	**15°C: Reference E_2, E_3 (MPa)**	**E_2, E_3 (MPa)**	**Δ (MPa)**	**Δ % Change**
5	9300	15090	5790	62.8%
10	9300	11880	2580	27.7%
15	9300	9300	0	0%
20	9300	6120	3180	-34.2%

drops to 5°C, E_1 increases to 11405 MPa, a 63% rise. Conversely, at 10°C, E_1 is 9310 MPa, showing a 33% increase from the reference temperature. However, at 25°C, E_1 decreases to 3245 MPa, a 54% reduction from 15°C. These observations indicate that bituminous material's stiffness is highly sensitive to temperature fluctuations and exhibits thermal sensitivity attributed to its elastic and viscoelastic nature. These results show that bituminous materials at high temperatures are prone to bias deflection value measurement.

— The data in Figure 3.8 and Table 3.6 showcases the temperature sensitivity of Layers 2 & 3 (BC-g2) within the 5°C to 20°C range. Similar to Layer 1 (HMA), BC-g2 also exhibits a decrease in stiffness (E_2 & E_3) as the temperature increases, indicating a softening effect as the material warms. However, the decrease in the magnitude of stiffness appears less pronounced than HMA. At 5°C, BC-g2 shows an increase of 62.8% (5790 MPa) compared to the reference temperature of 15°C. As the temperature rises to 10°C, there is a 27.7% decrease (2580 MPa), and at 20°C, a 34.2% reduction (3180 MPa). This suggests a potential "threshold temperature" around 15°C, below 15°C stiffness increases and above 15°C the material softens. These findings highlight the importance of considering the thermal properties of different pavement layer materials to achieve optimal deflection measurement that leads to accurate estimation and, eventually, better decisions to enhance pavement performance under varying temperature conditions.

3.5.4 Impact Analysis: Temperature Θ °C to deflection slope D_S

— The investigation delves into the impact of temperature uncertainty on deflection slope (D_S) measurements within pavement structures. Through simulation, the elastic modulus (E_i) of each pavement layer was systematically altered based on corresponding temperature profiles (ranging from 5°C to 25°C for surface temperature and 5°C to 20°C for structure temperature). Throughout the simulation, the

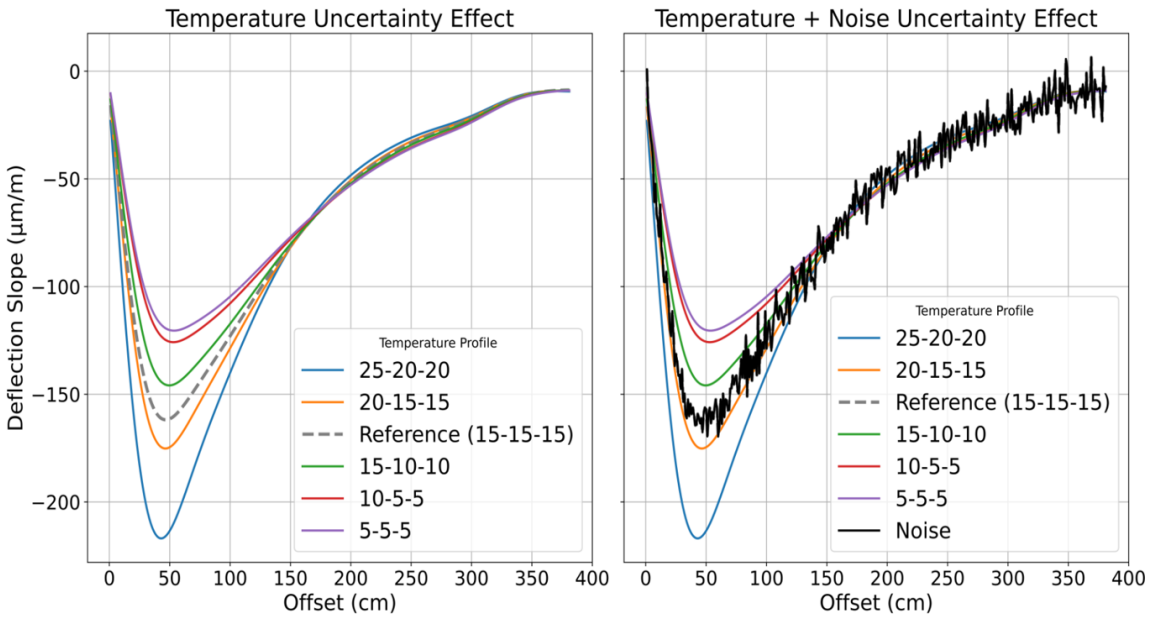

Figure 3.9 – Left-hand: Temperature uncertainty impact on D_S, Right-hand: Accumulated impact of noise (15 dB SNR) and temperature and uncertainty on D_S

soil modulus remained constant at 125 MPa, assumed independent of temperature. The results yield the following insights:

— Temperature-Dependent Deflection Slope: Analysis of Figure 3.9 highlights the substantial influence of individual layer temperatures on deflection slope (D_S). This underscores the direct correlation between the uncertainty in elastic modulus (E_i) due to temperature fluctuations and measured D_S. Higher temperatures lead to overestimating D_S, while lower temperatures result in underestimation. This underscores the pivotal role of considering E_i and temperature for accurate D_S data.

Impact of Noise: Figure of fig:c4bVVbta reveals the presence of noise in the data (15dB SNR), complicating interpretation. The noise overlaps with deflection slope curves, indicating that measurement errors arise from temperature uncertainty and external factors. This collective effect of temperature uncertainty and noise likely diminishes the accuracy of D_S estimations. Further investigation, which promises more accurate estimations, is warranted to quantify the accuracy loss attributable to these parameters.

These findings underscore the critical importance of engineers accounting for temperature variations and noise during pavement deflection measurements. As a pre-processing step, engineers must consider these factors to enhance the accuracy of D_S data. In addition, appropriate pavement materials tailored to different climatic zones ensure optimal deflection measurement performance across varied temperature ranges.

3.6 Conclusion

This chapter has developed a numerical forward model to estimate the soil elastic modulus M_R by analyzing TSD simulated deflection slope D_S.
The construction of the numerical forward model via Alizé software based on the Burmister elastic model by simulating TSD deflection slope D_S under the whole TSD wheels.
Based on the numerical forward model, a synthetic database has been carefully constructed. This database comprises four vital phases, including modeling pavement behavior under TSD, introducing additive noise to mimic real-world measurement noise, and conducting an exploratory Data and sensitivity analysis. To this point, the numerical forward Model findings encompass three leading points.
The research highlights three key points regarding TSD measurements: Firstly, focusing solely on the rear axle load in TSD deflection measurement leads to underestimation, whereas summing deflections from all TSD wheels (superposition) provides more accurate results. Secondly, for calibration and simplicity, TSD deflection velocity is assumed to be zero at the loading point and 3m away, introducing measurement uncertainty that requires careful interpretation. Finally, sensor placement affects deflection behavior assessment, with sensors near the loading point showing more consistent deflection slope values with soil modulus variations. At the same time, those farther away exhibit more variability. Conversely, sensors near the loading point show higher variability with surface modulus data, while those farther away are less responsive. Thus, sensor placement affects the assessment of pavement deflection behavior under TSD and, eventually, the estimation accuracy.
Moreover, the investigation on the Thermo-mechanical behavior of bituminous materials reveals a strong correlation between temperature-induced changes in elastic modulus (E_i) and deflection slope (D_S) data, with higher temperatures causing overestimations and lower temperatures causing underestimations. Additionally, noise (15dB SNR) complicates D_S interpretation, highlighting the influence of temperature uncertainty and external factors on measurement accuracy. Further research is required to quantify the accuracy loss due to these factors.
Overall, the exploration of these parameters, processes, and data in this chapter has established a groundwork for developing a numerical forward model to enhance pavement analysis under Traffic Speed Deflectometer (TSD). This in-depth investigation lays the groundwork for subsequent chapters, where advanced machine-learning techniques will be leveraged to elevate the accuracy and reliability of pavement assessments.

Chapter 4

Inverse Model: Numerical Validation

4.1 Introduction

This Chapter proposes a novel numerical model and methodology to accurately estimate the Subgrade Modulus (M_R) by directly utilizing TSD deflection slope D_S instead of traditional deflection methods, leveraging Machine Learning (ML). ML offers remarkable generalization capacity, surpassing conventional methods, particularly in extracting patterns, learning from complex data, and handling new and noisy data.
Therefore, this Chapter aims to propose a novel approach with methodological procedure for appraising the remaining life of pavement through precise M_R estimation. The methodology for implementing the ML model is presented in figure 4.1, where a numerical forward model dataset is constructed, comprising 235 simulated TSD deflection slope D_S measurements. It corresponds to variations in M_R values ranging from 16 to 250 MPa. The dataset is characterized by simulating the TSD (D_S) data acquired from seven sensors (Sn) serving as input independent variables (Features), and the output dependent variables (labels) represented by the soil modulus of elasticity (M_R).
To this end, the objective here is to create a numerical ML-based model for accurately estimating M_R. The model utilizes a supervised ML model for classification and regression, as shown in figure 4.1 based on the supervised ML algorithm Support vector Machine (SVM). However, to maximize the accuracy of the SVM model, an optimization step for initial hyperparameters will be performed. To this end, an advanced parametric study is conducted to analyze and validate the results, alongside assessing the model's robustness against changes in data size or type.
Moreover, a quantitative sensitivity analysis is carried out as mentioned in figure 4.1. This analysis explores the adverse effects of some challenges, including employing advanced modeling techniques to handle high-dimensional TSD data, examining the impact of measurement TSD sensor noise, studying temperature variation effects, and addressing uncertainties associated with E_i values on M_R estimation.

The subsequent sections will delve into procedural protocols, execution processes, and outcomes of implementing the (TSD + ML) model along with the advanced numerical validation framework.

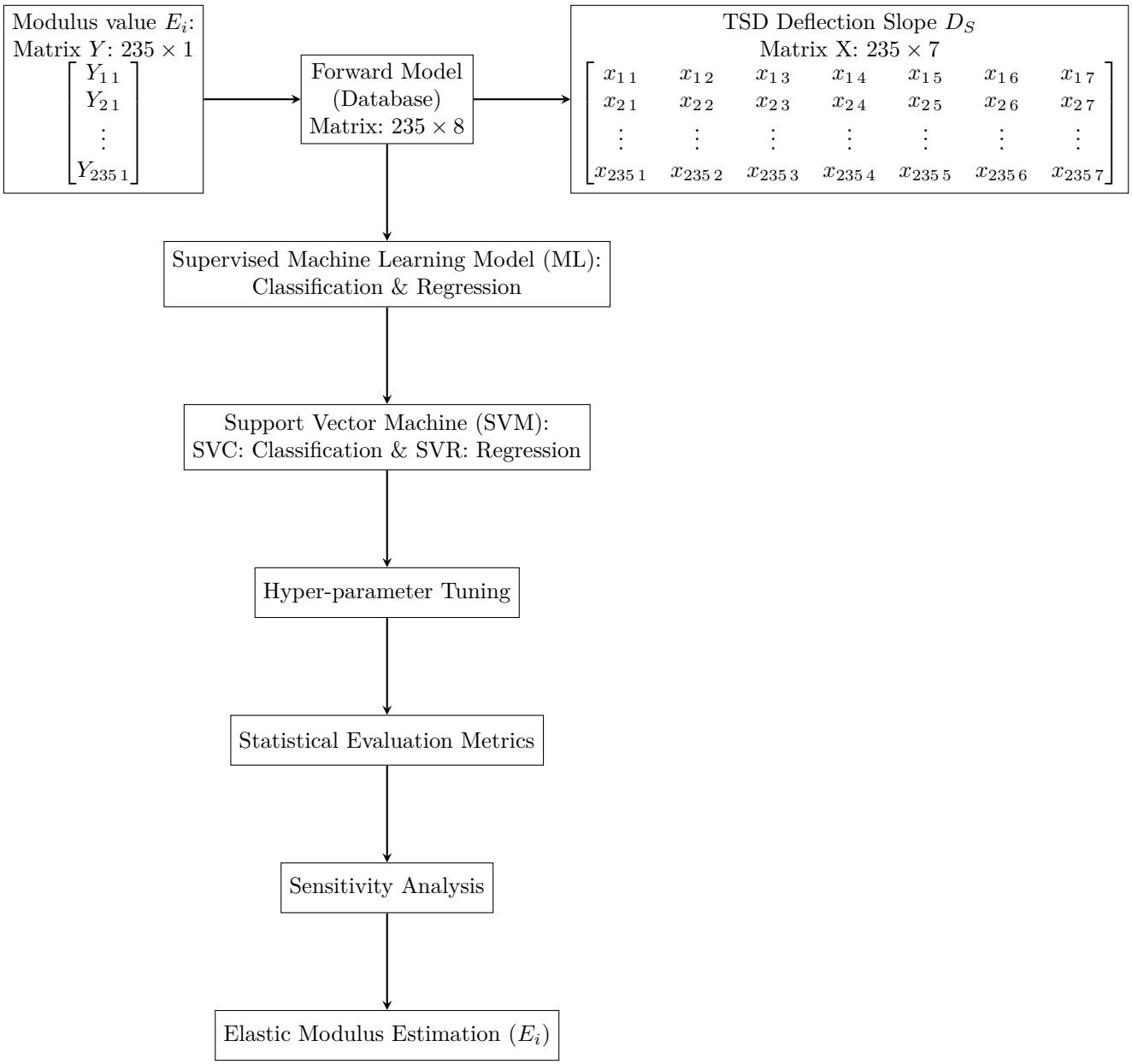

Figure 4.1 – Research framework and methodology for the estimation of (M_R) from TSD model: Numerical parametric study

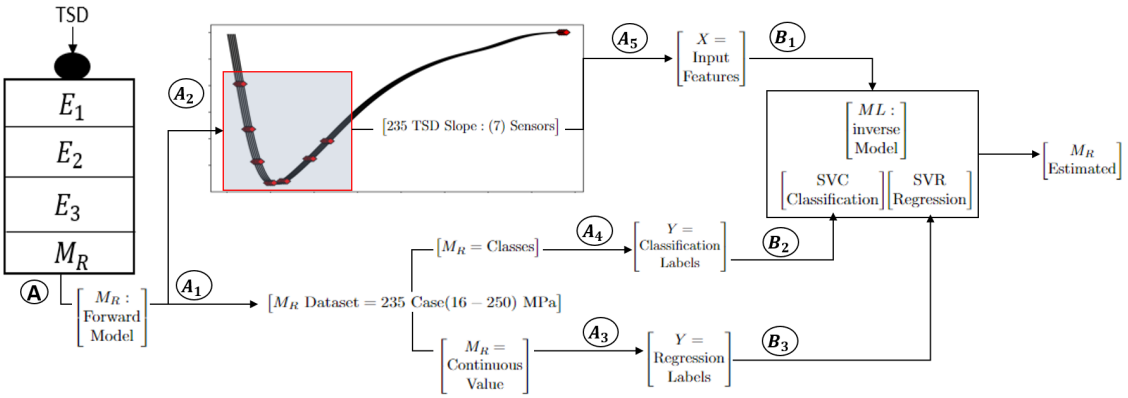

Figure 4.2 – Forward to inverse model framework

4.2 Forward to inverse model framework

— Objective: This study aims to estimate the soil modulus of elasticity M_R using a supervised machine learning model. Deflection slope D_S is the input parameter, while M_R is the target output.

A Support Vector Machine (SVM) algorithm is employed for constructing the inverse model. SVMs offer capabilities for both classification and regression analysis. This approach leverages the numerical forward model database established in Chapter II, enabling comprehensive M_R estimation.

— Data acquisition and preprocessing of Forward Model: As depicted in Figure 4.2, the initial step (A) involves predefining TSD load configuration and pavement structure as detailed in Table 3.1 of Chapter II. Then, these parameters will be fed into Alizé software. Alizé generates two files forming the forward model synthetic Database: one containing predefined mechanical properties like M_R values (A_1), and another containing corresponding simulated D_S measurements (A_2). The M_R values encompass a range from severely damaged (16 MPa) to sound structures (250 MPa) with 1 MPa increment, resulting in 235 data points.

The choice of this controlled synthetic Database approach will allow the creation scenarios where the underlying data structure is known, providing a clear understanding of the sensitivity analysis impact of TSD sensor noise and other influential physical parameters, such as temperature on the inverse model.

Therefore, these points are divided for training purposes: continuous values for regression analysis (A_3) and categorized classes for classification analysis (A_4). Conversely, the 235 M_R will generate a corresponding 235 deflection slope D_S curves. D_S are then represented by 7 TSD sensor measurements (marked in red within Figure 4.2 red frame). The position of the red points matches the sensor positions. Accordingly, in this step, an input feature matrix (A_5) will be constructed with

dimensions of 235x7, where each row represents a data point, and each column represents sensor data. This matrix serves as the input for the inverse model (B_1).

— Inverse Model Development: The inverse model for M_R estimation from D_S employs two primary analyses: Classification Model: This utilizes Support Vector Classification (SVC) with the input feature matrix (B_1) as the independent variable D_S and data in (B_2) as classification labels (M_R categories from (A_4)).
Regression Model: This utilizes Support Vector Regression (SVR) with the input feature matrix (B_1) as the independent variable D_S and data in (B_3) as the dependent variable (continuous M_R values from (A_3)).

— Model optimization and validation: To ensure accurate and reliable M_R estimations, the inverse model development incorporates additional procedures beyond the core classification and regression analyses. These include:
  — Train-test split: Dividing the data into training-testing sets for model evaluation.
  — Standardization: Scaling features to a common range for overfitting and underfitting prevention.
  — Exploratory Data Analysis (EDA): Understanding the underlying data distribution, patterns, and relationships between variables.
  — Data preprocessing: Techniques for handling missing values and outliers.
  — Hyperparameter tuning: Optimizing the SVM model's hyperparameters for optimal performance.
  — Sensitivity analysis: The model's sensitivity to external physical elements such as TSD sensor measurement noise and temperature.
  — Advanced parametric validation: Employing advanced techniques to ensure model generalizability and robustness.

— Computational environment: The inverse model development leveraged a Support Vector Machine (SVM) algorithm as its core. This implementation was realized through the sci-kit-learn library [141] in Python. To facilitate the computationally intensive tasks associated with SVM model training, Google Colab [142] served as the high-performance computing environment. This cloud-based platform offers accessibility and demonstrably expedites complex computations compared to traditional computing infrastructure. Within Google Colab, a virtual machine (VM) with hardware specifications was employed for the inverse modeling tasks. This VM boasted a powerful NVIDIA Tesla P100 graphics processing unit (GPU), 16 GB of dedicated memory, ample RAM (12 GB), and storage (100 GB). The operating system utilized was Ubuntu 18.04 LTS. These combined attributes ensured efficient resource allocation and successful training and execution of the inverse model, which will be explained in subsequent sections.

4.3 Inverse Model: Classification analysis

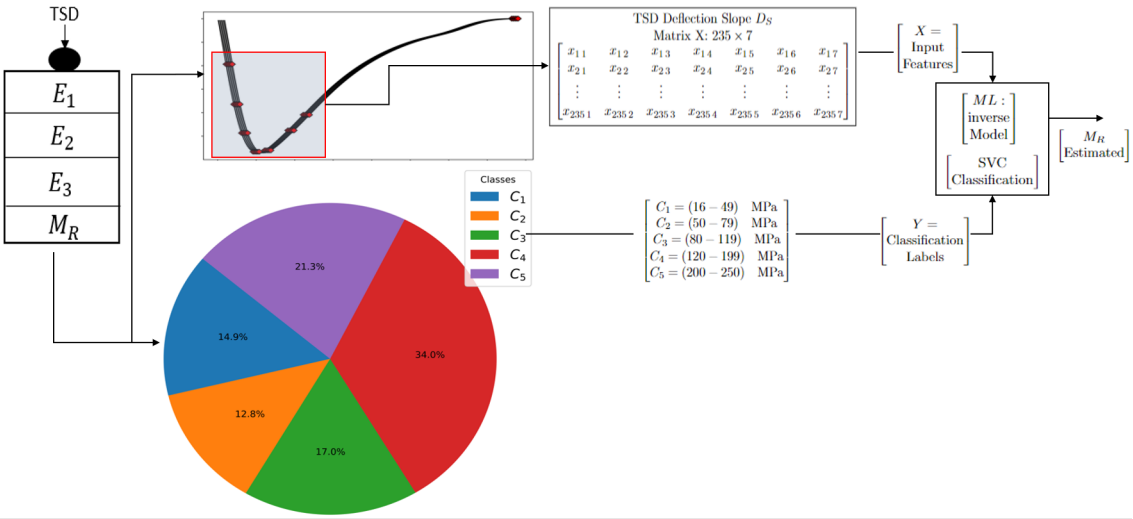

Figure 4.3 – SVC classification inverse model framework

This research section discusses the results of the inverse model, builds upon the soil classification framework established in the previous Chapter, and strictly adheres to the guidelines outlined in the French guide by SETRA (1998) [30].
A systematic approach is proposed for categorizing soil platform conditions based on their measured elastic modulus M_R values. A classification framework uses five distinct classes based on M_R ranges. These classes encompass the entire spectrum of pavement foundation conditions, ranging from severely damaged (C_1) to sound (C_5).
This framework is visualized in Figure 4.3, which is further utilized to depict the distribution of M_R values across these classes.
Initially, an analysis of the distribution of M_R values across the classes is conducted, considering both the number of instances (N°) and percentages (%) (Figure 4.3).
By analyzing the class distribution, an imbalanced dataset could be observed. For instance, class4 (120-199 MPa) contains the highest number of instances (34%), followed by CClass5 (200-250 MPa) at 21.7%. Conversely, Classes 1 (16-49 MPa), 2 (50-79 MPa), and 3 (80-119 MPa) constitute a combined 44.3%, with a relatively even distribution around 14.5%, 12.8%, and 17% respectively. This data imbalance may introduce two challenges for subsequent model development and analysis, which will be investigated as hypotheses.
The impact of data scarcity is the first challenge. Classes 1 and 2 have fewer data points than classes with higher M_R values. This scarcity could negatively impact the model's ability to learn and predict these classes accurately. The second challenge is predicting high-value classes. The model, trained on data with a minimum M_R value, will predict a maximum class. This range may pose challenges for the model, especially considering the

limited data points available for the higher-value classes.
The upcoming sections will explore how data characteristics influence the model's accuracy and investigate strategies to mitigate their negative impact via well-optimized hyperparameter tuning.

4.3.1 SVM-SVC hyperparameter tuning

To initiate the learning phase, akin to the calibration process required for any hardware device. However, ML employs hyperparameter tuning based on the target algorithm. Thus, this subsection delves into the impact of hyperparameter tuning on SVM-SVC performance optimization in classification tasks.

— Context: As previously highlighted, the investigation in the preceding chapter involved an assessment of feature noise stemming from TSD sensor uncertainty through a reputability test. This noise, characterized by random variations or errors in feature values, holds the potential to disrupt SVM learning processes, resulting in misclassifications and compromising classifier performance. Consequently, such disturbances may induce hyperplane deviation, representing the deviation of the SVM decision boundary from its optimal position, thus potentially leading to misclassification of data points and impacting the accuracy of the classification model [36, 132].

— SVM Kernel: To mitigate these challenges, the study proceeds with the optimization of C, γ, and ϵ values. However, before this, in the initial phase, the selection of an appropriate kernel function is important for achieving optimal model performance. Various kernels, including Linear, Polynomial, Radial Basis Function (RBF), and Sigmoid, are evaluated to determine their suitability based on factors such as data quantity, quality, and distribution shape. Notably, the RBF kernel consistently outperforms others in terms of accuracy and relevance to the data, thereby justifying its preference for modeling the classification task.

— (C): After choosing the appropriate kernel, then the regularization parameter (C) of SVMs plays a critical role in controlling the trade-off between overfitting and underfitting. Through an investigation into the interaction between different noise levels and the regularization parameter C, the study reveals that a high value of C encourages the SVM model to tightly fit the training data, potentially leading to overfitting. Conversely, a low value of C allows for greater flexibility in the decision boundary, making the model more susceptible to noise in the data.

— Gamma γ: On the other hand, defines the influence of a single training example, with high values meaning close range and low values meaning far range. It also takes a part in determining the flexibility of the decision boundary.

— Epsilon ϵ: ϵ is also a critical parameter representing the margin of error tolerance. It serves to achieve the desired balance between model complexity and generalization performance as it defines the width of the SVM tube, allowing some deviation from predicted values without penalty. Choosing an appropriate ϵ is essential as a low ϵ value makes the model less forgiving of errors, leading to potential overfitting. In contrast, a high value increases flexibility but may result in underfitting [34].

— GridSearchCV [143]: Using the sci-kit-learn Python library, a Grid Search Cross-Validation (Grid-Search-CV) process is employed to optimize hyperparameters. This method systematically investigates a grid of parameter combinations, a commonly adopted practice for identifying the optimal parameters for the selected kernel. In this research, focusing on the Radial Basis Function (Gaussian) - RBF kernel, which demonstrated superior accuracy compared to alternative kernels.

— Log-uniform: Ultimately, the study identifies optimal C, γ, and ϵ values that influence the decision boundary and strike a balance between fitting the data appropriately and maintaining resilience against noise and hyperplane deviation to secure the best possible accuracy, as shown in Table 4.1. A technique for continuous log-uniform random variable follows a logarithmic distribution over a constant range, a potential alternative to using a fixed set of discrete values for hyperparameter tuning [141]. A log-uniform random search would select values from a continuous distribution on a logarithmic scale. This allows for a more comprehensive exploration of the parameter space, potentially leading to the identification of even better hyperparameter combinations. For example, as shown in the table 4.1, instead of trying only values like 1, 10, and 100 for C, a log-uniform search would explore a broader range of values between 1 and 100 but with a bias towards lower values on the scale. Accordingly, the optimal values identified for the SVM hyperparameters are as follows: $C = 1000$, $\gamma = 100$, and ϵ=1, these optimum values align closely with those proposed in the existing literature for data of this type and characteristics

— Observations: In this study, SVMs adjust their decision boundaries to accommodate noise in high noise-level scenarios, increasing hyperplane deviation. Conversely, in lower noise scenarios, SVMs demonstrate a more effective response, aligning closer to the ideal decision boundary.

To this end, The following section will explore the discussion regarding classifications protocols and results discussion and analysis.

4.3.2 Classification model protocol setup

This section interprets the classification results of the inverse model. To ensure an accurate evaluation, a stratified train-test-split approach is employed. This method divides

Table 4.1 – SVC Grid search Hyperparameter Tuning

SVM Parameter	**Initial Values**		**Optimum**
	Lower	**Upper**	**Value**
Tested-Kernels	Linear/Poly/RBF/Sigmoid	Linear/Poly/RBF/Sigmoid	RBF
C tolerance parameter	1	10000	1000
γ kernel scale factor	0.01	1000	100
ϵ precision	0.001	10	1

the forward model dataset into training (70%) and testing (30%) sets while preserving the class distribution in both [141].

Beyond the standard split, a tailored Train-Test-Validation (TTV) framework, detailed in Figure 4.4 and Table 4.2, is implemented. This framework consists of five distinct iterations of training and testing, each focusing on specific "bands" of classes. For the model validation process of each of the five iterations, the 10-fold cross-validation technique is utilized. Here, the dataset is partitioned into ten equally sized subsets. The process iterates ten times, each iteration using a different subset as the validation set. In contrast, the remaining nine subsets are combined to form the training set.

With regards to the TTV framework, in the first iteration, 70% of all five classes (1-5) is used for training, and the remaining 30% is allocated for testing. This initial step establishes a baseline for the model's overall performance. Subsequent iterations (2-5) delve deeper by testing the model's ability to handle individual class bands. Each iteration excludes a specific class during testing while using the remaining courses for training. This approach, termed "band-wise testing," assesses the model's proficiency in predicting the excluded class when trained without it.

For instance, in the third iteration, classes 1 and 3-5 are included in the training set (70%), while class 2 serves as the testing band (30%). This allows us to evaluate how well the model predicts the class with the most minor data (smallest band, Iteration 3). Following a similar logic, other iterations sequentially test the model on different excluded bands: the lowest class values (Iteration 4) and the highest class values (Iteration 5). Via this approach, the model's strengths are assessed across the entire spectrum M_R conditions.

The upcoming section will focus on advanced parameter analysis. Analyzing the performance metrics across these iterations will provide further insights into the model's behavior and potential areas for improvement.

Table 4.2 – Classification Analysis: Training Testing Validation framework

Iteration	Training Band	Testing Band	Testing Objective
1	[1,2,3,4,5] (70%)	[1,2,3,4,5] (30%)	Overall Performance
2	[1,2,3,5]	[4]	Biggest band
3	[1,3,4,5]	[2]	Smallest band
4	[2,3,4,5]	[1]	Lowest band
5	[1,2,3,4]	[5]	Highest band

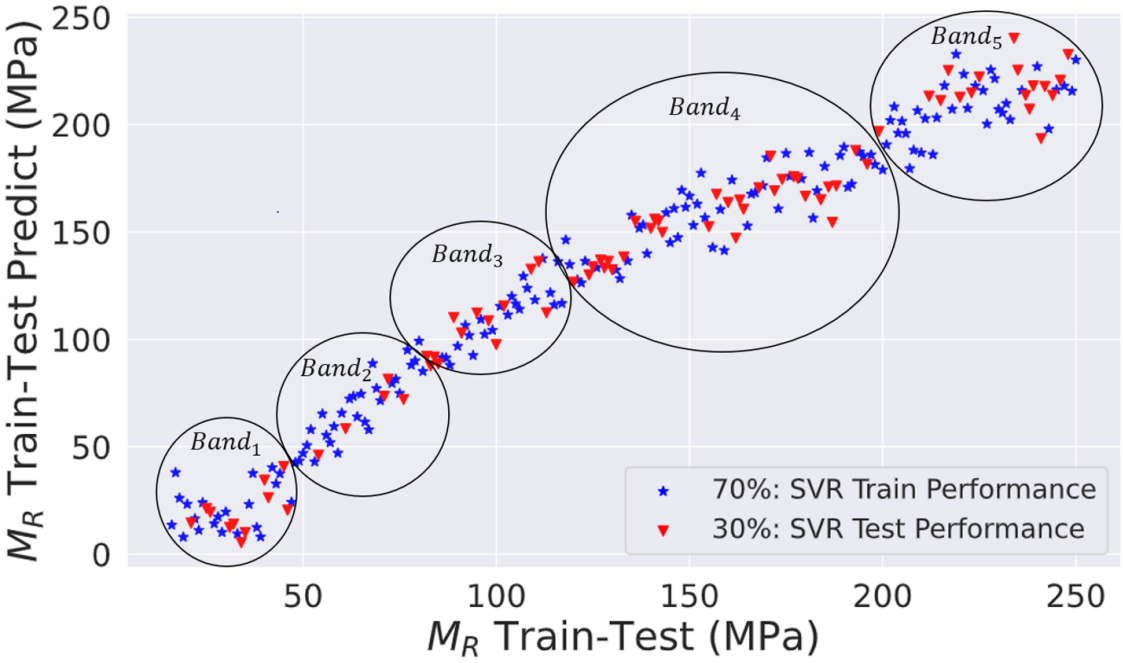

Figure 4.4 – Classification Analysis: Training Testing

4.3.3 Inverse model: Classification results discussion

Following the data preprocessing stage, which involved splitting the data into training and testing sets using a stratified train-test-split approach and a tailored Train-Test-Validation (TTV) framework with stratified bands, this section delves into the analysis of the model's performance within this framework as shown in Figure 4.5. As the initial investigation into the SVM-SVC classification model's performance, this section leverages the Dice Score coefficient (DSC-F1), a metric combining precision and recall, to analyze

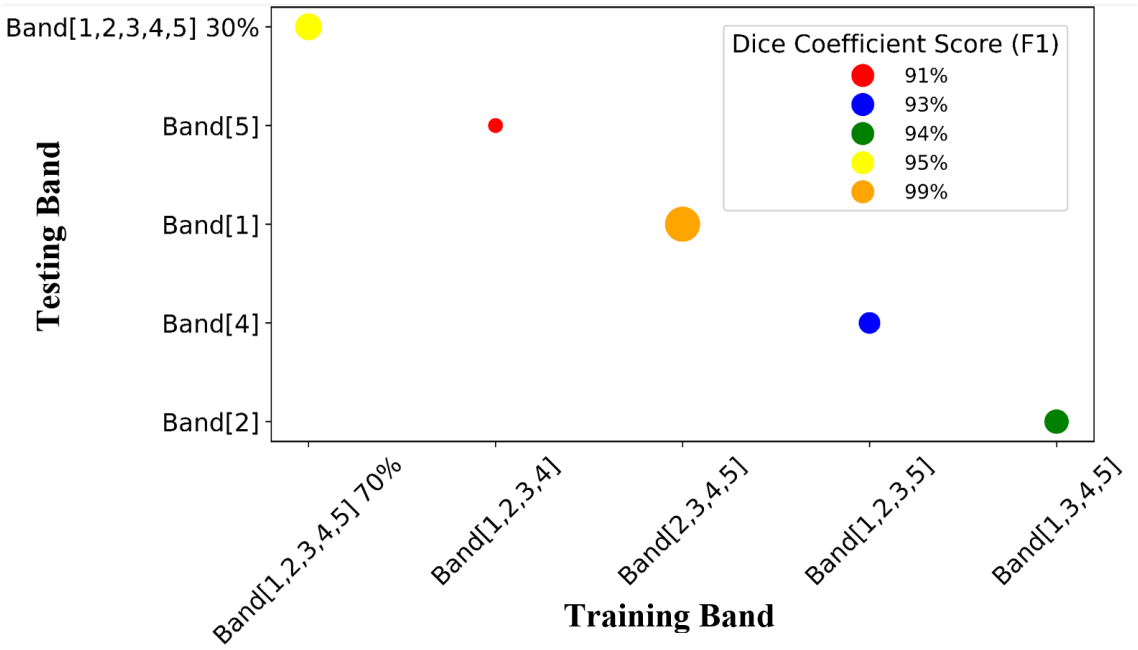

Figure 4.5 – TTV model's performance

results within the TTV framework. The observed range of Dice coefficient scores (91-99) across iterations suggests good performance in identifying and distinguishing between soil classes.

This analysis reveals key factors influencing performance, aligning with established scientific principles. Firstly, the training band in Iteration 3 likely offered a more balanced representation of soil classes. This aligns with the principle that balanced data distribution facilitates effective learning by the model. Conversely, Iterations with potentially imbalanced training bands (as suggested by slightly lower scores in Iterations 1, 2, 4, and 5) might lead to prioritization of well-represented classes and hinder learning for under-represented ones.

Secondly, the composition of the testing band in Iteration 3 might have also Contributed. If the soil conditions in this band presented clearer distinctions from the trained classes (e.g., Band 1), classification difficulty would be lower, leading to a higher Dice coefficient. Conversely, Iterations with testing bands featuring soil conditions more closely aligned with trained classes (as might be the case for Iterations 1, 2, 4, and 5) would necessitate more nuanced differentiation, potentially resulting in lower scores.

These findings, based on the Dice coefficient analysis within the TTV framework, provide a strong foundation for further investigation into the SVM-SVC model's performance in the upcoming subsection. Mainly by analyzing the confusion matrix to gain insights into specific classification patterns and potential misclassifications. Additionally, advanced performance evaluation metrics are incorporated to enhance the robustness of our classifica-

tion analysis. These metrics, including precision, recall, and the Dice coefficient score, for further insights into these metrics, refer to Table 2.6 in Chapter II.

4.3.4 Classification Model: Advanced evaluation metrics

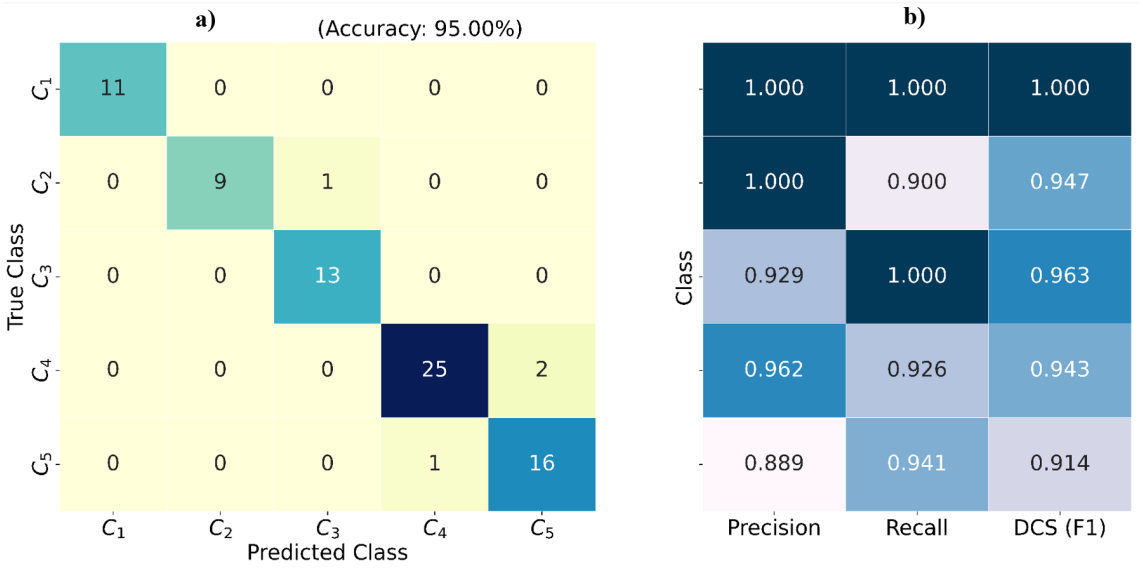

Figure 4.6 – a) Confusion Matrix b) Evaluation metrics for a classification model analysis

An advanced analysis of the SVM-SVC inverse classification model's performance using quantitative metrics reveals strengths and areas for improvement.
In the current investigation. A Confusion Matrix (CM) assessed the model's performance. The CM provides a detailed breakdown of the model's predictions, with correct classifications along the diagonal and misclassifications in off-diagonal entries.
As shown in the CM of Figure 4.6, the model achieves a high overall accuracy of 95%, indicating its effectiveness in correctly classifying a portion of the data. This suggests the model has the potential to make accurate predictions on unseen data.
However, a closer look at class-wise performance using precision and recall metrics reveals some variation. Classes 1 and 2 show perfect precision (1.00), meaning that most predicted instances for these classes genuinely belong to them. In contrast, Classes 4 and 5 have slightly lower precision (0.96 and 0.89), suggesting some misclassifications occurred for these classes.
The recall metric paints a similar picture. While recall values range from 0.90 to 1.00, the model successfully identifies a high proportion of actual instances within each class. Class 2 has a slightly lower recall (0.90). This suggests the model might miss some true positives for Class 2.
The F1 score, also known as the Dice coefficient, offers a balanced view of the model's

performance for each class by combining precision and recall. While all classes achieve high scores (0.91 to 1.00), Class 5 exhibits the lowest F1 score (0.91). This necessitates further investigation into the factors impacting Class 5 performance. A potential explanation lies in the model encountering higher uncertainty due to TSD sensor noise, which is cussing (measurement uncertainty). This noise could introduce ambiguity, leading to misclassifications within Class 5. However, from a practical standpoint, the consequences of misclassifications need to be considered. In this case, misclassifications within Class 5 might be less critical than those in lower-valued classes.
Lower-valued classes might represent vital situations, such as severely damaged areas. Misclassifying these could have negative consequences, potentially leading to delayed repairs and compromising infrastructure integrity. Conversely, misclassifications within Class 5, potentially due to noise, might represent less critical situations in the immediate term. While these misclassifications are not ideal, they might be preferable to overlooking an indeed damaged section (lower-valued class due to a misclassification.
Therefore, the slightly lower F1 score in Class 5, potentially influenced by noise, needs to be evaluated in the context of the relative importance of misclassifications across different classes. While striving to improve overall model performance is essential, it is paramount to consider the practical implications of misclassifications and prioritize mitigating those with the most passive consequences.
Overall the high accuracy is promising, but the variations in class-wise metrics and the Dice coefficient scores suggest there might be challenges in differentiating certain classes, particularly Classes 4 and 5 with lower precision, and Class 2 with lower recall. These findings warrant further investigation into these specific classes and the data used to train the model. Techniques like visualizing the confusion matrix and examining the characteristics of these classes could reveal factors like overlapping features or data imbalances. Addressing these issues through techniques like oversampling or undersampling data could improve the model's performance in future refinements.

4.4 Inverse model: Regression Analysis

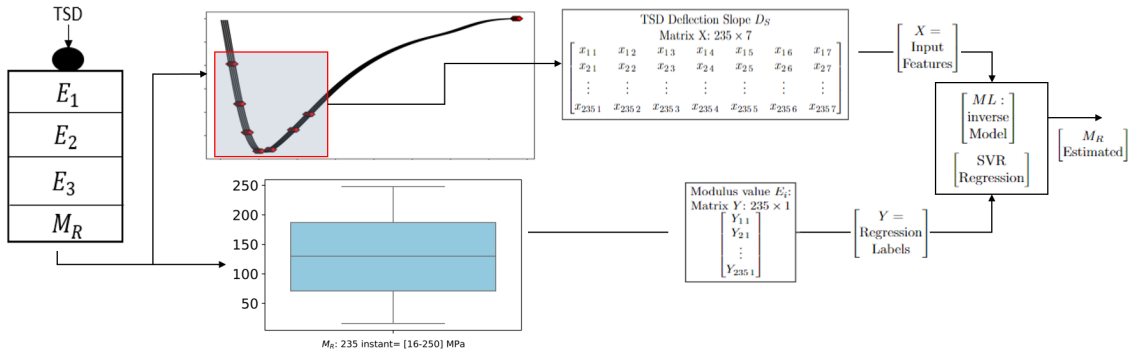

Figure 4.7 – SVR inverse model framework

Following the classification analysis using the SVM-SVC model, this section explores the inverse problem – regression analysis – employing a Support Vector Regression (SVR) model. Figure 4.7 shows that the inverse regression framework leverages the numerical forward model. This forward model generates a continuous dataset of M_R values ranging from 16 MPa to 250 MPa with an interval of 1 MPa. Additionally, for each M_R value, a corresponding simulated deflection slope measurement D_S is obtained.

The SVR model takes two inputs: Firstly, deflection Slope Matrix D_S that has dimensions of 235 x 7, representing the independent variable features. Each row signifies a data point with seven features potentially considering a deflection slope.

M_R Label Vector: This vector has dimensions of 235 x 1, representing the dependent variable labels. Each element corresponds to the M_R value associated with a specific data point in the deflection slope matrix as depicted in Figure 4.7.

In contrast to the classification model based on SVM-SVC, which assigns instances to specific classes based on M_R values, the SVR regression model aims to estimate the exact M_R value for a given set of deflection slope features.

The upcoming section will delve into the SVR algorithm Hyperparameters Tuning for maximizing the inverse regression model accuracy.

4.4.1 SVR hyperparameters tuning

Similar to SVC, fine-tuning SVR hyperparameters is used for enhancing model performance. Based on the results of GridSearchCV, as presented in Table 4.3, it is obvious that optimal performance for the SVM model is achieved using the RBF kernel, consistent with the classification outcomes. RBF is commonly preferred for nonlinear tasks due to its flexibility.

In this context, the optimization process begins with tuning the C tolerance parameter to have an optimal accurecy value at 10, indicating a penalty for errors.

Table 4.3 – SVR GridsearchCV hyperparameter tuning

SVM Parameter	**Initial Values**		**Optimum**
	Lower	**Upper**	**Value**
Tested-Kernels	Linear/Poly/RBF/Sigmoid	Linear/Poly/RBF/Sigmoid	RBF
C tolerance parameter	0.1	100	10
γ kernel scale factor	0.01	10	1
ϵ precision	0.001	1	0.1

Balancing a high C value to avoid overfitting with a low value to prevent underfitting is essential for model performance. Subsequently, the adjustment of the γ parameter, indicated by a value of 1 in Table 4.3, defines a relatively smooth decision boundary, with a stronger emphasis on training examples farther from this boundary. Finally, the optimization of the ϵ precision at 0.1 defines the tolerance margin for data points, aiding the model in better generalizing to unseen data.
To this end, the fine-tuning of hyperparameters enables the SVR model to achieve the highest possible accuracy even in the presence of noise and uncertainty as will be presented in the upcoming section. This underscores the efficacy of the fine-tuning process in identifying an optimal hyperparameter combination tailored to the dataset's characteristics, rendering the SVR model a reliable tool for predictive tasks within this context.

4.4.2 Regression model protocol setup

Table 4.4 – Regression analysis: Training Testing Validation Framework

Iteration	Training Zone	Testing Zone	Testing Objective
1	[C] (70%)	[C] (30%)	Overall Performance
2	[A]	[B]	Highest band
3	[B]	[A]	Lowest band

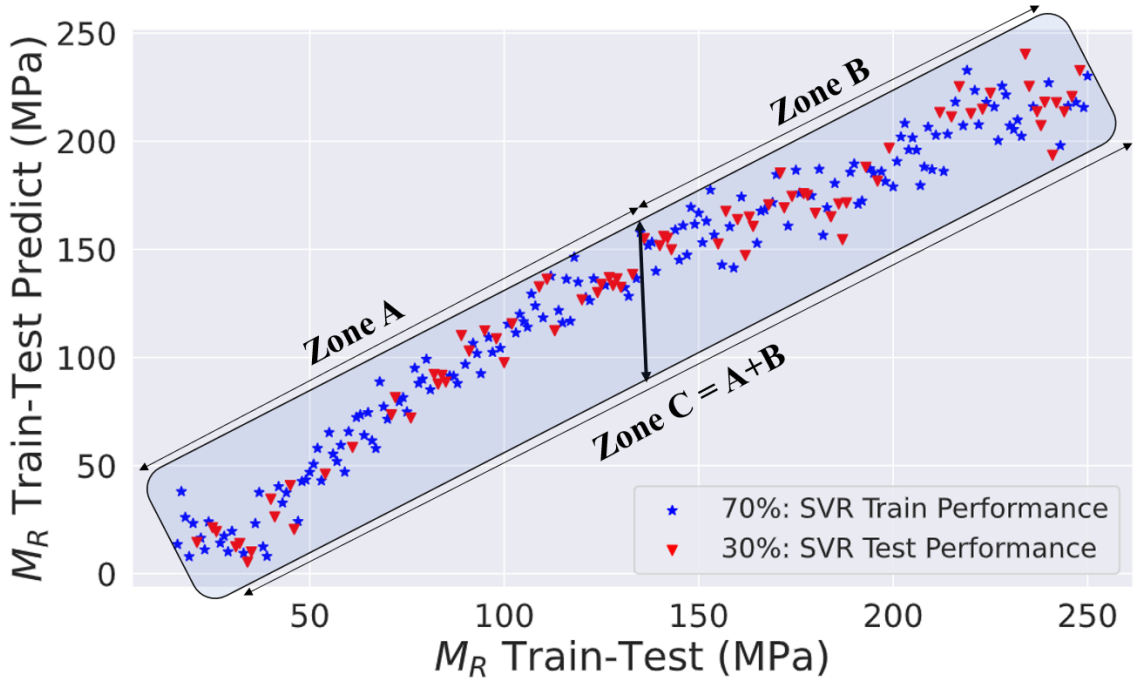

Figure 4.8 – Regression analysis: M_R Train-Test split

Table 4.4 and Figure 4.8 illustrate the data partitioning process employed in SVR regression analysis using the Multi-Iteration Framework. Unlike classification analyses, which utilize stratified sampling to ensure class balance, regression analysis adopts random sampling for the train-test split (typically 70% training, 30% testing). This deviation stems from the primary objective of regression models: capturing the underlying relationships between features D_S and target variable labels M_R. However, there is the risk of data leakage (improper inclusion of testing data into the training process as it leads to overly optimistic model performance estimates and undermines the model's generalizability to new, unseen data). The Multi-Iteration Framework addresses this issue, ensuring the model learns from an independent set of features. This preserves data integrity by safeguarding the original distribution and prevents overfitting by avoiding data leakage.
Moreover, the Multi-Iteration Framework enables the iterative assessment of the SVR model's performance across a range of M_R values, potentially capturing various soil conditions. Consequently, the dataset is partitioned into three zones A), B), and C), as shown in Figure 4.8. The middle line in the figure is set at 125 MPa, representing the closest midpoint of equality between 16 and 250: Zone A (16-125 MPa) denotes the initial half of the data or the lower band zone, Zone B signifies the upper band of the data (125-250 MPa), and Zone C denotes the fusion and concatenation of both zones, forming a unified zone (16-250 MPa).
In other words, this framework provides an evaluation strategy, with each iteration con-

centrating on distinct facets of the model's performance
As it depicts Table 4.4 and Figure 4.8 in Iteration 1: The primary objective of this iteration is to assess the model's ability to generalize. A portion of the training data zone (Zone C) is used for testing overall (typically 70% training, 30% testing).
However, in Iterations 2 & 3, the focus shifts towards assessing performance across the spectrum of M_R values by focusing on the model's performance in specific M_R value ranges. Zone assignments (A, B) likely correspond to distinct ranges within the overall M_R value dataset. In iterations 2 and 3, allocating Zone A and B for the highest band and Zone B and A for the lowest band, respectively, allows us to assess the model's proficiency in estimating M_R values for potentially varying soil conditions, including both stiffer and damaged soil conditions.

4.4.3 Inverse model overall performance

This section conducts an initial regression analysis, analyzing the overall performance of SVR in estimating the M_R based on D_S values. The investigation encompasses different scenarios, as shown in Figure 4.9 SVR regression results indicate promising performance. For instance, in Iteration 1 (Zone C), where the primary goal is to evaluate generalization, the model achieves a high coefficient of determination (R^2) of 95%. This suggests that the model captures a portion of the variability in the data and demonstrates healthy performance in predicting M_R values.
Subsequent iterations (2 & 3) focus on assessing performance across the spectrum of M_R values by examining specific ranges. Zone assignments (A, B) likely represent distinct M_R value ranges within the dataset. The high (R^2) values observed across iterations (93% and 97%) indicate the continued strong performance of the model in capturing the relationships between deflection slope features and M_R values. This suggests that the model's predictive ability extends beyond generalization to specific M_R value ranges, enabling reliable estimation of soil elastic modulus across diverse soil conditions, including potentially damaged soil conditions.
However; further analysis is essential to comprehend the variance in the results, particularly to investigate the underlying reasons for the observed decrease in the coefficient of determination (R^2) value. This forthcoming section will delve deeper into the root cause of this reduction, explaining the factors influencing the model's performance.

4.4.4 Regression model performance analysis

This section is of paramount importance as it delves into the underlying reasons for the observed decrease in the coefficient of determination (R^2) value for evaluating the performance of SVR models in predicting soil properties. The investigation delves into the

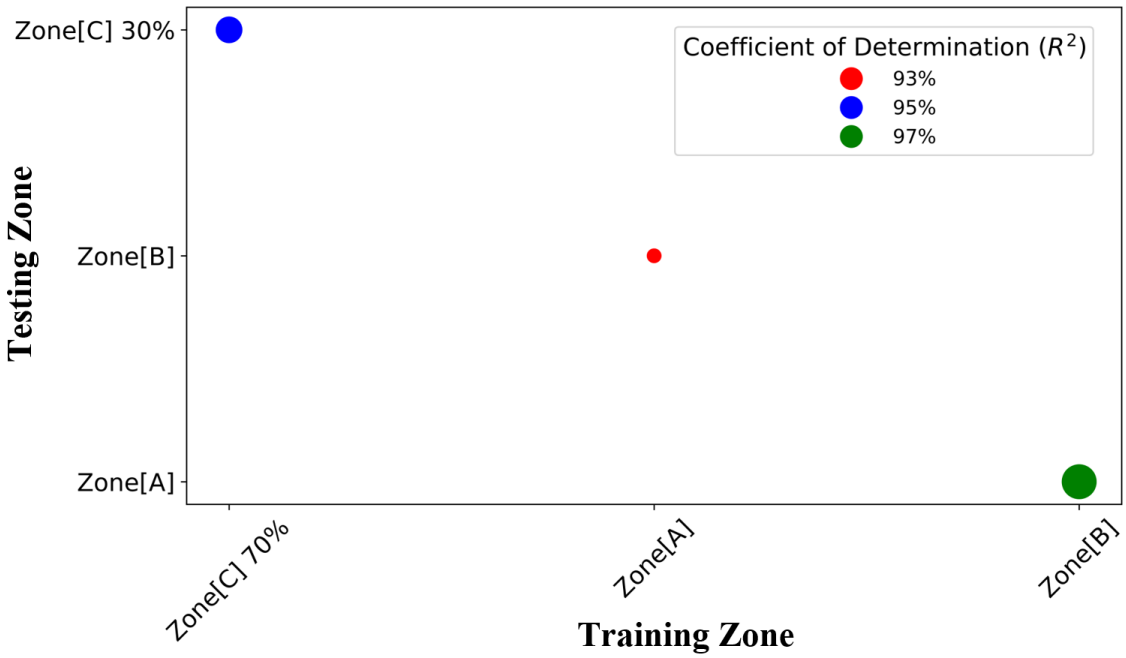

Figure 4.9 – Evaluation metrics for a classification model analysis

effect of noise on the inverse SVR regression model's performance in estimating M_R.

The study undertakes a quantitative comparison of two SVR models to assess the impact of noise on the prediction accuracy of M_R. The two models contrast in their training data conditions—Model 1 uses noise-influenced data, and Model 2 utilizes noiseless data, providing a framework to examine how noise affects model performance.

In terms of quantitative metrics; model 1 exhibited a coefficient of determination (R^2) of 0.951 and a Pearson correlation coefficient (R) of 0.976. These high values indicate a strong positive correlation between the model predictions and the actual M_R values from D_S. However, the model also reported a Root Mean Squared Error (RMSE) of 14.784 MPa, suggesting an average error in predictions, which is a result of noise within the data. On the other hand, Model 2, trained on noiseless data, demonstrated even stronger correlation values with an (R^2) of 0.997 and an (R) of 0.999. Additionally, it achieved a much lower (RMSE) of 3.618 MPa. These stats only suggest a tight fit between the predicted values and the actual and point to superior performance when noise is absent from the modeling data.

In the analysis, as indicated by the red circle, clusters of deviated data are evident in the top and bottom portions. These deviations are primarily attributed to the presence of noise. When the SVR model is tested without noise, these noise-related clusters disappear. This comparison highlights the degradation of model performance due to noise. The quantitative disparity between the two models underscores this impact. Under ideal, noise-free conditions, Model 2 captures a considerable proportion of variance in M_R data

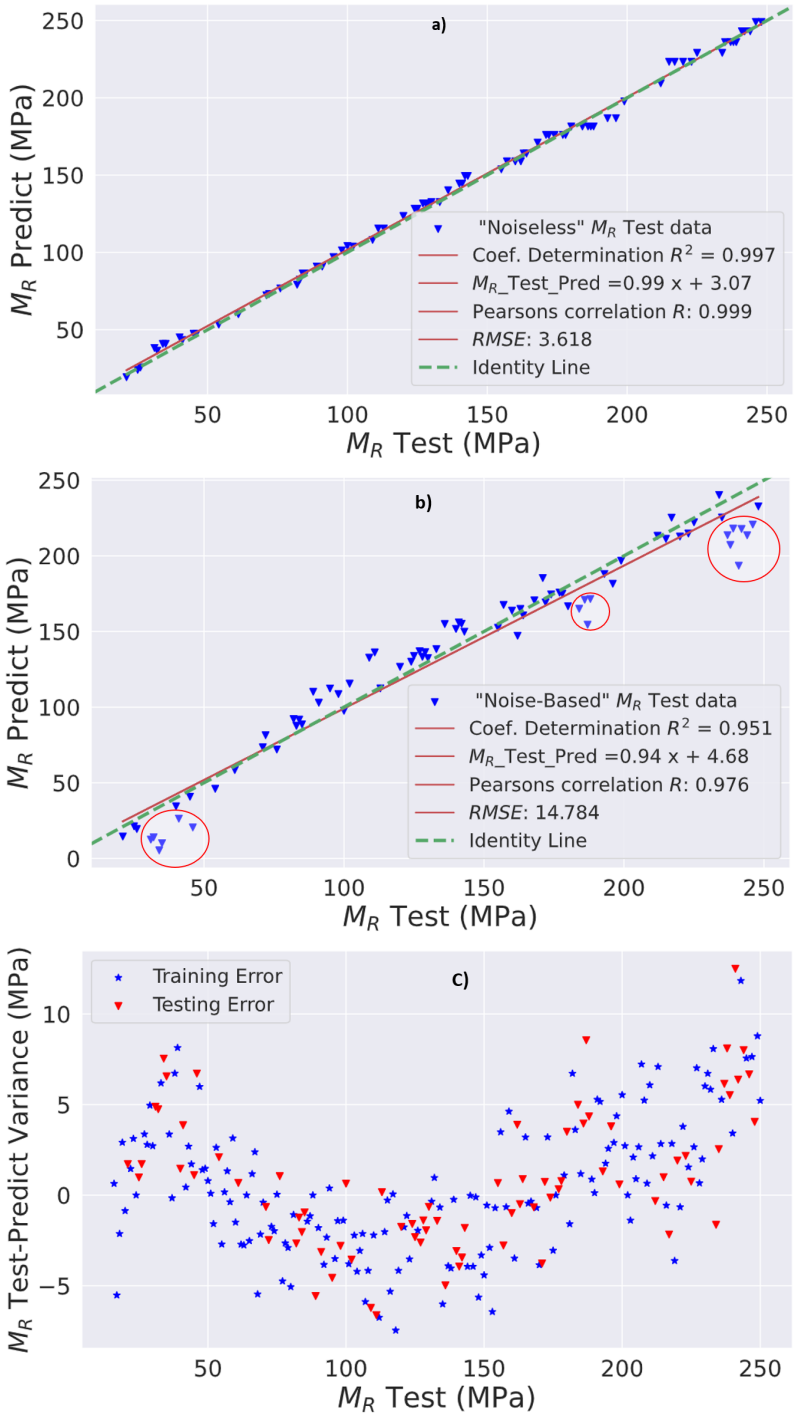

Figure 4.10 – SVR model analyses: (a) Noiseless regression model, (b) Noise-based regression model, (c) Variance analysis (actual to predict error).

and exhibits a substantially lower prediction error. Conversely, Model 1, affected by noise, shows an elevated RMSE and slightly lower R, reflecting the adverse effects of noise. These

effects include increased predictive error and reduced accuracy in capturing the underlying soil behavior.

In the same context, a variance analysis was conducted to assess the uncertainty embedded in the SVR model quantitatively. The outcomes of this analysis, illustrated in Figure 4.10 C), involved an intricate examination of the predicted values compared to the actual test values. Approximately 95% of the differences between these values fell within an acceptable range of ±15 MPa. This range is deemed sufficient, considering the inherent variability of the data. It also aligns with the current state-of-the-art practices in this domain [131].

To this end, the statistical and physical analysis provided by the variance analysis underscores the robustness of the SVR model, showcasing its efficiency in navigating and mitigating uncertainties within the dataset. In essence, this analysis shows the critical influence of noise on the accuracy of predictive modeling using SVR for soil properties. Therefore, future applications should consider applying techniques such as Kalman Filtering or Fourier Transform Filtering during data preprocessing to reduce noise and improve predictive accuracy in real-world environmental conditions.

By acknowledging noise's impact and employing appropriate data processing strategies, pavement engineers could harness ML models more effectively, enhancing accuracy in M_R prediction and ultimately facilitating better-designed and more durable pavements.

Thus, before delving into the sensitivity analysis, it is essential to address the aspect that could influence the model's performance: the tuning of hyperparameters, which need to be carefully configured to ensure the SVR model generalizes well to unseen data while avoiding overfitting or underfitting. This preliminary optimization is foundational to the robustness and reliability of the SVR model, setting the stage for exploration in subsequent sections, particularly in the context of sensitivity analysis.

4.5 Influence of temperature uncertainty on estimating soil Modulus from deflection slope

Table 4.5 – Characteristics of the pavement structure used to derive the forward model

Layer (i)	Thickness (m)	Material	E_i (MPa)	ν	Interface	°C
1	0.06	HMA	7000	0.35	(1) bound	5-25
2	0.09	BC-g2	9300	0.35	(1) bonded	5-20
3	0.09	BC-g2	9300	0.35	(1) bonded	5-20
4	∞	M_R	**125**	**0.35**	(1) **bonded**	**15**

As per the forward model structure presented in (Table 4.5), the study investigates the influence of uncertain temperatures on estimating soil modulus M_R using TSD deflection slope D_S simulated measurements. This research uses the SVR model to examine the correlation between temperature uncertainty and soil modulus estimation. A case study explores multiple scenarios with varying levels of temperature uncertainty and elastic modulus (E_i) values for different layers.

The data are organized into four distinct cases with differing degrees of uncertainty. Each case includes information on temperature profiles, which serve as input features of the SVR model beside D_S for the estimation of M_R as 125 MPa

The critical findings from the study present that,

— Case 1 (Table 4.6): It is the most challenging scenario, where both temperature and modulus values for all pavement layers are unknown, and estimation errors range from 6.4% to 18.4% (Table 4.6). This highlights the principle uncertainty associated with M_R estimation without temperature data. Furthermore, Figure 4.11 confirms this high level of uncertainty, with wider variance bands indicating substantial prediction variability due to the lack of temperature information across layers.

— Moving on to Case 2, Table 4.7, where temperature data is introduced only for the first layer ($L1$), a marginal improvement is observed in prediction errors compared to Case 1. Errors still range from 3.2% to 16%, but even partial knowledge of temperature for the surface layer contributes to a reduction in uncertainty (Table 4.7).

— This trend continues in Case 3 (Table 4.8), where temperature information becomes

available for the second layer ($L2$) only, resulting in a more substantial improvement in prediction errors, ranging from 2.4% to 9.6% (Table 4.8).

— However, in Case 4 (Table 4.9), where temperature information is available only for the deepest layer ($L3$), prediction errors remain comparable to previous cases, ranging from 1.6% to 6.4%. This suggests that temperature knowledge in the bottom layer could be highly informative for M_R estimation compared to any other layer.

Overall, the comparative analysis across these four cases reveals a hierarchy in the importance of temperature data for different pavement layers.

Moreover, while information from any layer improves estimation accuracy, knowledge of the deepest layer appears particularly valuable. This underscores the necessity of incorporating temperature data into pavement M_R estimation methodologies to achieve reliable results. Future research could delve into the underlying physical mechanisms explaining the effectiveness of layers' temperature data.

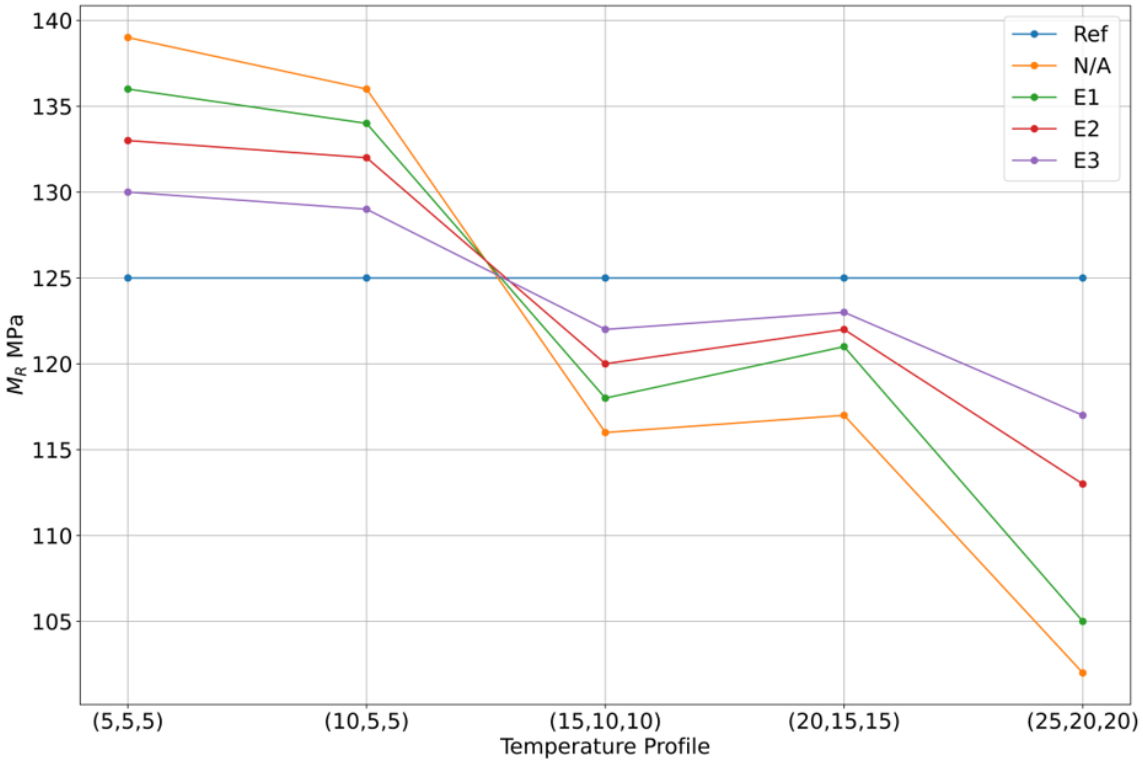

Figure 4.11 – Influence of temperature uncertainty on M_R modulus from D_S

Table 4.6 – Both temperature and modulus values of all layers (L_1, L_2, L_3) are unknown

Θ °C			E_i **(MPa)**			M_R	**Δ**
L_1	L_2	L_3	E_1	E_2	E_3	(MPa)	%
-	-	-	-	-	-	139	11.2%
-	-	-	-	-	-	136	8.8%
-	-	-	-	-	-	116	7.2%
-	-	-	-	-	-	117	6.4%
-	-	-	-	-	-	102	18.4%

Table 4.7 – Only temperature and modulus values for the first layer (L_1) are known

Θ °C			E_i **(MPa)**			M_R	**Δ**
L_1	L_2	L_3	E_1	E_2	E_3	(MPa)	%
5	-	-	11405	-	-	136	8.8%
10	-	-	9310	-	-	134	7.2%
15	-	-	7000	-	-	118	5.6%
20	-	-	4690	-	-	121	3.2%
25	-	-	3245	-	-	105	16%

Table 4.8 – Only temperature and modulus values for the second layer (L_2) are known

Θ °C			E_i **(MPa)**			M_R	**Δ**
L_1	L_2	L_3	E_1	E_2	E_3	(MPa)	%
-	5	-	-	15090	-	133	6.4%
-	5	-	-	15090	-	132	5.6%
-	10	-	-	11880	-	120	4%
-	15	-	-	9300	-	122	2.4%
-	20	-	-	6120	-	113	9.6%

Table 4.9 – Only Temperature and Modulus values for the third layer (L_3) are known

Θ °C			E_i **(MPa)**			M_R	**Δ**
L_1	L_2	L_3	E_1	E_2	E_3	(MPa)	%
-	-	5	-	-	15090	130	4%
-	-	5	-	-	15090	129	3.2%
-	-	10	-	-	11880	122	2.4%
-	-	15	-	-	9300	123	1.6%
-	-	20	-	-	6120	117	6.4%

4.5.1 Temperature and noise uncertainty: Key Findings

1. Bituminous materials like asphalt are highly responsive to temperature variations, undergoing critical changes in stiffness and mechanical properties. Understanding this temperature sensitivity is crucial for effective pavement management.
2. Pavement engineers could improve inverse model optimization by utilizing prior knowledge of known pavement structures, focusing on the top layer (E_3), which impacts (M_R) determination. Integrating these layer properties into analysis methods substantially enhances soil modulus prediction accuracy. By incorporating data from these structures into the core of the inverse model, engineers could achieve more precise estimations of soil modulus and overall pavement performance.
3. Seasonal temperature variations could significantly impact deflection data for pavement assessment. Excessively high or low temperatures could distort values, leading to inaccurate pavement condition assessments. Even though temperature correction factors simplify measurement interpretation, addressing associated uncertainty is essential to maintaining accuracy in pavement performance assessments.
4. Measurement errors in deflection slope curves often stem from temperature uncertainty and external factors like noise. This combined effect likely diminishes the accuracy of deflection slope estimations.

In summary, temperature, seasonal variations, the properties of overlying pavement layers, and measurement noise are critical factors in pavement evaluation. Integrating these factors into analysis methods enables engineers to obtain more reliable pavement condition assessments and optimize pavement design and maintenance strategies for improved performance and durability.

4.6 Conclusion

This Chapter presents an innovative method for estimating soil resilient modulus (M_R) by integrating simulated Traffic Speed Deflectometer (TSD) data with a machine learning (ML) supervised model, specifically utilizing Support Vector Machine (SVM) for classification (SVC) and regression (SVR) analyses based on a previously developed numerical forward model database.
The findings from both classification and regression inverse analyses reveal some insights and demonstrates the efficacy of ML in estimating soil M_R from simulated D_S data across various test scenarios, highlighting its ability to effectively capture the D_S-M_R relationship.

However, noise in the data adversely affects model performance, leading to increased prediction errors and reduced accuracy. Despite this, the SVM model demonstrates robustness in handling uncertainties within the dataset, with many prediction errors falling within an acceptable range. Thus, implementing noise reduction techniques during data preprocessing is essential for enhancing model accuracy, especially in scenarios with noisy real-measurement data.

Additionally, addressing data imbalance within the distribution of M_R class data requires fine-tuning hyperparameters to mitigate potential biases during the model learning phase. The research underscores the influence of the combination of temperature and noise on pavement behavior estimating accuracy.

Temperature sensitivity of bituminous materials like asphalt directly impacts deflection behavior and pavement performance assessments. Incorporating temperature data, mainly focusing on in-depth layer properties, enhances the accuracy of M_R predictions, leading to a more comprehensive understanding of pavement response under varying thermal conditions.

Nontheless, the combined effects of temperature uncertainty and noise pose challenges in deflection slope D_S measurements, complicating pavement response interpretation. Thus, robust noise reduction techniques and meticulous temperature data handling are essential to ensure accurate pavement performance assessments.

This multidimensional approach advances accurate modulus estimation and contributes to ML in pavement engineering.

However, further exploration of the model's performance and adaptability to diverse environmental conditions is necessary for broader applicability. The upcoming chapter will present future validation through experimental testing to examine the gap between numerical modeling and practical implementation, strengthening the research's impact on pavement engineering practices.

Chapter 5

Experimental Validation

5.1 Introduction

This chapter delves into the experimental validation of the numerical model and inversion process developed in the preceding chapters. However, rather than directly estimating soil resilient modulus (M_R), the focus shifts to using Machine Learning (ML), specifically Support Vector Machine (SVM), to estimate the surface modulus (E_1) from experimental deflection slope (D_S) measurement data. This decision stems from two primary reasons: The scarcity of experimental labeled data for M_R. Secondly, the intention was to assess the model's generalization capabilities by leveraging different data types with diverse distributions and scales .

To achieve these objectives, a systematic methodology was implemented, as depicted in Figure 5.1. The experimental dataset originated from bearing capacity tests conducted within the I-Street project [38], spanning four months at the fatigue Carousel of the University Gustave Eiffel (formerly IFSTTAR). Throughout the experimental setup, adherence to French pavement standards [144] was ensured, maintaining a dual-wheel load configuration and velocity. Instruments such as strain gauges [145], temperature sensors, and a Geophone [146] were deployed to capture pavement behavior data.

However, a notable challenge encountered during this experimental phase was the insufficient availability of relevant structured data (labeled), which is indispensable for machine learning (ML) applications. To overcome this limitation, numerical data augmentation techniques were employed via the simulation of Geophone measurements, enabling the construction of a hybrid database comprising synthetic and experimental data.

Subsequently, the experimental forward model underwent two approaches: global and local. In the global approach, all seven original features from the dataset were utilized as input for the SVM model. Conversely, the local approach, based on Principle Component Analysis (PCA) [147, 148], employed dimensionality reduction by utilizing two principal components (PCs) derived from the data as input for SVM.

Ultimatly, as depicted in Figure 5.1 an advanced parametric validation encompassing both classification and regression inverse models was conducted, aimed at optimizing the model's performance and validating its effectiveness and efficiency.

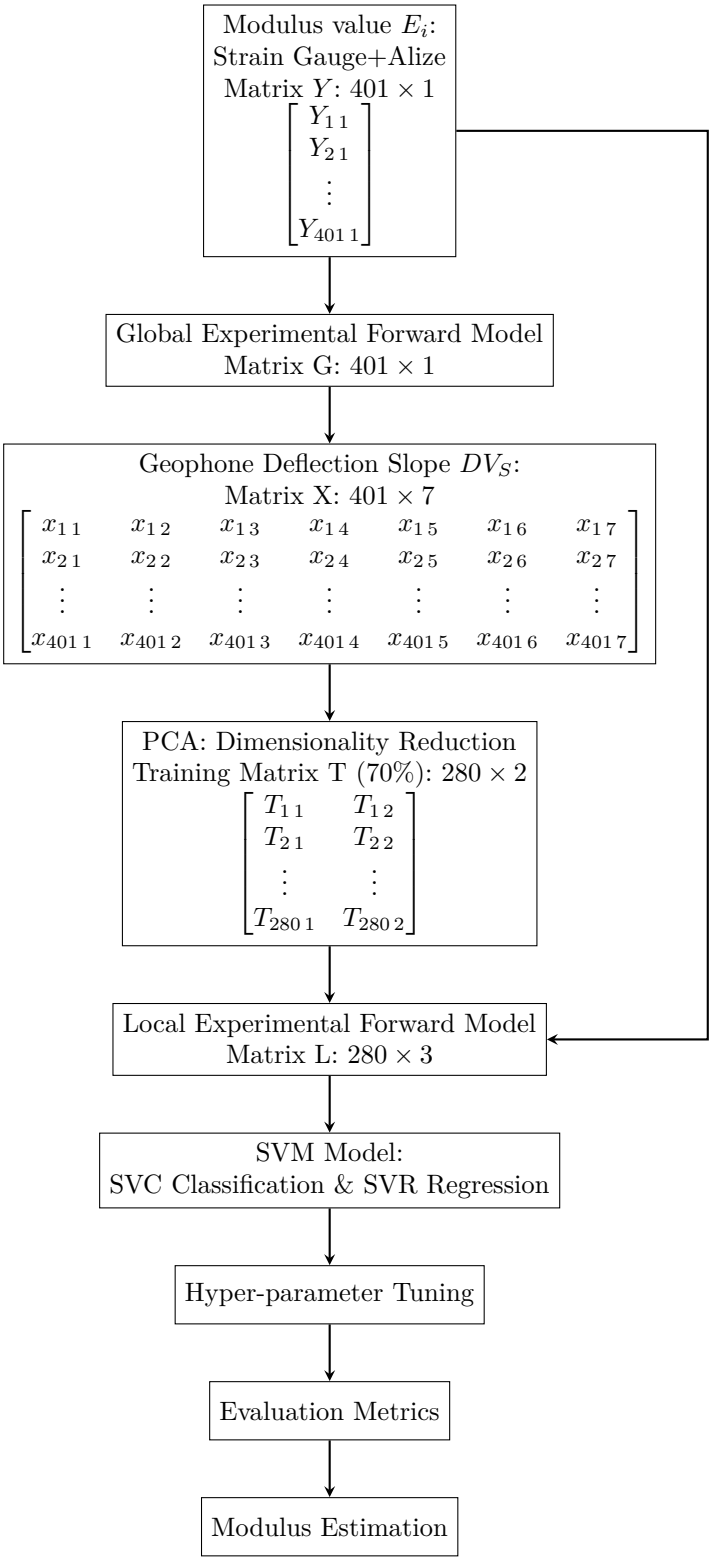

Figure 5.1 – ML based Global Approach for the Estimation of (E_1)

5.2 Experimental forward model Framework

5.2.1 Data acquisition

The research data was collected at the University Gustave Eiffel Nantes as part of the I-street project. The data collection involved the use of an advanced outdoor road traffic simulator known as the fatigue carousel, as shown in figure 5.2, which is a specialized facility designed for simulating real-world road conditions under the influence of heavy traffic loads [38].
The fatigue has a 40-meter diameter. It is equipped with four loading arms, and each arm has the capability to carry dual-wheel loads with a maximum capacity of thirteen tons and can operate at speeds of up to 100 km/h [144].
One of the notable features of this simulator is its ability to replicate the deterioration experienced by a moderately used road over twenty years in just a brief two-month testing interval [144].
In terms of load configuration, the consolidation simulation involved executing 30,000 spinning charging cycles after pavement construction. This added up to 120,000 loadings distributed across the four carousel arms. The simulation maintained a constant speed of approximately 22.5 m/s and utilized a dual-wheel load of 65 kN, aligning with France's pavement load limit [146].

Figure 5.2 – The pavement fatigue Carousel at Univ. Eiffel Nantes [144].

5.2.2 Pavement structure

Table 5.1 – Characteristics of the experimental pavement structure

L_i	h (m)	Material	E_i (MPa)	ν	Interface	(°C)
1	0.10	**HMA**	**2000 - 10000**	**0.35**	**(1) bonded**	**5 - 35**
2	0.05	UGM	126	0.35	(1) bonded	5 - 35
3	0.25	UGM	126	0.35	(1) bonded	5 - 35
4	∞	M_R	104	0.35	(1) bonded	5 - 35

The characteristics data of the pavement structure in this study were obtained through bearing capacity tests, presented in Table 5.1. Whereas, (L_1), the uppermost layer, constructed with a Hot Mix Asphalt (HMA) material with broad variation range of (E_1), indicating that both traffic loads and temperature play a basic role in its fatigue behavior. In the same structure, (L_2) and (L_3) consist of Unbound Granular Material (UGM), chosen with specific fixed attributes for the sake of analysis simplicity. (L_4) with its soil modulus (M_R), which corresponds to the third platform (Pf_3), features a comparatively lower modulus value than others.
Additionally, uniform deformation is obvious in this structure due to consistent Poisson's ratio, aided by strongly bonded interfaces that enhance structural integrity along with fixed temperature profiles related to measurements taken at specific depths from the surface, at 2.5 cm, 10 cm, and 30 cm respectively.

5.2.3 Measurement instruments

The pavement instrumentation utilized in this experimental study consisted of strain gauges, temperature sensors, and a Geophone sensor as shown in Figure 5.3.
Dynatest PAST-IIA strain gauge is utilized for the measurement of strain, which represents the instantaneous surface deformation of a material under the Carousel arms, particularly within the bituminous surface layer at a depth of 9 cm [145]. These strain gauges boast a measurement range of ± 1500 μ strain (microstrain), with a sensitivity of 0.11 N/μ-strain. Importantly, they are designed to withstand the high temperatures encountered during asphalt concrete construction, reaching 150 °C. Furthermore, alongside the strain gauge,

a vertically oriented Geophone Sensor, specifically the Model GS-ONE LF from Geospace Technology [149], is employed, boasting a sensitivity of 89.2 V/m/s, a natural frequency

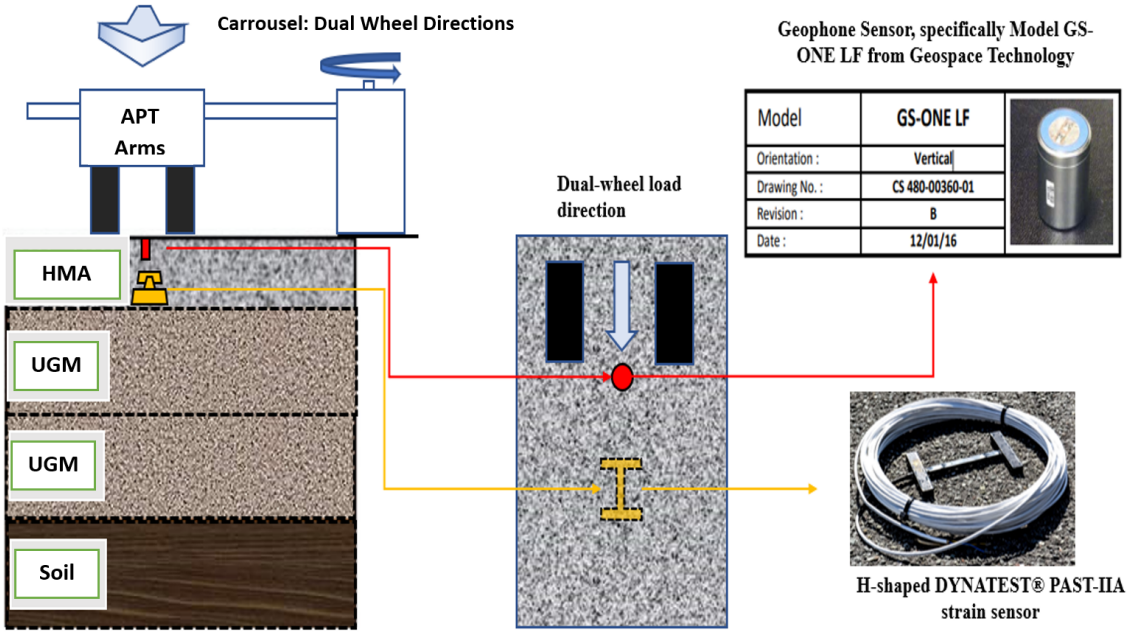

Figure 5.3 – Strain gauge and Geophone sensor orientation along with the load direction

of 4.5 Hz, and a closing resistance of 47 kΩ. Geophone sensors are commonly utilized to measure deflection slope resulting from the motion of carousel dual load arms [146].
Furthermore, real-time temperature data is collected using temperature sensors that are placed at various depths, including the surface, 2.5 cm, 10 cm, and 30 cm within the bituminous layer. The objective is to capture variations in the structure temperature profile at different layers, which can influence its mechanical properties.
After defining the pavement and structure and the measurement instrumentation's, a series of spinning charging cycles was applied as a consolidation step on the pavement. The number of loads applied during this consolidation step was 120,000, which, considering the four arms of the carousel, corresponds to a total of N = 4 arms × 30,000 cycles = 120,000 loadings. The load applied by the dual-wheel load during the entire experimental test was 65 kN at a velocity of 12.5 m/s, which corresponds to the maximum load allowed on pavements in France.
In the upcoming section will explore the data processing techniques and measurement principles utilized for both the Geophone and Strain Gauge sensors for constructing the experimental forward model database that to be used by machine learning algorithms (SVM) for the estimation of the pavement elastic modulus.

5.3 Data processing

5.3.1 Strain Guage

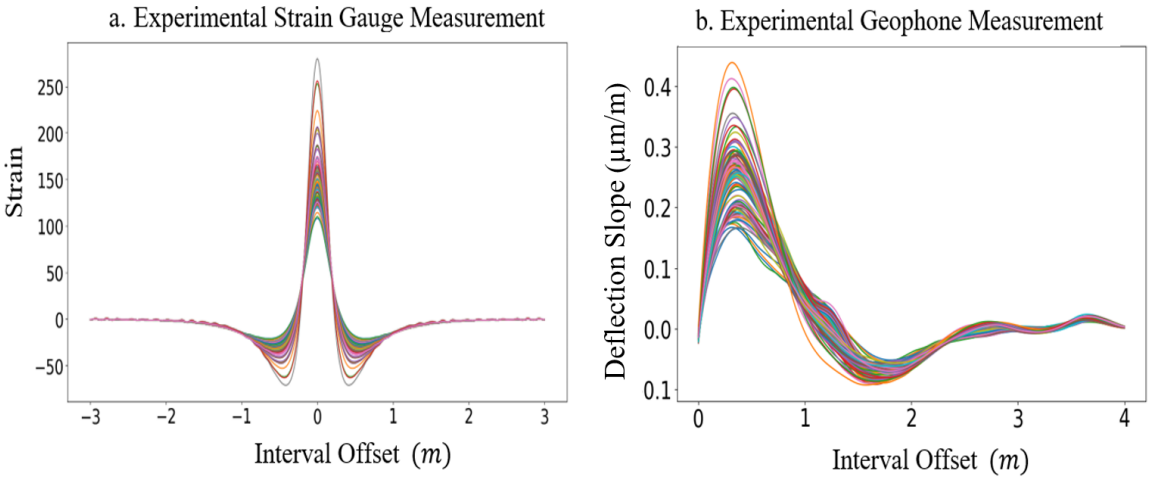

Figure 5.4 – Forward Model Components: a) Strain Gauge, b) Geophone Measurement

In this experimental study, seventy-one (71) measured data points were simultaneously collected from the predefined pavement structure presented in Table 5.1. The mechanism for collecting measurement data of strain and deflection slope (D_S) is as follows: In this configuration, the center of the two twin loading wheels was traversed directly above the embedded strain gauge during the spinning cycles. The signal from the gauge comprises measurements over time, with each peak indicating an extension of the gauge whenever a dual-wheel load passes over the sensor.

Given that the velocity of the loading arms is known, it becomes feasible to infer the distance of the dual-wheel load from the gauge by considering the time associated with the peak as the zero distance. Consequently, the strain signal as a function of the position of the loading arms, with distance ranges set between -3 and $+3$ meters, has been deduced as shown in Figure 5.4 (a).

Following the collection of 71 strain measurements, the data will be inputted into Alize software to compute the corresponding surface modulus values for each measurement. When applying machine learning techniques, these surface modulus values will serve as the dependent variables (labels).

5.3.2 Geophone Measurement Process

The geophone [149] recorded the Vcc output voltage as a function of time, which represented the vertical displacement velocity, also referred to as the deflection velocity. Each arm of the carousel produced distinct signal peaks associated with corresponding time

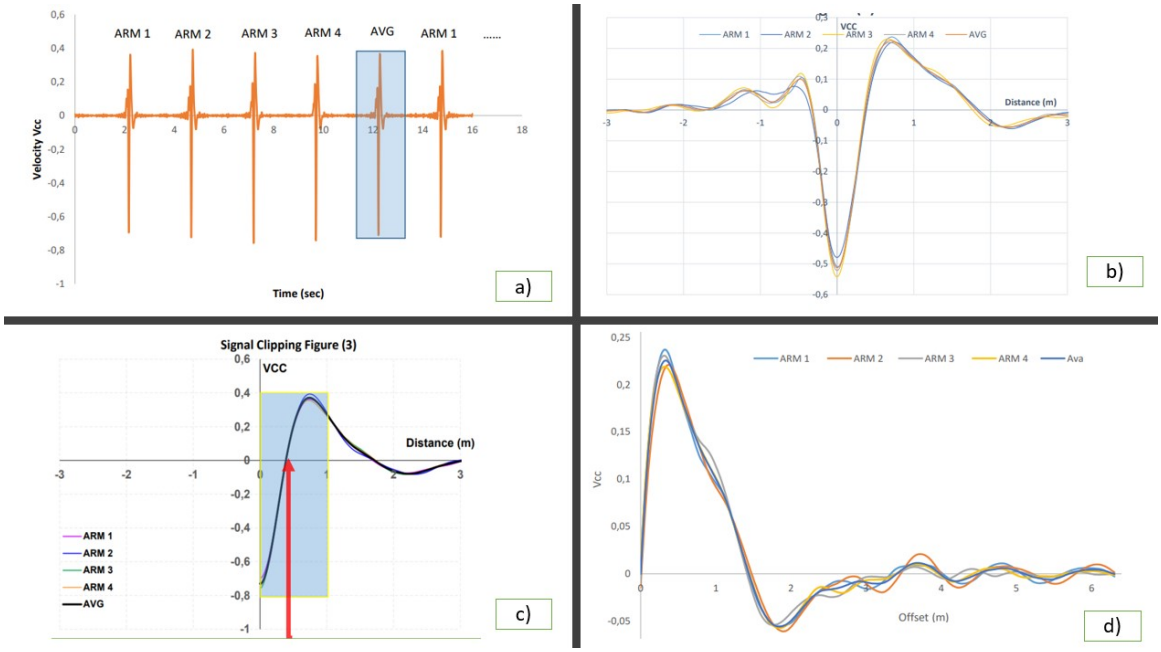

Figure 5.5 – Geophone Measurement: a) Time-based signal, b) Non-symmetric full signal, c) Absolute value, d) TSD equivalent

intervals.

as shown in Figure 5.5 a), the geophone operated at a frequency of 600 Hz, capturing 600 samples per second with a time interval of 0.0016 seconds between each recorded data point. The signals were initially captured in the time domain, showing variations over time as the carousel arms passed over the geophone. To convert these time-domain signals into the spatial domain, the physical characteristics of the carousel were taken into account. The radius of the carousel was 19.5 meters, and the perimeter of the 6th section was 122.52 meters. The rotational speed of 12.2 meters per second was used to calculate the distance covered by each Vcc value.

A conversion factor was determined by dividing the velocity by the time step, enabling the computation of the distance corresponding to each Vcc value. This transformation allowed the representation of the signal in the spatial domain, with distances ranging from -3 meters to +3 meters. The maximum signal occurred at 0 meters, which corresponded to the loading point where the carousel arm passed closest to the geophone as shown in Figure 5.5 b).

The analysis concentrated on the positive segment of the signal, ranging from 0 to +3 meters, to align with the measurement principles of the Traffic Speed Deflectometer (TSD). The negative portion of the signal, between -3 and 0 meters, was excluded from consideration due to noise, ensuring the reliability of the data. Thus, to measure the signal's magnitude, the absolute value of the Vcc signal was calculated. By identifying the abso-

lute minimum value, a new reference point for zero distance was established Figure 5.5 c). To derive the deflection velocity from the recorded Vcc signals, the geophone's sensitivity, specified as 89.4 V/m/s in the factory datasheet, was used. The deflection velocity was obtained by dividing the Vcc signal by this sensitivity factor. Additionally, to compute the slope or gradient of the deflection velocity, the signal was divided by the instantaneous vertical velocity of the carousel arm, which was approximately 12.5 meters per second Figure 5.5 d) and in Figure 5.4 (b).

5.3.3 Data augmentation:

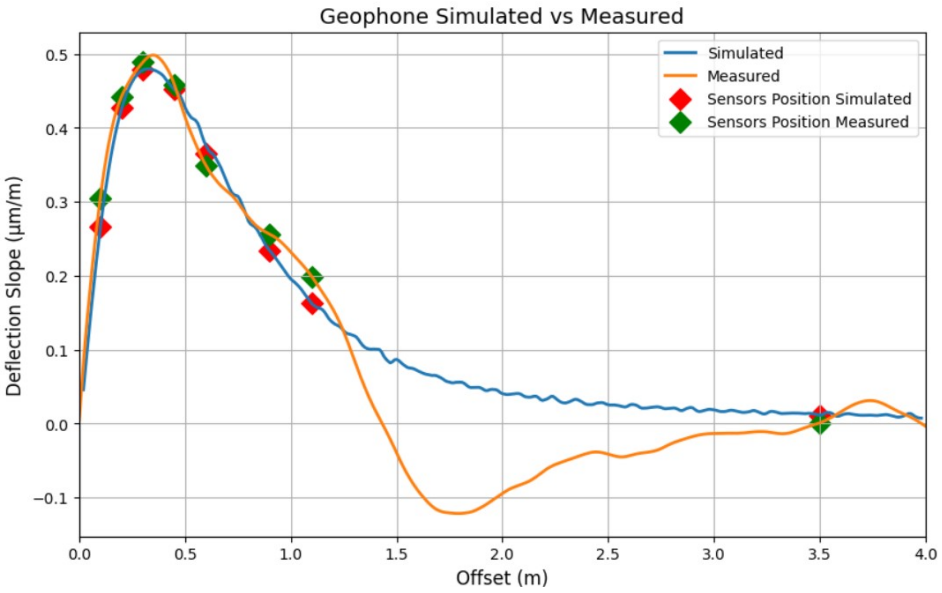

Figure 5.6 – Forward Model: Measured to simulated Geophone

Due to the limited dataset containing only 71 measurement labelled outputs, numerical data augmentation was employed to enhance the effectiveness of learning and training processes via simulating the Geophone deflection slope measurement. The simulation process followed similar steps and hypotheses presented in Chapter II for simulating the deflection slope behavior under TSD. The only difference was systematically varying the E_1 instead of M_R, with values between 2000 and 10000 MPa in intervals of 20 MPa. This augmentation process resulted in a total dataset of 401 cases, comprising 71 actual measurements and 330 simulated ones as shown in Figure 5.6.

To conclude, the strain gauge data was utilized as input for Alizé software to extract the equivalent Modulus value (E_1) for each measurement, as depicted in Figure 5.4 (a). These E_1 values served as labels for the Support Vector Machine (SVM) algorithm, constituting the input variable. Additionally, seven independent variables or features were extracted from Geophone measurements as depicted in Figure 5.4 (b), corresponding to the Traffic

Speed Deflectometer (TSD) sensor positions on the deflection slope curve, similar to what have been presented in the numerical chapters.
At this stage, the subsequent section will undertake exploratory data analysis for the deflection slope database. This analysis aims to lay the groundwork for developing an experimental inversion model for both the regression and classification for estimating E_i.

5.3.4 Forward Model: Exploratory Data Analysis

In this analysis phase, an Exploratory Data Analysis (EDA) of D_S is conducted to gain valuable insights into the deflection slope characteristics. Key observations resulting from statistical and physical analyses are summarized. These insights are derived from the data depicted in Figure 5.7, illustrating the characteristics of input features Sn_1 to Sn_7.

— Figure 5.7 (a), presents a box-and-whisker plot that illustrates the trend observed in the D_S data set. The plot depicts a gradual decrease in the mean and standard deviation values of D_S as the distance from the loading points increases, indicating a diminishing variability trend towards the reference sensor.
Conversely, this observed behavior deviates from the trend illustrated in Figure 3.6 of Chapter II concerning the M_R forward model. In that model, the mean and standard deviation of D_S increase as the distance from the loading points increases, with nearly zero values at the loading point and the reference sensor. This observation corroborates the established hypothesis that the deflection slope is influenced by the position of the TSD load and the sensor's location.

— Upon analysis Figure 5.7 (b), calculating the interquartile range (IQR), Q3 - Q1, reveals the data's variability. Larger IQR values indicate more variability. $S7$ shows the most minor IQR variation, while $S1$ exhibits the highest IQR variability. This observation suggests that when estimating E_1, the deflection slope near the loading point displays higher variability but gradually stabilizes with increasing distance. Consequently, the behavior of E_1 appears to be particularly sensitive to upstream sensors, such as Sn_1 and Sn_2, compared to those situated farther away, like Sn_6.
However, these findings diverge from those obtained in the M_R forward model (Figure 3.7 Chapter II), where $S1$ shows the lowest IQR variation, and $S7$ demonstrates the highest IQR variability. In the context of M_R, the deflection slope remains consistent near the loading point but becomes more variable as the distance increases. Estimation of M_R notably relies on downstream sensors, such as Sn_6 and Sn_7, rather than those in closer proximity, like Sn_1 and Sn_2.
Hence, the placement of sensors influences the assessment of pavement deflection behavior under TSD, with specific sensors proving more effective in capturing deflection behavior depending on their precise location and the targeted E_i.

— These findings are consistent with most of the previous studies, exemplified by [79] (discussed in Chapter II), which focused on benchmarking the structural condition of flexible pavements using deflection bowl parameters (BLI, LLI, MLI). However, these parameters are derived through a simplified approach that excludes the measurement of other sensors positioned beyond the defined distance scope of each one of the three parameters. It is obvious from Figure 5.7 that these additional sensors still provide valuable information about pavement behavior. Disregarding them could potentially result in a loss of accuracy associated with the utilization of these simplified methods, emphasizing the need for comprehensive data collection and analysis in pavement assessment.

The subsequent section will quantify the impact and influence of reducing the data dimensionality on regression and classification models for estimating E_i using dimensionality reduction techniques.

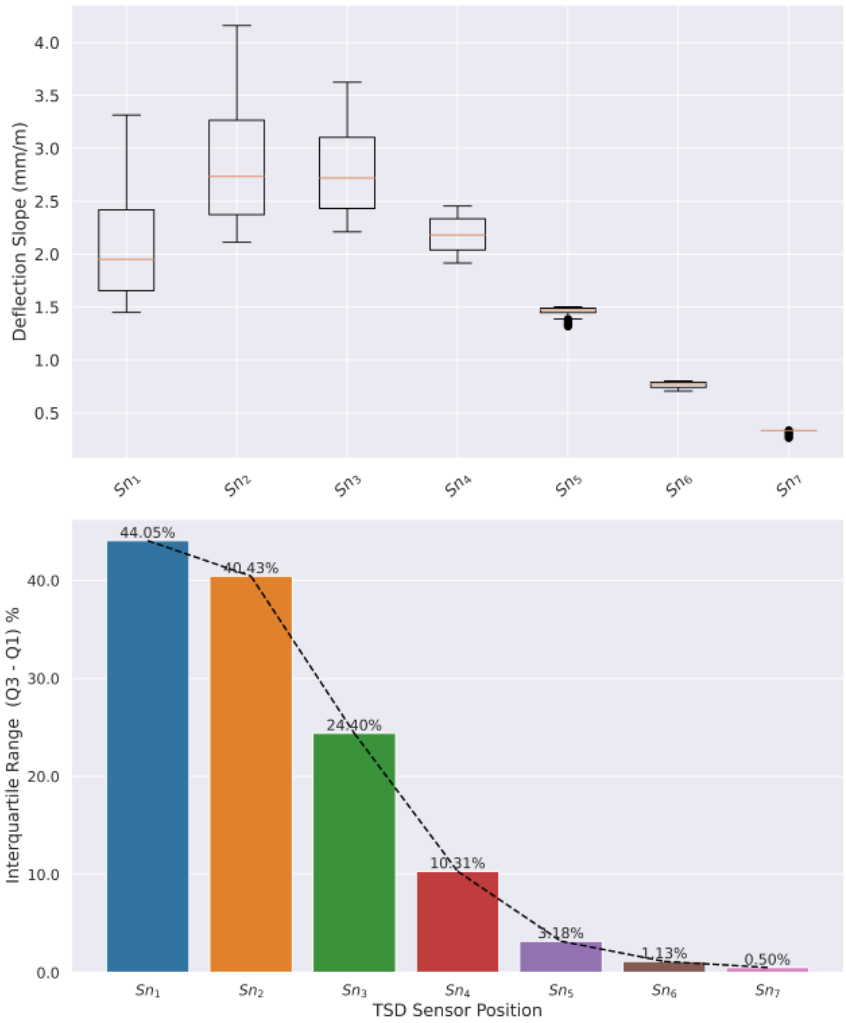

Figure 5.7 – D_S Exploratory Data Analysis a) S_n Characteristics b)IQR ratio

5.4 Global to local feature engineering

5.4.1 PCA-based dimensionality reduction

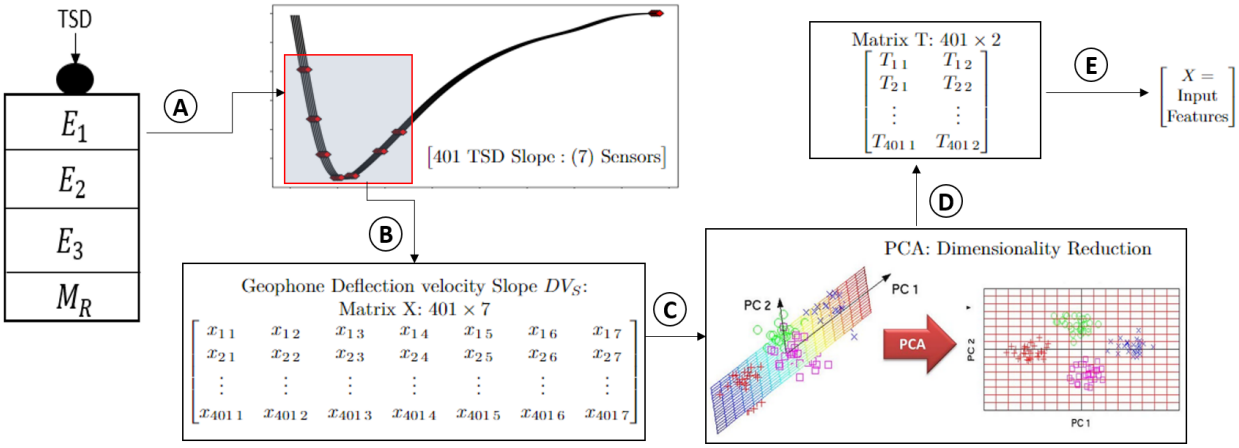

Figure 5.8 – PCA Global-to-Local Approach for the Estimation of M_R via deflection slope D_S

Large datasets have become increasingly prevalent in today's data-driven landscape, as shown in Figure 5.8. However, these datasets often pose challenges in interpretability due to their high dimensionality. Principal Component Analysis (PCA) emerges as a powerful technique designed to address this issue by reducing the dimensionality of complex datasets while enhancing interpretability and minimizing the loss of essential information [147, 148].

PCA achieves this dimensionality reduction by creating new variables, known as principal components, which are uncorrelated with one another and successively maximize the variance present in the original data. Identifying these principal components involves solving an eigenvalue/eigenvector problem, and these new variables are defined based on the specific dataset at hand. This adaptability makes PCA a valuable tool in data analysis [150, 151].

This section conducts a feature engineering analysis to explore the consequences of data dimensionality reduction through a cost-benefit analysis, aiming to quantify the information loss resulting from the application of the PCA algorithm. Subsequently, the research delves into integrating PCA with SVM for regression and classification tasks. The objective is to observe the model's performance when utilizing reduced data dimensions (PCA-local) compared to the scenario without data dimension reduction (Global). This analysis applies explicitly to the seven input features derived from the deflection slope (D_S) sensor values used in estimating the surface elastic modulus (E_1).

The following points outline the PCA setup protocol implemented in this research.

5.4.2 PCA-based dimensionality reduction implementation protocol

1. **Database:** Matrix of dimensions (280×8)

   In this study, Principal Component Analysis (PCA) is implemented on an experimental global forward model dataset, depicted in Figure 5.1. This dataset is structured with dimensions 280×8. Where 280×7 correspond to input Training features (70%) derived from total dataset of deflection slope (D_S) sensor values (Sn_1 to Sn_7), aiming to estimate the surface elastic modulus (E_1) with the dataset contains 280×1 training output labels, generated in the preceding section.

2. **Standardize the Data:** (with mean = 0 and variance = 1) [147, 150, 151]

   Once the database parameters and dimensions have been defined, PCA standardizes the data to avoid dominance by features with larger scales. Standardization transforms each feature X_i (deflection slope) to have a mean μ of 0 and a variance σ^2 of 1:

$$Z_i = \frac{X_i - \mu}{\sigma} \tag{5.1}$$

3. **Compute the Covariance Matrix** [147, 150, 151]

   The third step is to compute the covariance matrix Σ, which captures the relationships between the standardized features. It's a square matrix of dimensions $d \times d$, in this case (7×7), where d is the number of original features (7, corresponding to the number of TSD sensors Sn_1 to Sn_7 that capture the deflection slope D_S). The covariance between features i and j is calculated as:

$$Cov(X_i, X_j) = \frac{1}{n-1} \sum_{k=1}^{n} (X_i^k - \bar{X}_i)(X_j^k - \bar{X}_j) \tag{5.2}$$

   Where n is the number of data points (280 simulated measurements), and $\bar{X}_i$ and $\bar{X}_j$ are the means of X_i and X_j.
   The covariance matrix results, where the diagonal elements represent the variances of individual variables, all greater than zero, implying variation. In contrast, off-diagonal elements indicate covariances between pairs of variables, with larger absolute values signifying stronger linear relationships.

4. **Eigenvector and Eigenvalue from the Covar. Matrix** [147, 150, 151]

   In PCA, a crucial step involves the acquisition of eigenvectors and eigenvalues from the covariance matrix Σ. This process is characterized by the following equation:

$$\Sigma v = \lambda v \tag{5.3}$$

The expression Σv is represented as the result of multiplying the covariance matrix Σ obtained in step 3, by an eigenvector v. This operation encompasses a linear transformation of the eigenvector.
Conversely, λv represents the same eigenvector v, scaled by a factor of eigenvalue λ. It is indicated by the equation that the Eigen decomposition is performed via the multiplication of the covariance matrix Σ with an eigenvector v, the outcome is a scaled version of the original eigenvector v, with the scaling factor provided by the eigenvalue λ.
This concept assumes a central role in PCA. Eigenvectors denote the principal directions within the data space where data exhibits maximal variability (variance), and eigenvalues quantify the magnitude of variance along these principal directions.

5. **Eigen Vectors Verification** [147, 150, 151]

   To verify that the Eigenvectors are correctly computed, the sum of the squares of each value in an Eigenvector should equal to 1.

$$\sum_{i=1}^{d} v_i^2 = 1 \tag{5.4}$$

   This confirms that the Eigenvectors are unit vectors.

6. **Sort Eigenvalues and Select Top k Eigenvectors** [147, 150, 151]

   After sorting the eigenvalues in descending order. It is time to choose the top k eigenvectors corresponding to the k largest eigenvalues. These Eigenvectors form the new basis for the feature space. The sum of the selected eigenvalues indicates the proportion of total variance retained.
   Deciding how many principal components to keep is critical. The "explained variance" quantifies how much of the original data's variability each principal component captures. Mathematically, the explained variance (EV) for the i-th principal component is computed as:

$$EV(PC_i) = \frac{\lambda_i}{\sum_{j=1}^{d=7} \lambda_j} \tag{5.5}$$

   Where: - $EV(PC_i)$ is the explained variance for the i-th principal component. - λ_i is the eigenvalue associated with the i-th principal component. - p is the total number of principal components (equal to the original feature count).

7. **Construct the Projection Matrix W** [147, 150, 151]

   The projection matrix W is constructed by stacking the selected k Eigenvectors as columns. It has dimensions $d \times k$ (7×2):

$$W = [v_1, v_2, \ldots, v_k] \tag{5.6}$$

8. **Transform Data to the New Feature Subspace** [147, 150, 151]

   To obtain the reduced-dimensional data in the new feature subspace T (280×2), multiply the original data matrix X (280×7) by the projection matrix W (7×2):

$$T = X \cdot W \tag{5.7}$$

   Here, T represents the transformed data with k dimensions, where each row corresponds to a data point in the new feature space.

5.4.3 PCA results: Variance explanation and information Loss

The analysis delves into the intricacies of variance explanation and the associated information loss, particularly concerning Principal Component Analysis (PCA). PCA reveals insights into the inherent variability of the original dataset and the effectiveness of dimensionality reduction techniques. Figure 5.9 shows the cumulative explained variance which represents the sum of the explained variances of the principal components up to a certain point. The cumulative explained variance is often used in practice to decide the number of principal components to retain. Based on this PCA generates PCs, each capturing distinct directions of variation observed in the original data. PC1, representing the primary principal component, encapsulates the direction of maximum variance, followed by PC2, which captures the remaining variance orthogonal to PC1.

Figure 5.9 emphasizes that PC1 accounts for 81% of the total variation, while PC2 contributes 17%. The cumulative variance explained by these first two components is substantial, totaling 98.00% of the original dataset's variability. This correlation between PC1, PC2, and the original database indicates their joint capture of the majority of the variability present in the original measurements.

However, challenges arise during the application of PCA, particularly in the presence of noisy components characterized by high variance. These noisy components hinder the accurate representation of the data structure, leading to issues such as amplification during reconstruction and the potential for overfitting, all contributing to information loss. PCA's reliance on higher-variance components becomes problematic in such scenarios, resulting in a suboptimal decomposition that obscures meaningful patterns and yields a less informative representation.

Moreover, eigenvalue decomposition, a fundamental aspect of PCA, introduces further complexity. Reducing dimensionality and selecting a subset of principal components inherently lead to information loss. Striking the right balance in determining the optimal

number of components to retain is crucial: retaining too few may lead to major information loss, whereas retaining too many undermines the goal of dimensionality reduction. Given these challenges, the subsequent investigation aims to evaluate the influence of in-

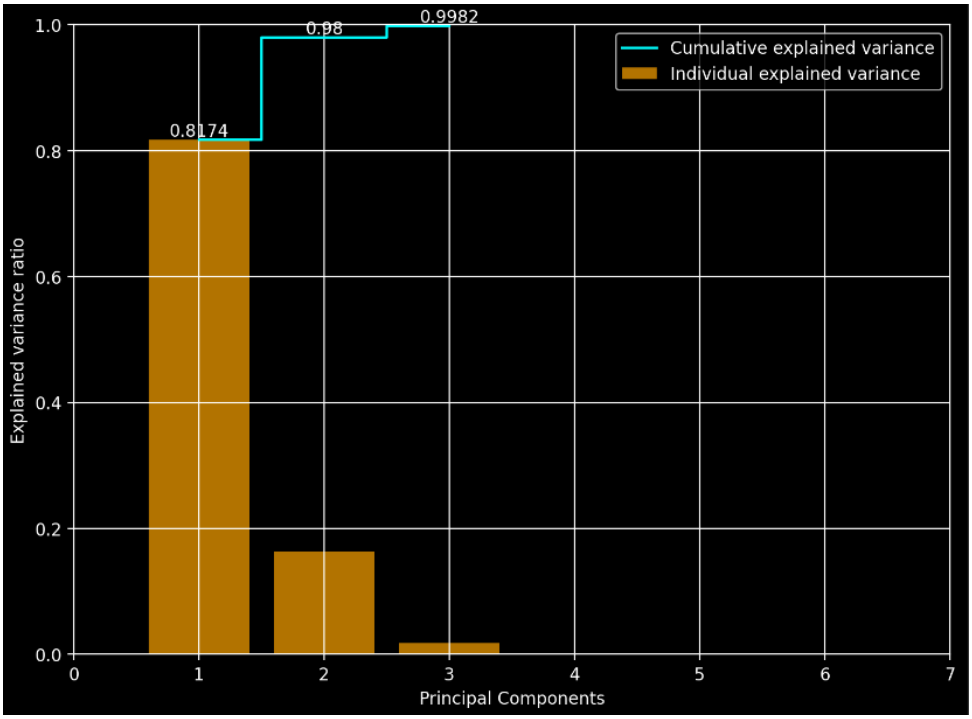

Figure 5.9 – Cumulative explained variance

formation loss on the estimation of pavement elastic modulus (E_1), considering scenarios both with and without PCA. This analysis introduces a trade-off between reducing dimensionality and compromising estimation accuracy due to information loss. The goal is to assess whether the reduction in accuracy remains acceptable, thereby evaluating the effectiveness of PCA in balancing dimensional reduction with the preservation of critical estimation accuracy.

5.5 Experimental inverse model: Results discussion

Following the development of the experimental forward model and the construction of the database, this section explores the application of machine learning techniques, specifically utilizing the Support Vector Machine (SVM) method for both the regression and classification for the regression support vector regression will be used, whereas for the classification Support vector classification is applied. So, this approach mirrors the methodology introduced in the preceding numerical chapters.

For this purpose: two distinct types of databases are introduced as shown in Figure 5.1: one employing a global approach, and the other adopting a local approach. The global

approach dataset exhibits dimensions of 401×8, with 401×7 allocated for features extracted from the deflection slope D_S, and an additional 401×1 for the modulus E_1 as labels. In contrast, the local approach dataset is obtained after applying PCA, resulting in dimensions of 280×2. This format encompasses 280×2 for training features represented by two principal components PCs derived from the deflection slope D_S, alongside 280×1 for the surface modulus E_1 labels.
The ensuing section commences with a classification analysis utilizing both the global approach dataset and the local approach.

5.5.1 Inverse Model: Classification analysis

5.5.1.1 E_1 classes distribution with Stratify-train_test_split

Aligned with the forward model framework established in the previous section, this study systematically classifies surface conditions outlined in the structure presented in Figure 5.10. The surface modulus was distributed into four distinct classes based on their values within E_1. The distribution of surface elastic modulus E_1 values is depicted in Figure 5.10. The figure shows that the dataset utilized in this investigation comprises 400 measurements, ranging from 2000 MPa, indicating severely damaged conditions, to a maximum of 10000 MPa, indicating a structurally sound surface modulus. Following the establishment of the database and exploratory data analysis of the input/output variables D_S/E_1 respectively, the learning phase will be initiated accordingly.
During the learning process, a consistent approach is maintained throughout the study involves a balanced-based training and testing set ratio. They are utilizing a stratified train-test split of 70% for training and 30% for testing. Stratified train-test split ensures uniformity in evaluating model accuracy in the later process.
To this end, the forward model dataset is partitioned into a training set consisting of almost 269 cases and a testing set comprising 132 cases, with each class of the four classes containing 100 cases. These classes are distributed according to specific ranges of modulus values: 2000-3999 MPa for the first class, 4000-5999 MPa for the second class, 6000-7999 MPa for the third class, and 8000-10000 MPa for the fourth class as illustrated in Figure 5.10. Employing this approach maintains the original class distribution. It addresses potential imbalances within the dataset, enhancing the reliability and performance of the model evaluation process.
The following section will analyze the classification analysis outcomes by comparing SVC's performance using both global and local approaches as seen in Figure 5.8. The evaluation will be presented using primary performance evaluation tools such as Confusion Matrix and various evaluation metrics.

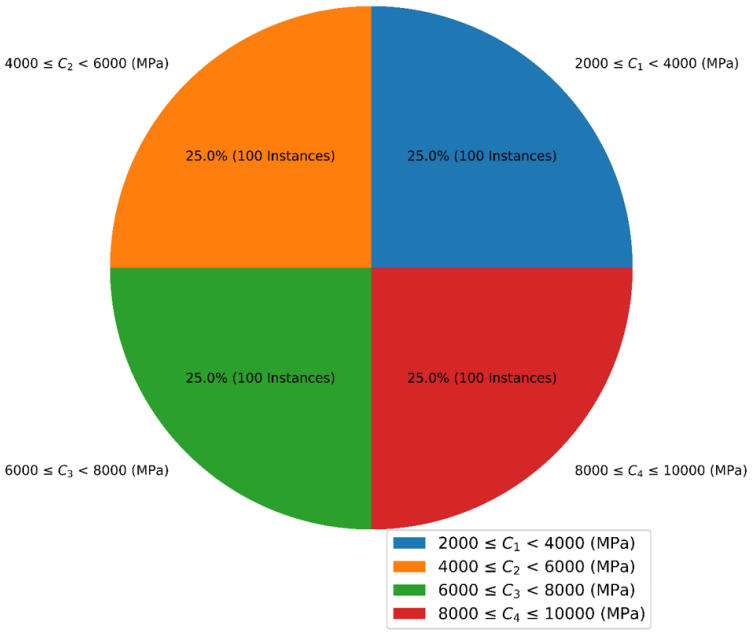

Figure 5.10 – Percentage distribution of E_i classes

5.5.1.2 SVC Hyperparameter tuning

Table 5.3 compares the initial and optimized values of SVC parameters for the inverse classification model in both the local (PCA) and global approaches.
The overall observation is that there are similar values between the optimized hyperparameters of the numerical inverse classification results presented in Table 4.1 of the previous chapter and the inverse classification optimized hyperparameters presented in Table Table 5.3 of this chapter. Below is a breakdown of the main findings:

— Kernel Selection: In the local (PCA) approach, there is a transition from a linear kernel to a radial basis function (RBF) kernel, indicating that the optimized model benefits from the non-linear separation of classes. Conversely, the global approach maintains the RBF kernel for its optimized models, suggesting that a linear decision boundary is insufficient for capturing the relationships between features and surface modulus, particularly in the presence of uncertainty caused by elements such as noise.

— Tolerance Parameter (C): The local (PCA) approach shows a moderate increase in the tolerance parameter reach an optimized value at 1×10^3 optimization, indicating a relaxation in the margin constraints to allow for more flexibility in the classification. In contrast, the global approach experiences a substantial increase in C reach an optimized value at 2×10^3, suggesting a preference for a harder margin classification with less tolerance for misclassification and this will reflect in the

Table 5.2 – SVC hyper Parameter tuning with and without PCA Application

SVC	**Local (PCA)**		**Global**	
Parameter	**Initial Values**	**Optimized**	**Initial Values**	**Optimized**
Kernal	Linear/Poly/RBF/Sigmoid	RBF	Linear/Poly/RBF/Sigmoid	RBF
C	$[1\ ;\ 10^4]$	1×10^3	$[1\ ;\ 10^4]$	2×10^2
γ	$[10^{-1}\ ;\ 10^3]$	1×10^2	$[10^{-1}\ ;\ 10^3]$	5×10^2
ϵ	$[10^{-3}\ ;\ 10^1]$	2×10^{-1}	$[10^{-3}\ ;\ 10^1]$	5×10^{-1}

accuracy of the model as will be discussed in the upcoming sections.

— Kernel Scale Factor (γ): Both approaches start with a small value of 1×10^{-1} for the kernel scale factor. After optimization, the local (PCA) approach sees an increase to 1×10^2, indicating a higher influence of individual training samples on the decision boundary. Similarly, the global approach increases γ to 5×10^2, suggesting a more localized influence of training samples on the decision boundary.

— Precision (ϵ): Both approaches try to tight the margin around the support vectors, the local (PCA) approach increases its precision to 2×10^{-1}, indicating a tighter margin around the support vectors. On the other hand, the global approach sees a slight improvement in precision, reaching 2×10^{-1}, suggesting that the model becomes more discriminating in its classification.

In summary, the optimization of SVM hyperparameters through grid search reveals distinct preferences between the local (PCA) and global approaches. While the local (PCA) approach tends to favor a non-linear decision boundary with a relaxed margin and moderate influence of individual samples, which may lead to some misclassifications, the global approach leans towards a non-linear decision boundary as well, with a harder margin and localized influence of samples. These differences reflect the varying complexities and characteristics of the datasets handled by each approach, highlighting the importance of tailored model tuning for optimal performance.

5.5.1.3 Confusion Matrix analysis

This study investigates the effectiveness of a Support Vector Classifier (SVC) algorithm in an inverse model for predicting pavement surface conditions based on D_S data.

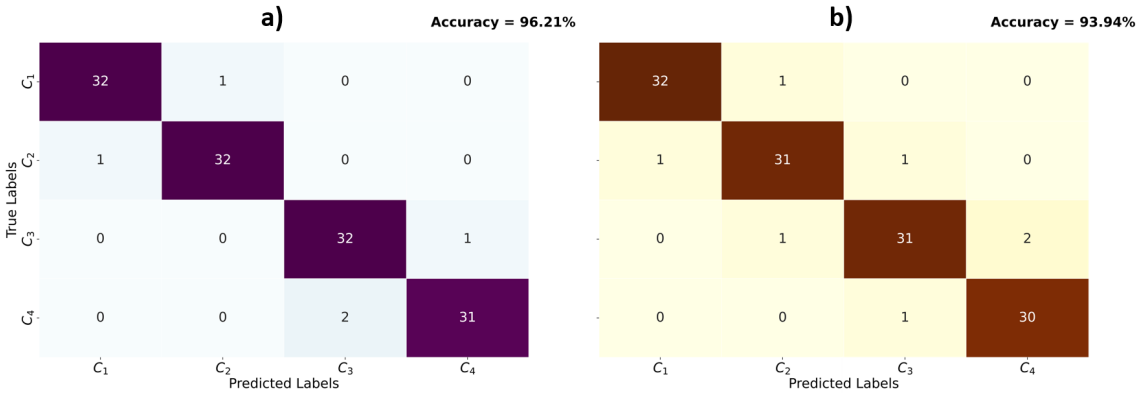

Figure 5.11 – E_i classification Confusion matrix: a) Global b) Local

This section explores the findings of CM analysis.

— The analysis of the confusion matrix in Figure 5.11 compares two distinct approaches within the inverse model. While both approaches achieve acceptable performance, it is notable that the global approach, utilizing all seven initial features, attains notably higher accuracy, exceeding 96%. In contrast, the local PCA approach, employing only two principal components (PCs), achieves nearly 94%, a relatively high accuracy when compared to existing literature..

— This observation underscores the retaining of the most initial features to furnish the model with comprehensive information. This allows the model to discern more effectively between diverse pavement conditions, particularly for classes with potentially overlapping features. However, while Principal Component Analysis (PCA) serves as a valuable tool for reducing data complexity, it may inadvertently discard crucial information essential for distinguishing pavements with similar characteristics. This limitation becomes more pronounced when dealing with classes exhibiting overlapping features in the lower-dimensional space captured by the PCs, as illustrated in classes 4 and 5 of Figure 5.11. Thus, there exists a trade-off: while PCA enhances computational efficiency by reducing data complexity, it may lead to diminished accuracy, particularly for classes with overlapping features.

— As depicted as Figure 5.11, even the global approach utilizing all seven features exhibits some misclassifications, indicating that noise in the data may introduce inaccuracies into the model. Despite this, both approaches demonstrate promise, with the retention of all features offering key advantages in accurately classifying pavement conditions. However, the presence of noise underscores the importance of potential data pre-processing techniques to enhance accuracy. The following subsection will delve into advanced evaluation metrics derived from the confusion matrix results.

5.5.1.4 Evaluation metrics analysis

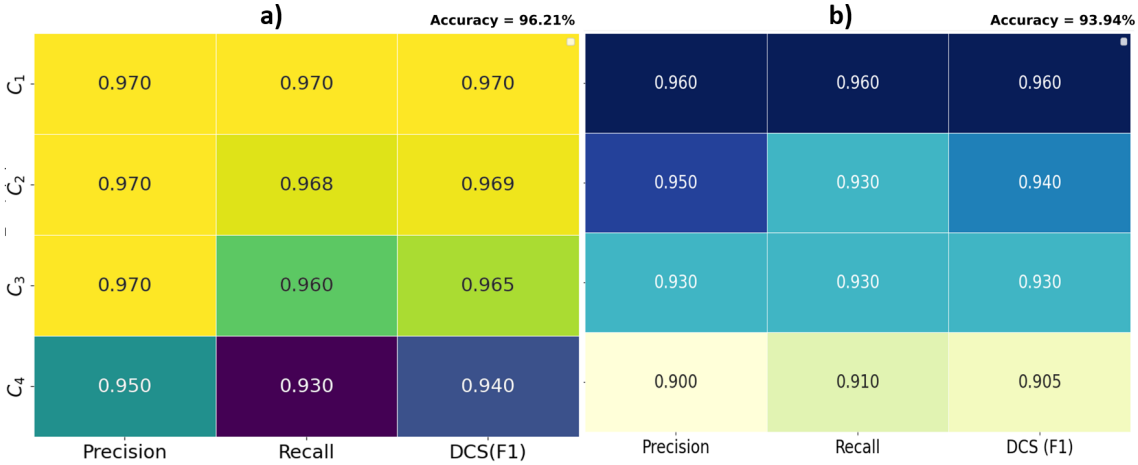

Figure 5.12 – Evaluation metrics a) Global b) Local

To evaluate the effectiveness of the global and local approaches, we utilized advanced performance metrics, including precision, recall, and F1-Dice score, as depicted in Figure 5.12. These metrics offer a comprehensive evaluation of the model's accuracy in classifying pavement conditions.

— Precision analysis: Precision measures the accuracy of a model in correctly identifying positive cases among all cases it predicts as positive. In this context, the global model achieved a precision of 0.965, indicating that when it labeled a pavement condition as damaged, it was correct 96.5% of the time. Conversely, the local model achieved a precision of 0.935, meaning it was correct 93.5% of the time. This shows that the global model was better at accurately classifying pavement conditions correctly.

— Recall Evaluation: Recall, on the other hand, assesses a model's ability to identify all positive cases correctly. The global model achieved a recall of 0.957, indicating that it successfully identified 95.7% of all damaged pavement conditions. In comparison, the local model achieved a recall of 0.933, meaning it identified 93.3% of the damaged pavement conditions. The improvement in recall with the global model suggests it was better at capturing all relevant damaged pavement conditions.

— F1-Dice Score Calculation: The F1-Score (Dice Coff. score) combines precision and recall into a single metric, providing a balanced assessment of a model's performance. The global model achieved an F1-Score of 0.961, while the local model scored 0.934. This indicates that the global model's overall effectiveness in correctly identifying true positives and avoiding false positives was higher than the local model. Additionally, the Dice score shows how well the model can draw the lines between where it predicts damage and where it is. This is especially useful

when the data is noisy, so the model doesn't make mistakes by saying there's more or less damage than there really is.

— Room for Improvement: To this point, while potential is shown by the inverse classification model based on ML, there is still room for improvement. Issues such as data noise and potential overlap between pavement condition categories can increase assessment accuracy and dependability. Additionally, methods to handle noisy data and manage overlapping features can further boost the model's effectiveness. The compromises linked with techniques like PCA for reducing data complexity are underscored by this examination.

However, delving into the regression aspect of SVM through Support Vector Regression (SVR) in the subsequent section could provide more intriguing opportunities for a deeper analysis of SVM's performance. Exploring SVR may unveil insights into the correlations between features and pavement condition, offering valuable input for proactive maintenance approaches.

5.5.2 Inverse model: Regression analysis

In this part, the efficiency of Support Vector Regression (SVR) in predicting surface modulus (E_1) from deflection slope (D_S) is explored. The potential of SVR as a robust tool for regression tasks in pavement assessment is investigated by examining the relationship between deflection slope and surface modulus. This examination and validation aim to reveal valuable insights into the applicability and effectiveness of SVR as an inverse modeling technique.

5.5.2.1 Regression analysis: Train Test Split

In this section, the SVR model's performance is evaluated under various conditions, including two regression approaches, global and local, As shown in Figure 5.13.
The dataset used for training and testing is sourced from the forward model chapter. In the global regression approach, all seven original features from the dataset serve as input for the SVR model with input matrix X (401×7). On the other hand, the local regression (PCA) approach utilizes dimensionality reduction by employing two principal components (PCs) derived from the data with input matrix T (280×2).
Random sampling is employed to split the data into training and testing parts to prevent bias and ensure generalizability. Figure 5.13 shows 70% training and 30% testing sets, departing from the stratified sampling typically used in classification tasks. Data preprocessing is conducted before the split to prevent data leakage and overfitting. This ensures that the model learns from the inherent relationships within the data during training and is subsequently evaluated on unseen data from the testing set.

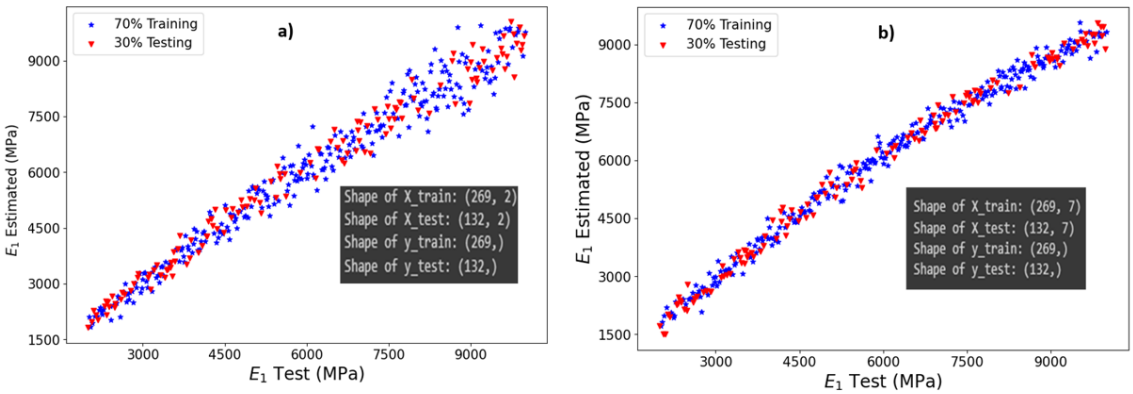

Figure 5.13 – Target variable E_1 Train-Test split: a) Local approach b) Global approach

5.5.2.2 SVR hyperparameters tuning

Table 5.3 – SVR hyperparameter tuning with and without PCA Application

SVC	**Local (PCA)**		**Global**	
Parameter	**Initial Values Range**	**Optimized**	**Initial Values Range**	**Optimized**
Kernal	Linear/Poly/RBF/Sigmoid	RBF	Linear/Poly/RBF/Sigmoid	RBF
C	[0.1 ; 100]	20	[0.1 ; 100]	50
γ	[0.01 ; 10]	1	[0.01 ; 10]	5
ϵ	[0.001 ; 1]	0.1	[0.001 ; 1]	0.2

In the context of SVR hyperparameter tuning, the comparison between the local (PCA) and global approaches reveals interesting insights into optimizing the estimation of surface modulus.

— Non-linearity: Both approaches favored the RBF kernel after optimization, highlighting the importance of capturing non-linear relationships between features and surface modulus.

— Margin Trade-off: The local (PCA) approach with a lower optimized C value prioritized flexibility, potentially leading to a more adaptable model but with a risk of higher deviations in predictions. Conversely, the global approach with a higher C value emphasized robustness, aiming for a more accurate model with stricter

margins.

— Sample Influence: The local (PCA) approach with a higher optimized γ placed greater emphasis on individual training samples, potentially capturing intricate details in the data. The global approach with a lower γ focused on broader trends, leading to a more generalized model.

— Precision and Generalizability: Both approaches aimed to tighten the margins around support vectors, but the local (PCA) approach achieved higher (ϵ), potentially could impact its generalizability to unseen data. The global approach with slightly lower precision might be more suitable for real-world applications.

These findings emphasize the importance of carefully selecting hyperparameters based on the specific requirements for surface modulus estimation. Tailoring the model's flexibility, margin tolerance, and sample influence can optimize performance for the desired level of accuracy and generalizability.

5.5.2.3 Inverse model analysis: Results discussion

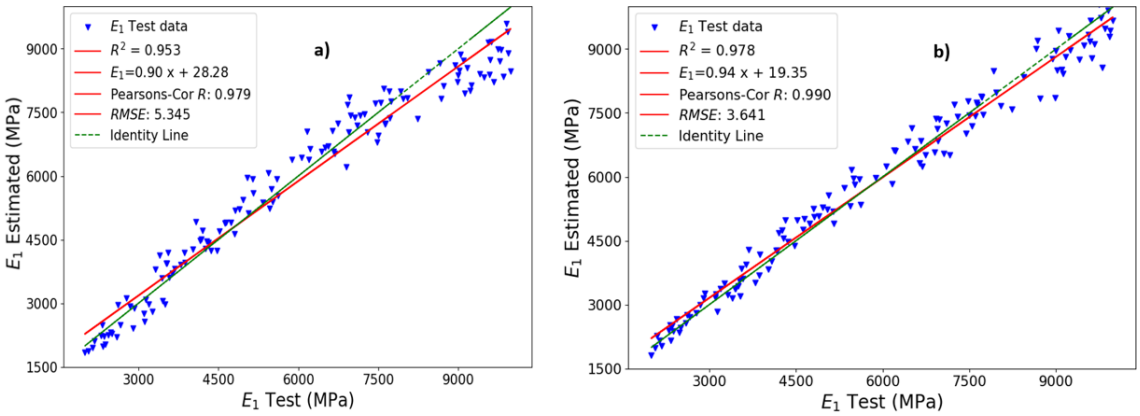

Figure 5.14 – SVR regression analysis a) Local b) Global

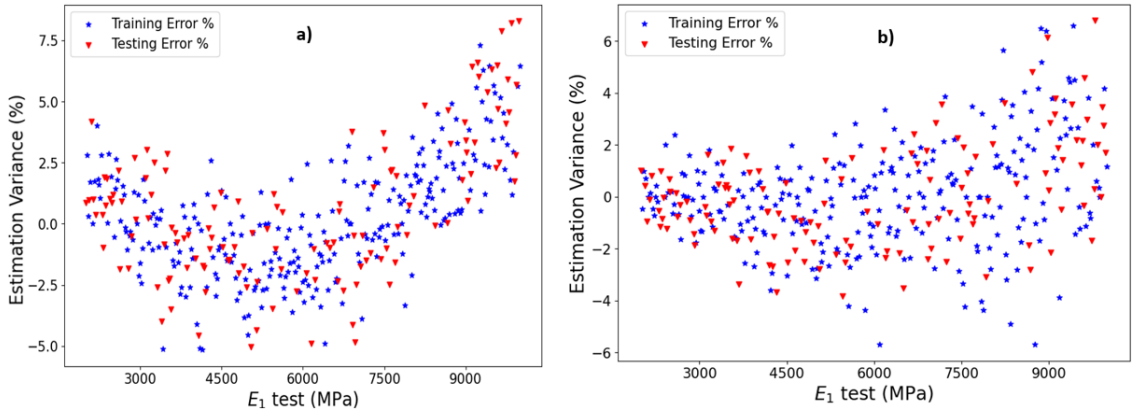

Figure 5.15 – Regression Variance analysis a) Local b) Global

This section delves into the application of Support Vector Regression (SVR) within an inverse model framework, focusing on both local and global approaches and assessing their performance using regression metrics such as R-squared (R^2), Root Mean Squared Error (RMSE), and Correlation Coefficient (R). Higher R^2 values signify a better fit, lower RMSE values suggest improved prediction accuracy, and R values closer to 1 or -1 indicate stronger relationships between predicted and actual values.

— As depicted in Figure 5.14, the global approach achieves slightly higher R^2 (0.978) and lower RMSE (3.641%) compared to local regression, indicating that the model utilizing all seven original features captures the relationship between deflection slope D_S and modulus more accurately on average.

— In contrast, despite a lower R^2 (0.95), the local PCA approach still exhibits a strong correlation ($R = 0.97$) and reasonable RMSE (5.345%), implying that the two principal components capture most of the relevant information for prediction, potentially leading to better generalization capabilities, particularly for datasets with high dimensionality.

— While the global approach provides a more comprehensive understanding of how various factors influence surface modulus, the local PCA approach offers a balance by sacrificing some detail for computational efficiency. This balance is advantageous for larger datasets or real-time applications where faster processing times are required.

— Going beyond mere comparison of local and global SVR approaches, this analysis integrates a variance analysis as shown in Figure 5.15 to scrutinize the uncertainty within the models for both the global and the local approaches. The global SVR approach demonstrates a lower variance (6%) compared to the local approach (7.5%), suggesting slightly higher consistency in predictions.

— Regarding prediction uncertainty, approximately 95% of the differences between predicted and actual values fall within a 5% variance range for both approaches, which is considered acceptable given the inherent data variability.

— Furthermore, the establishment of a 5% variance threshold serves as a means for potential outlier detection within the dataset, warranting further investigation into anomalous data points.

— Overall, the observation of low variance and acceptable uncertainty across both local and global models affirms the acceptable predictive accuracy of the SVR model. While the global approach may exhibit slightly tighter consistency, both methodologies demonstrate commendable performance well within the expected range of data variability.

— However; it's important to note the limitation of the analysis, which utilized a

dataset of moderate size (401 samples). Pavement engineering involves variability due to factors like materials, traffic loads, and environment, necessitating a more extensive and diverse dataset for a robust and generalizable model. Future research could explore techniques to increase data quantity and incorporate more pavement-related features, potentially enhancing accuracy and applicability.

To this end, the SVR model shows promising capabilities for predicting surface modulus from deflection slope measurements. Further research with more diverse datasets is warranted to enhance pavement condition assessment, optimize maintenance strategies, and improve overall pavement performance.

5.6 Global and local approaches

Based on the empirical findings derived from the classification and regression results, this section delves into the findings of factors that influence the selection between global and local approaches, as also shown in Figure 5.4.

— Accuracy to Efficiency Trade-off: The global inverse SVM model emphasizes accuracy, retaining all original features to capture intricate relationships between deflection slope and surface modulus, yielding slightly higher accuracy. Conversely, the local PCA-based SVM prioritizes computational efficiency, employing PCA for dimensionality reduction. In scenarios involving large datasets or real-time applications, this approach enhances efficiency with only a minor sacrifice in accuracy while maintaining robustness for various applications.

— Generalizability and Data Limitations: The local PCA approach also highlights generalizability. For smaller datasets where extrapolating performance to unseen data is critical, extracting essential information through principal components proves effective in enhancing generalizability.

— Dataset-specific Selection and evaluation: Choosing between global and local approaches depends on the dataset's specific attributes. Datasets featuring complex, non-linear feature relationships may favor the global approach. Thorough cross-validation with both methods provides insights into performance, aiding tailored decision-making based on the dataset's unique characteristics.

To this point, there is no universally optimal approach, as the best choice depends on the dataset's unique priorities and attributes. By considering these factors, informed decisions can be made to enhance pavement condition assessment methodologies, achieving a balance between accuracy, efficiency, and generalizability.

Table 5.4 – Experimental inverse model: local to global performance analysis

Factor	**Global**	**Local (PCA)**
Accuracy	Higher	Slightly Lower
Data Efficiency	Lower (Computation-intensive)	Higher (faster processing)
Generalizability (limited data)	Potentially lower	Potentially higher
Strength	mitigate uncertainty	Balancing accuracy and efficiency

5.7 Conclusion

This chapter showcases the effective experimental validation of a numerical model using Support Vector Machines (SVM) for estimating pavement surface modulus E_1 based on deflection slope D_S measurements. The rationale behind this choice stems from the scarcity of labeled measurement data initially available for soil resilient modulus M_R, along with assessing the model's adaptability across diverse datasets.

Through various classification and regression tests, the proposed machine learning (ML) based inverse model demonstrates a robust correlation between numerical modeling and experimental data including hyperparameter tuning. This substantial agreement across all tests highlights the accuracy and reliability of the estimated E_1 values obtained from the model.

The experimental validation effectively showcases the ML-based numerical model's capability in assessing pavement condition using real deflection slope measurements. The successful application of SVM for both regression and classification tasks further reinforces the validation process.

The methodology employed a three-pronged approach: Firstly, data acquisition involved utilizing data from bearing capacity tests conducted under controlled conditions, providing a solid foundation for model development. Secondly, data augmentation techniques were employed to address the challenge of limited labeled data, thereby enhancing the model's robustness by simulating the deflection slope using industry reference software (Alizé-LCPC). Lastly, two distinct SVM model configurations were explored: a global approach utilizing all features and a local approach employing two principal components for dimensionality reduction.

The performance of both the global approach (all features) and the local PCA approach (two principal components) proved to be acceptable and The notable alignment in performance observed between the both approaches further strengthens the validation.

While the global method showcased slightly higher accuracy due to its ability to leverage richer data, the local PCA method achieves a favorable balance between accuracy and efficiency. This renders the local method suitable for large datasets or real-time applications. Consequently, the optimal choice between these methods depends on user priorities.

From the empirical findings, it is concluded that prioritizing accuracy may favor the global method, while those concerned with data efficiency or generalizability with limited data may prefer the local PCA method. Ultimately, the specific dataset characteristics and user needs will dictate the optimal selection.

At this stage, the research has arrived at the overarching conclusion outlined in the forthcoming chapter.

Chapter 6

General Conclusion

6.1 Thesis objective

This thesis aims to develop a Machine learning based intelligent framework that integrates data science techniques and pavement modeling to interpret data from simulating pavement deflection behavior under Traffic Speed Deflectometer (TSD) network-level measurement.

The primary objective is to address existing knowledge gaps and make a contribution to the pavement engineering field by proposing an innovative methodology and computational tools for directly estimating pavement mechanical properties, specifically the pavement elastic modulus E_i, from TSD deflection slope data D_S instead of simulated deflection measurements. To the best of the author's knowledge, the inverse model and framework proposed in this research represent one of the first reported attempts in the literature to estimate E_i solely based on numerical TSD deflection velocity D_S using supervised machine learning model.

To this point, before summarizing the research findings, a brief overview of the overall thesis contribution area, structure, and protocols is presented.

6.2 Research gaps and thesis contribution areas

— The pavement mechanics community identifies critical gaps in current pavement management systems (PMS) related to structural assessment, particularly in accurately evaluating pavement structural integrity. Current practices often rely on surface cracking as indicators, which may not fully capture the pavement's structural capacity. This reliance on surface distresses as lagging indicators poses challenges in precise decision-making for maintenance and rehabilitation (M&R) actions within PMS.

— Accurate assessment of pavement structural condition necessitates effective backcalculation of pavement layer moduli (E_i). However, traditional methods like Destructive Testing (DT) pose sustainability, efficiency, and safety concerns. Conversely, Non-Destructive Testing (NDT) methods offer a more sustainable alternative, par-

ticularly those utilizing deflection measurements. Yet, network-level structural assessment using NDT methods remains uncommon due to limitations in traditional deflection measurement devices like the Falling Weight Deflectometer (FWD).

— To address these challenges, Traffic Speed Deflectometers (TSDs) emerge as promising solutions for collecting structural data at the network level without disrupting traffic flow. Unlike traditional methods, TSD measurements occur at traffic speeds, ensuring improved traffic safety and efficiency while offering high productivity and cost-effectiveness.

— To this end, currently, a critical gap exists in backcalculating pavement layer moduli from TSD data, making road authorities hesitant to utilize backcalculated moduli for pavement evaluation or design without understanding the associated error. These challenges arise from the discrepancies in converting TSD measurements to FWD equivalents by integrating the deflection velocity, leading to loss of information and data processing challenges. These challenges underscore the need for a robust and generalizable approach to pavement structural assessment using TSD data.

— Machine Learning (ML) presents a potential solution to address these limitations by learning complex patterns within datasets. ML algorithms offer a generalized approach for estimating pavement modulus (E_i) from TSD data, overcoming the limitations of traditional techniques by adapting to various loading configurations. By leveraging ML models trained on diverse datasets, road authorities can enhance accuracy and reliability in pavement structural assessment, facilitating more informed decision-making within PMS.

6.3 Research methodology

The methodology employed in this research unfolds across several chapters, each contributing to the overarching goal of estimating pavement modulus using TSDs deflection slope via ML.

— In the introductory Chapter I, the theme is introduced, and research hypotheses and objectives are established.

— Building upon this foundation, Chapter II delves into the identification of research gaps by analyzing existing literature, paving the way for proposing supervised learning ML as a solution for modulus estimation.

— With the groundwork laid, Chapter III focuses on the development and validation of a numerical forward model for TSDs, aligning with French pavement standards and creating a synthetic database for further analysis.

— Transitioning from forward modeling, Chapter IV dives into the development and validation of the inverse model, specifically targeting the estimation of M_R from D_S using SVM techniques, augmented by advanced parametric study, sensitivity analysis and hyperparameter tuning.
— As the research progresses, Chapter V puts theory into practice by validating the models with real measurement data, implementing data augmentation techniques to address data limitations, and conducting a comparative global and local analysis to enhance model accuracy.
— Finally, Chapter VI serves as the culmination of the thesis, summarizing key findings, discussing their implications for pavement engineering, and offering recommendations for future research directions and methodology enhancements.

6.4 Research findings

1. Forward Model: The findings from the numerical forward model regarding the TSD system encompass three main points.
   Firstly, regarding the load configuration, the research indicates that focusing solely on the rear axle load in TSD deflection measurement while neglecting other loads would lead to an underestimation of the deflection velocity measurement. Therefore, adopting the approach of summing the deflection from each TSD wheel (superposition) yields more accurate results.
   Secondly, concerning the TSD principle of operation, for calibration purposes and simplifying calculations, the TSD deflection velocity measurement is artificially assumed to be zero at the loading point and at a distance of 3m from the loading point where the reference sensor is located. However, these assumptions introduce TSD measurements uncertainty, necessitating attention for accurate interpretation.
   Finally, concerning sensor positions, the exploratory data analysis shows the variations among specific sensors, depending on the target modulus E_i data. Sensors near the loading point exhibit more consistent deflection slope values form the variation of the corresponding soil modulus data, while those farther away show greater variability. Conversely, for surface modulus data, sensors nearest to the loading point demonstrate higher variability and responsiveness, whereas those farther away show less variability and response to modulus variation. Thus, sensor placement affects the assessment of pavement deflection behavior under TSD and eventually the estimation accuracy.

2. Numerical inverse Model: The findings from both classification and regression inverse analyses using supervised machine learning, notably Support Vector Machine

(SVM), unveil several noteworthy insights.
Firstly, the study showcases the effectiveness of ML in estimating soil M_R from D_S simulated measurements, suggesting its potential practical utility via exhibiting high accuracy across various test scenarios, indicating its adeptness in capturing the D_S-M_R relationship effectively.
However, the presence of TSD noise in the data impacts model performance, resulting in elevated prediction errors and decreased accuracy. Despite the TSD noise, the SVM model demonstrates robustness in handling uncertainties within the dataset, with a considerable portion of prediction errors falling within an acceptable range. Nonetheless, implementing noise reduction techniques during data preprocessing becomes crucial for improving model accuracy, especially in real-measurement scenarios characterized by noisy data.
Furthermore, the observed data imbalance within the distribution of M_R class data highlights the need for fine-tuning hyperparameters to mitigate potential biases during the model learning phase.

3. Temperature-Noise sensitivity and uncertainty: The research findings emphasize the influence of the combination of temperature and TSD noise on pavement behavior.
Firstly, the study highlights the temperature sensitivity of bituminous materials like asphalt, which undergo substantial changes in stiffness and mechanical properties as temperatures fluctuate. These variations directly affect deflection behavior, influencing pavement performance assessments.
Secondly, this research underscores the importance of temperature data in inverse modeling for pavement analysis. Acquiring detailed data about the vertical temperature profile near the soil surface and incorporating it can enhance the accuracy of M_R estimation. This approach aligns with the observed proportional relationship, $E_i = f(\Theta\,^{\circ}\mathrm{C})$.
Correcting deflection measurements to a specific temperature, as is common in the industry, may result in misleading data. However, the findings suggest that incorporating vertical structural temperature information reduces uncertainty in pavement analysis. To enhance the accuracy of estimating E_i from D_S, it is strongly recommended that advanced studies be conducted on predicting vertical structural temperature based on surface and ambient temperatures. Alternatively, having a database of a thermal model would be beneficial.
Moreover, the combined effects of temperature uncertainty and TSD sensor noise pose a visible additional challenges in deflection slope D_S measurements and complicating the interpretation of pavement responses. This overlap underscores the

need for robust noise reduction techniques and meticulous handling of temperature data to ensure accurate pavement performance assessments.

4. Experimental Validation: The research findings affirm the effectiveness of the ML numerical inverse model for assessing pavement conditions using real deflection slope measurements. This validation is established by efficiently SVM in regression and classification tasks to estimate E_1 from D_S, with acceptable performance across global approach (utilizing all features) and local (employing PCA-reduced features, specifically 2-PCs) approaches.
   The experimental and numerical ML model's show a notable alignment in performance between the two models, including in hyperparameter tuning, indicating accurate capture of essential relationships by both.
   Furthermore, the consistent performance agreement between the global and local approaches further reinforces validation. While the global method demonstrates slightly higher accuracy due to its ability to capture richer data, the local PCA method exhibits a favorable balance between accuracy and efficiency, suitable for large datasets or real-time applications. Thus, the choice between the methods depends on user priorities, with the global method favored for maximizing accuracy and the local PCA method preferred for concerns regarding data efficiency or generalizability with limited data. The optimal approach selection ultimately hinges on the specific dataset characteristics and user needs.

6.5 Research limitations and challenges

This research encountered two challenging limitations:

— Limited Labeled Data: Supervised Machine learning algorithms heavily rely on labeled data for training and effective performance. This research faced challenges due to the limited availability of labeled experimental data which is common issue internationally.
  To address this limitation, a numerical data augmentation techniques is employed using an industry reference software (Alize-LCPC) to build a hybrid database.

— Applicability Across Diverse Environments: While the developed methodology has been validated under specific conditions (within the context of the thesis hypothesis and parameters), its generalizability to a wider range of pavement structures and environmental factors remains a potential challenge. The variations in pavement materials, layer thicknesses, and climatic conditions can influence pavement mechanical properties.

6.6 Future work and recommendations

— Model usability recommendation: Further validation with real TSD or Raptor measurement data from diverse pavement sections would be beneficial to assess the inverse model's performance and facilitate better optimization. Therefore, when applying the model in different configurations, adhering to the overall developed methodology is recommended while considering potential discrepancies in these properties. Further validation with real-measurement data from diverse environments would be beneficial to assess the model's performance and potentially refine it for broader applicability.

— Concrete and composite pavement: Although Traffic Speed Deflectometers (TSD) have demonstrated potential in evaluating the structural condition of flexible pavements, there has been limited exploration of their application to concrete and composite pavement slabs and load-carrying joints. Despite their extensive use in the pavement network, research related to TSD has primarily neglected these pavement types. Hence, future studies should focus on filling this gap by investigating the feasibility of using TSD to assess the structural integrity of concrete and composite pavements.

— Enhancing the precision of estimating E_i from D_S would profit from conducting advanced investigations focused on predicting vertical structural temperature through surface and ambient temperature data. Alternatively, establishing a database of thermal models could also be advantageous.

— While this thesis has contributed to the advancement of pavement mechanics by employing artificial intelligence to analyze deflection slope measurements and interpret pavement behavior to estimate structural and mechanical properties, it also highlights challenges in optimizing the inverse approach. Specifically, it emphasizes the importance of prior knowledge of pavement structure properties and the necessity of a well-labeled database. Building on these insights, it is recommended to integrate Traffic Speed Deflectometer (TSD) and Ground Penetrating Radar (GPR) data while constructing generative-based AI models to understand pavement behavior efficiently.

List of publications

[1] A. Abdelmuhsen, J.-M. Simonin, F. Schmidt, D. Lievre, A. Cothenet, and A. Ihamouten, "On the variants of svm method for the estimation of soil elastic modulus from tsd model: Numerical parametric study," *Transportation Engineering*, vol. 13, p. 100187, 2023. [Online]. Available: https://www.sciencedirect.com/science/article/pii/S2666691X23000271

[2] A. Abdelmuhsen, J.-M. Simonin, F. Schmidt, and A. Ihamouten, "Ml-based model for the estimation of the pavement elastic modulus via deflection," in *Transport Research Arena (TRA)*, 2024.

[3] A. Abdelmuhsen, J.-M. Simonin, F. Schmidt, A. Ihamouten, and D. Lièvre, "Database construction based upon numerical modelling of pavement deflection behaviour under the traffic speed deflectometer," in *25e Congrès Français de Mécanique*, 2022.

[4] A. Abdelmuhsen, J.-M. Simonin, F. Schmidt, and A. Ihamouten, "Machine learning-based modelling for numerical evaluation of the traffic speed deflectometer performance," in *YRS2023-11th Young Researchers Seminar*. Zenodo, 2023.

RÉSUMÉ EN FRANÇAIS

Aperçu

La détérioration progressive de l'état des chaussées routières nécessite une évaluation structurale rapide, efficace et automatisée afin d'estimer la durée de vie résiduelle de la chaussée. L'estimation précise du module d'élasticité des différentes couches de la chaussée (E_i) joue un rôle essentiel dans ce processus, permettant la conception de chaussées résilientes, l'optimisation des stratégies de maintenance et l'amélioration de la sécurité routière globale. Cependant, les méthodes et dispositifs conventionnels utilisés pour estimer E_i, tels que le Falling Weight Deflectometer (FWD), présentent plusieurs limitations en raison de contraintes opérationnelles et de sécurité lors des mesures à l'échelle du réseau.

Pour surmonter ces obstacles, les dispositifs de Traffic Speed Deflectometer (TSD) sont proposés comme des solutions innovantes pour l'évaluation continue de la capacité portante des chaussées, éliminant ainsi le besoin de contrôle de la circulation. en effet, TSD fonctionne à la vitesse normale de circulation jusqu'à 80 km/h, et repose sur la mesure de la vitesse de déflexion verticale (D_V) de la chaussée au lieu de la déflexion elle-même. Les mesures continues du TSD fournissent des données beaucoup plus adaptées que le FWD, ce qui permet une planification de la maintenance plus précise et efficace. Par contre, le traitement efficace de la quantité importante de données qu'il génère présente de défi. Cela pourrait cependant être surmonté en utilisant des techniques spécialisées, telles que l'apprentissage automatique (ML).

Ainsi, cette thèse présente un modèle et une méthodologie efficaces basés sur la combinaison (ML+TSD) pour l'estimation de E_i. Cette approche novatrice utilise des mesures de pente de déflexion D_S par TSD, plutôt que sur la méthode classique de déflexion. Le modèle développé dans le cadre de cette recherche repose sur des données issues de logiciels (Alizé-LCPC) reconnus par les praticiens et d'un simulateur extérieur expérimental, garantissant ainsi leur conformité aux conditions du monde réel. De plus, pour valider leur performance, un processus de validation paramétrique avancé a été exécuté de manière méticuleuse.

Ce modèle relève non seulement les défis liés à l'estimation précise de E_i, mais il mène également une analyse de sensibilité quantitative rigoureuse. Cette analyse examine systématiquement les impacts de quatre défis majeurs: la complexité des données TSD en

haute dimension, l'influence du bruit de mesure, les variations de température, et Les incertitudes de E_i des autres couches des chaussées.

Objectif de la thèse

Cette thèse vise à proposer un cadre intelligent basé sur l'apprentissage automatique qui intègre les techniques de la science des données et la modélisation des chaussées pour interpréter les données issues de la simulation du comportement en déflexion des chaussées sous les mesures de Le déflectomètre à grande vitesse (TSD) à l'échelle du réseau.
L'objectif principal est de combler les lacunes de connaissances existantes et de contribuer de manière significative au domaine du génie des chaussées en proposant une méthodologie innovante pour estimer directement les propriétés mécaniques des chaussées, spécifiquement le module élastique E_i, à partir des données de pente de déflexion TSD D_S plutôt que des mesures de déflexion simulées. À la connaissance de l'auteur, le modèle inverse et le cadre proposés dans cette recherche représentent la première tentative rapportée dans la littérature pour estimer E_i uniquement à partir de la de pente de déflexion D_S du TSD en utilisant un modèle d'apprentissage supervisé.
À ce stade, avant de résumer les résultats de la recherche, un bref aperçu de la zone de contribution globale de la thèse, de sa structure et de ses protocoles est réalisé.

Lacunes de recherche et domaines de contribution

La communauté de la mécanique des chaussées identifie des lacunes critiques dans les systèmes actuels de gestion des chaussées (PMS) liées à l'évaluation structurelle, notamment dans l'évaluation précise de l'intégrité structurelle des chaussées. Les pratiques actuelles s'appuient souvent sur les fissures de surface comme indicateurs fonctionnels, ce qui peut ne pas refléter pleinement la capacité structurelle réelle de la chaussée. Cette dépendance aux détériorations de surface comme indicateurs retardataires pose des défis dans la prise de décisions précises pour les actions de maintenance et de réhabilitation (M&R) au sein des PMS.
Or, une évaluation précise de l'état structurel des chaussées nécessite un recalcul efficace des modules des couches de chaussées (E_i).
Cependant, les méthodes traditionnelles comme les tests destructifs (DT) posent des problèmes de durabilité, d'efficacité et de sécurité. D'autre part, les méthodes de tests non destructifs (NDT), en particulier celles utilisant les mesures de déflexion, offrent une alternative plus durable. Pourtant, l'évaluation structurelle à l'échelle du réseau à l'aide des méthodes NDT reste rare en raison des limitations d'utilisation des dispositifs de mesure

de déflexion traditionnels comme le déflectomètre à masse tombante (FWD).
Pour relever ces défis, le TSD émergent comme des solutions prometteuses pour collecter des données structurelles à l'échelle du réseau sans perturber le flux de trafic. Contrairement aux méthodes traditionnelles, les mesures du TSD se font à la vitesse du trafic, ce qui assure une meilleure sécurité et efficacité du trafic tout en offrant une productivité et un rapport coût-efficacité élevés.
Actuellement, un écart critique existe dans le recalcul des modules des couches de chaussée à partir des données du TSD, rendant les autorités routières réticentes à utiliser les modules recalculés pour l'évaluation ou la conception des chaussées sans comprendre l'erreur associée. Ces défis découlent des divergences dans la conversion des mesures du TSD en équivalents FWD en intégrant la vitesse de déflexion, ce qui entraîne une perte d'information et des défis de traitement des données. Ces défis soulignent le besoin d'une approche robuste et généralisable pour l'évaluation structurelle des chaussées à partir des données du TSD.
L'apprentissage automatique (ML) présente une solution potentielle pour répondre à ces limitations en apprenant des schémas complexes au sein des ensembles de données. Les algorithmes ML offrent une approche généralisée pour estimer le module des chaussées (E_i) à partir des données du TSD, surmontant les limitations des techniques traditionnelles en s'adaptant à diverses configurations de chargement. En exploitant des modèles ML entraînés sur des ensembles de données diversifiés, les autorités routières peuvent améliorer la précision et la fiabilité de l'évaluation structurelle des chaussées, facilitant ainsi une prise de décision plus éclairée au sein des PMS.

Méthodologie de recherche

La méthodologie utilisée dans cette recherche se déploie à travers plusieurs chapitres, chacun contribuant à l'objectif général d'estimation du module des chaussées en utilisant les pentes de déflexion des TSD via l'apprentissage automatique.
Dans le Chapitre d'introduction I, le sujet et le contexte sont introduits, et les hypothèses et objectifs de recherche sont établis.
S'appuyant sur cette fondation, le chapitre II se plonge dans l'identification des lacunes de recherche en analysant la littérature existante, ouvrant la voie à la proposition de l'apprentissage supervisé ML comme solution pour l'estimation du module.
En suite, le chapitre III se concentre sur le développement et la validation d'un modèle numérique direct pour les TSD, en alignement avec les normes françaises de chaussées et en créant une base de données synthétique pour une analyse ultérieure.
En transition depuis la modélisation directe, le chapitre IV plonge dans le développement et la validation du modèle inverse, ciblant spécifiquement l'estimation de M_R à partir de

D_S en utilisant des techniques Support Vector Machine (SVM), augmentées par une étude paramétrique avancée, une analyse de sensibilité et un ajustement des hyperparamètres.
dans la continuation de ce travaux, le chapitre V, met la théorie en pratique en validant les modèles avec des données de mesure réelles, mettant en œuvre des techniques d'augmentation de données pour traiter les limitations des données initiales, et menant une analyse comparative globale et locale pour améliorer la précision du modèle.
Enfin, le chapitre VI résume les principales conclusions, discute de leurs implications pour le génie des chaussées et propose des recommandations pour les orientations futures de la recherche et les améliorations méthodologiques.

Résultats de la recherche

1. Modèle direct : Les conclusions du modèle direct numérique concernant le système TSD englobent trois points principaux. Premièrement, en ce qui concerne la configuration de repartion charges sur les essieux, la recherche indique que se concentrer uniquement sur la charge de l'essieu arrière dans la mesure de déflexion TSD tout en négligeant les autres charges entraînerait une sous-estimation de la mesure de la vitesse de déflexion. Par conséquent, adopter l'approche de sommation des déflexions de chaque roue TSD (superposition) donne des résultats plus précis. Deuxièmement, en ce qui concerne le principe de fonctionnement du TSD, à des fins d'étalonnage et pour simplifier les calculs, la mesure de la vitesse de déflexion du TSD est artificiellement supposée être nulle au point de chargement et à une distance de 3 mètres du point de chargement où se trouve le capteur de référence. Cependant, ces hypothèses introduisent une incertitude dans les mesures TSD, nécessitant une attention pour une interprétation précise. Enfin, en ce qui concerne les positions des capteurs, l'analyse exploratoire des données montre des variations significatives entre des capteurs spécifiques, en fonction des données du module cible E_i. Les capteurs près du point de chargement présentent des valeurs de pente de déflexion plus cohérentes, tandis que ceux plus éloignés montrent une plus grande variabilité. Au contraire, pour les données de module de surface, les capteurs les plus proches du point de chargement démontrent une variabilité à la variation du module plus élevées, tandis que ceux plus éloignés montrent moins de sensibilité à la variation du module. Ainsi, le placement des capteurs affecte significativement l'évaluation du comportement en déflexion de la chaussée sous TSD et, finalement, la précision de l'estimation.
2. Modèle inversé numérique : Les résultats des analyses inverses de classification et de régression utilisant l'apprentissage supervisé par machine, en particulier SVM,

dévoilent plusieurs points remarquables. Premièrement, l'étude met en avant l'efficacité de l'apprentissage automatique dans l'estimation du module de réaction du sol M_R à partir des mesures simulées de la pente de déflexion D_S du TSD, suggérant son utilité pratique potentielle en exhibant une précision élevée à travers divers scénarios de test, ce qui indique sa capacité à capturer efficacement la relation D_S-M_R. Cependant, la présence de bruit dans les données affecte les performances du modèle, entraînant une augmentation des erreurs de prédiction et une diminution de l'exactitude. Néanmoins, le modèle SVM démontre une robustesse dans la gestion des incertitudes au sein de l'ensemble de données, avec une partie considérable des erreurs de prédiction tombant dans une plage acceptable. Néanmoins, la mise en œuvre de techniques de réduction du bruit lors de la prétraitement des données devient cruciale pour améliorer la précision du modèle, surtout dans les scénarios de mesure réelle caractérisés par des données bruitées. De plus, le déséquilibre observé dans la distribution des données de la classe M_R met en évidence la nécessité d'ajuster finement les hyperparamètres pour atténuer les biais potentiels lors de la phase d'apprentissage du modèle.

3. Sensibilité à la température et au bruit, et incertitude : Les résultats de la recherche mettent en avant l'influence significative de la combinaison de la température et du bruit sur le comportement du revêtement de chaussée. Tout d'abord, l'étude souligne la sensibilité à la température des matériaux bitumineux comme l'asphalte, qui subissent des changements substantiels de rigidité et de propriétés mécaniques au gré des variations de température. Ces variations affectent directement le comportement de déflexion, influençant les évaluations des performances du revêtement de chaussée. Deuxièmement, la recherche met en évidence l'importance des données de température dans la modélisation inverse pour l'analyse du revêtement de chaussée. En incorporant les données de température, en se concentrant notamment sur les propriétés des couches en profondeur, l'exactitude des prédictions de M_R au sein de ces modèles est améliorée. De plus, l'intégration des informations de température permet une compréhension plus complète de la réponse du revêtement de chaussée dans différentes conditions thermiques, conduisant à des estimations de M_R plus fiables. En outre, les effets combinés de l'incertitude sur la température et du bruit posent des défis supplémentaires dans les mesures de pente de la déflexion D_S, et compliquent l'interprétation des réponses du revêtement de chaussée. Ce chevauchement souligne l'importance de réduire le bruit et de manipuler les données de température pour des évaluations précises du revêtement de chaussée.

4. Validation expérimentale : Les résultats de la recherche confirment l'efficacité du modèle inverse numérique ML pour évaluer l'état du revêtement de chaussée en

utilisant des mesures réelles de pente de déflexion. Cette validation est établie par l'utilisation efficace de SVM dans des tâches de régression et de classification pour estimer le module de la première couche de chaussée E_1 à partir de D_S, avec des performances acceptables dans les approches globale et locale. Les modèles ML expérimentaux et numériques montrent un alignement notable dans leurs performances, y compris dans le réglage des hyperparamètres, ce qui indique une capture précise des relations essentielles par les deux. De plus, la performance constante entre les approches globale et locale renforce davantage la validation. Bien que la méthode globale démontre une précision légèrement supérieure en raison de sa capacité à capturer des données plus riches, la méthode locale PCA présente un équilibre favorable entre précision et efficacité, adapté aux ensembles de données volumineux ou aux applications en temps réel. Ainsi, le choix entre les méthodes dépend des priorités de l'utilisateur, la méthode globale étant privilégiée pour maximiser la précision et la méthode locale PCA étant préférée pour les préoccupations concernant l'efficacité des données ou la généralisabilité avec des données limitées. En fin de compte, la sélection de l'approche optimale dépend des caractéristiques spécifiques de l'ensemble de données et des besoins de l'utilisateur.

Limitations et défis de la recherche

Cette recherche a rencontré deux limitations majeures :

— Données étiquetées limitées : Les algorithmes d'apprentissage automatique supervisés reposent fortement sur des données étiquetées pour l'entraînement et des performances efficaces. Cette recherche a été confrontée à un défi significatif en raison de la disponibilité limitée de données expérimentales étiquetées, ce qui est un problème courant à l'échelle internationale et dans la plupart des domaines. Pour pallier cette limitation, des techniques d'augmentation de données numériques sont employées en utilisant un logiciel de référence industriel (Alize-LCPC) pour construire une base de données hybride.

— Applicabilité dans des environnements diversifiés : Bien que la méthodologie développée ait été validée dans des conditions spécifiques (dans le contexte des hypothèses et des paramètres de cette thèse), sa généralités à une gamme plus large de structures de chaussée et de facteurs environnementaux reste un défi potentiel. Les variations significatives dans les matériaux de chaussée, les épaisseurs de couches et les conditions climatiques peuvent influencer les propriétés mécaniques de la chaussée.

Travaux futurs et recommandations

— Recommandation d'utilisation du modèle : Une validation supplémentaire avec des données de mesure réelles provenant de TSDDs sur différentes sections de chaussée serait bénéfique pour évaluer les performances du modèle inverse et faciliter une meilleure optimisation. Par conséquent, lors de l'application du modèle dans différentes configurations, il est recommandé de suivre la méthodologie générale développée tout en tenant compte des éventuelles divergences dans ces propriétés.

— Chaussée en béton et composite : Bien que les déflectomètres de vitesse de trafic (TSD) aient démontré leur potentiel dans l'évaluation de l'état structural des chaussées flexibles, il y a eu peu d'exploration de leur application aux dalles de chaussée en béton et composite, ainsi qu'aux joints porteurs de charge. Malgré leur utilisation extensive dans le réseau routier, la recherche liée aux TSD a largement négligé ces types de chaussées. Par conséquent, les études futures devraient se concentrer sur le comblement de cette lacune en examinant la faisabilité d'utiliser les TSD pour évaluer l'intégrité structurelle des chaussées en béton et composite.

— Bien que cette thèse ait contribué à l'avancement de la mécanique des chaussées en utilisant l'intelligence artificielle pour analyser les mesures de pente de déflexion et interpréter le comportement des chaussées pour estimer les propriétés mécaniques structurelles, elle met également en évidence des défis dans l'optimisation de l'approche inverse. Plus précisément, elle souligne l'importance des connaissances préalables des propriétés de structure des chaussées et la nécessité d'une base de données bien étiquetée. Sur la base de ces constatations, il est recommandé d'intégrer les données des déflectomètres de vitesse de trafic (TSD) et des radars à pénétration de sol (GPR) lors de la construction de modèles d'IA generative pour une compréhension efficace du comportement des chaussées.

APPENDIX

Rapid Pavement Tester (RAPTOR)

The Raptor (Figure 6.1) is a cutting-edge device developed in collaboration between Dynatest and the Technical University of Denmark (DTU), which represents a significant advancement in pavement evaluation technology. This state-of-the-art TSDDs device is specifically designed for in-motion measurement of pavement deflections, providing real-time data on road conditions [88]. The Raptor is a semi-trailer truck featuring rear-mounted independent single-wheel suspension systems, with one system on each side. The sensor beam is installed in a protected compartment at the platform's bottom, approximately 200 mm above the pavement surface. This beam comes near one of the tires (from the inner side) and is equipped with an array of laser-based line profilers [86].
(Figure 6.2 *a*) presents a plan view of the Raptor platform, while (Figure 6.2 *b*) showcases a side view. The platform designation "2×50 kN" signifies no connection between the rear wheels. Additionally, (Figure 6.2 *b*) depicts a sketch of the deformed pavement surface for a cross-section directly below the sensor beam. It should be noted that this sketch is based on a linear elastic half-space model and aims to offer a qualitative understanding of the anticipated laser readings [86].

Raptor principle of operation

The Raptor's sensor beam carries individual lasers, each of which measures its self-distance to the pavement surface along a line transverse to the travel direction. This specific line is referred to as the "detection window" Figure 6.3 *a*, covering approximately 200 mm in length and containing over 1280 individually measured distance points, with each point having an approximate diameter of 200 micrometers. The lasers operate at a sample rate of approximately 4000 Hz, generating around four million data points per second from a single laser line profiler [87].
As the Raptor advances, a three-dimensional scan ($3D$) of the road surface is formed when the individual laser measurements are arranged as rows in a matrix Figure 6.3 *b* for lasers (i and $i-1$). Therefore, any arbitrary point on the pavement surface that enters the detection window of the forwardmost sensor (Laser I, Figure 6.3 *a*) can be identified in the readings of all other lasers. This identification process relies on an image correlation technique, which matches texture patches surrounding the evaluated point for each laser.

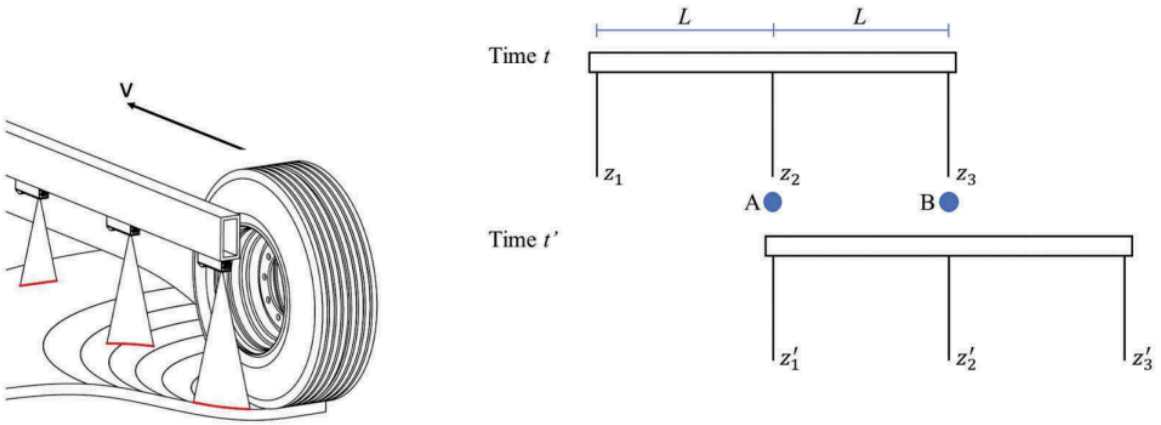

(a) Laser mounting on beam. (b) RAPTOR measuring principle.

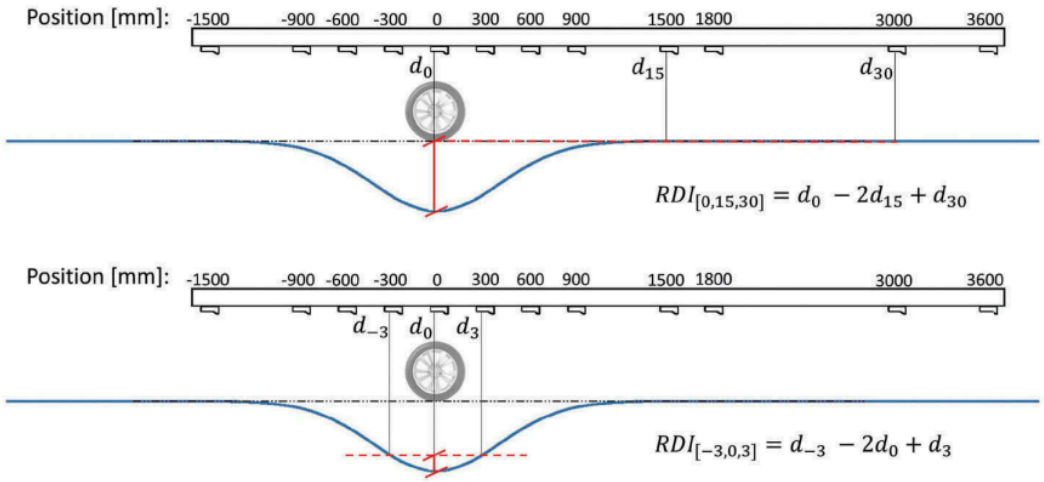

(c) RAPTOR Deflection Indices (RDI).

Figure 6.1 – Raptor [88].

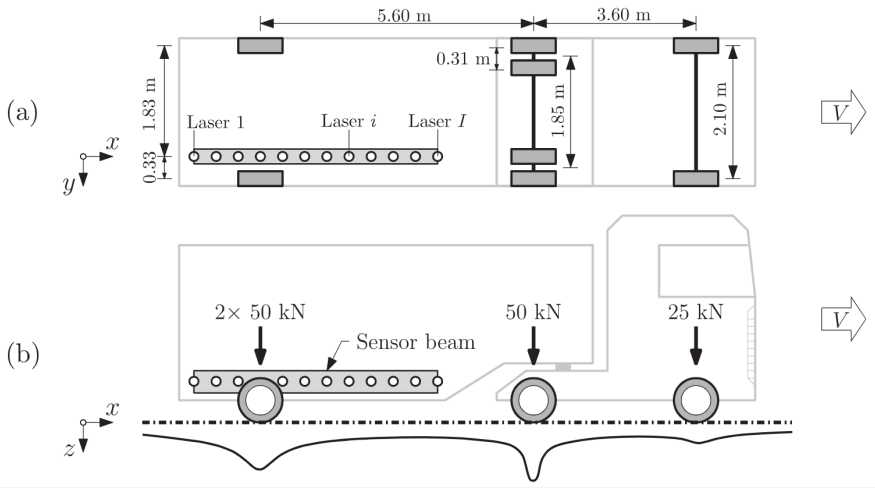

Figure 6.2 – Raptor's sketch, (a) top view in $x-y$ plane, (b) side view in $x-z$ plane [86].

Figure 6.3 b illustrates two such texture patches, represented by dashed square frames, each with dimensions of (64 × 64 pixels) [87]. Since the natural texture surrounding a point on the pavement surface is unique, the identification of a patch across all scans is achieved with a high level of confidence.

The length of the detection window, which spans 200 mm, compensates for any beam roll, yaw rotations, or a combination of both, ensuring that the sought patch remains within the detection boundaries across all lasers. Furthermore, if these rotations are independently measured, patch-matching can also be extended to identify sideway displacements of the tracked point [86].

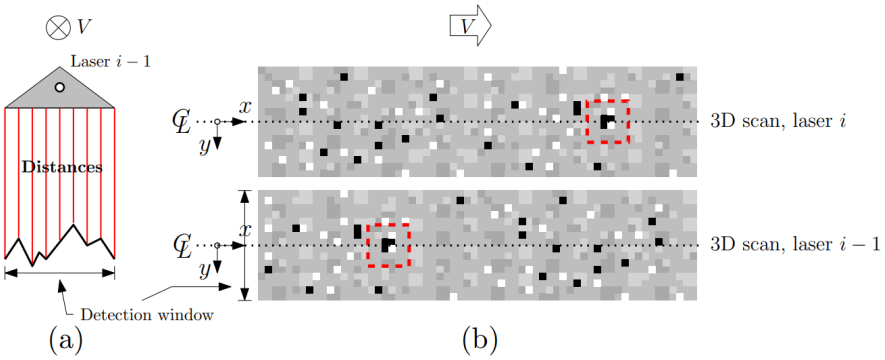

Figure 6.3 – Linelaser sensor, (a) grayscale pixels detection window, (b) 3D surface scan [86]

.

Raptor measurement data

The Raptor sensor beam has motion-tracking sensors, including gyroscopes and accelerometers. These sensors track changes in beam pitch angle and height over short intervals through integration. To demonstrate the collected data during a standard Raptor

operation, Figure 6.4 represents a segment of the sensor beam containing two lasers, i and $i-1$, moving at a constant speed V. The unloaded pavement surface (before deformation) is represented by a straight dashed-dotted line, and the loaded pavement surface (after deformation) is depicted by a curved solid line. The coordinate system attached to the beam is right-handed, with the origin located at the unloaded surface. The x-axis aligns with the travel direction, while the z-axis points downward into the medium [86].

Figure 6.4 *a*, the distance d_i^M to a random evaluation point A on the pavement surface is measured by laser i. When laser i detects point A, the beam's angle is θ_i, and the height is h_i (measured concerning a reference point on the beam). The displacements of the point in the x-z plane are represented by u_x and u_z, illustrating two orthogonal displacements. At a later time, Figure 6.4 *b*, the distance d_{i-1}^M to the same point A is measured by laser $i-1$. The corresponding beam angle is θ_{i-1}, and the height is h_{i-1} [86].

Therefore, the fundamental measurement data provided by the Raptor device for a random evaluation point includes distance readings from each laser, denoted by d_i^M's, as well as the changes in sensor beam angle ($\Delta\theta_{i\to i-1}$) and sensor beam height ($\Delta h_{i\to i-1}$) between consecutive detections obtained from the motion tracking sensors. These changes are calculated as $\Delta\theta_{i\to i-1} = \theta_{i-1} - \theta_i$ and $\Delta h_{i\to i-1} = h_{i-1} - h_i$ [86].

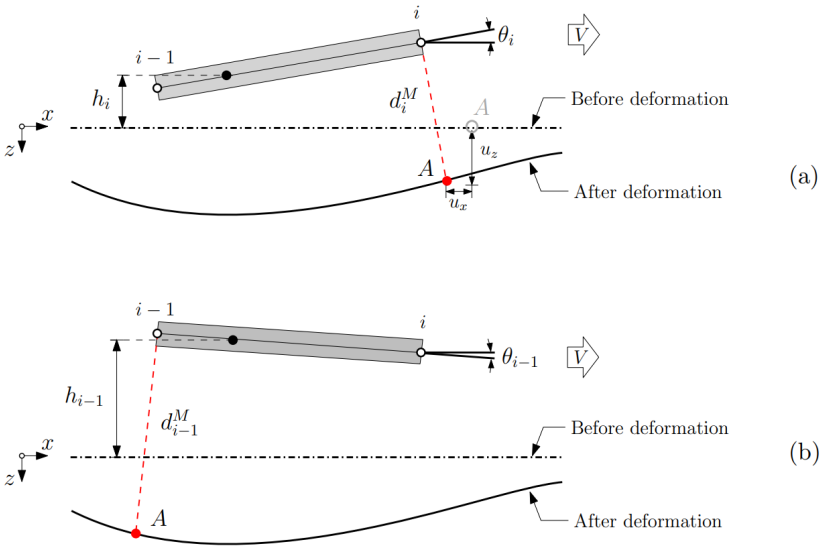

Figure 6.4 – Raptor measurement data: (a) distance d_i^M and (b) distance d_{i-1}^M [86].

Raptor limitations

Practical implementation of Raptor reveals limitations related to the system's high-sensitivity lasers, which introduce noise and erratic behavior (surface texture). Also, the current analytical approach overlooks surface displacements along the y-axis. Moreover, the untapped potential of patch-matching techniques to identify lateral displacements adds to these limitations.

BIBLIOGRAPHY

[1] French Ministry of Ecological Transition, "Chiffres clés du transport - edition 2021," 2021. Source: Ministry of Ecological Transition.

[2] W. Bank, *World development report 1994: Infrastructure for development*. 1994.

[3] M. Bexell and K. Jönsson, "Responsibility and the united nations' sustainable development goals," in *Forum for development studies*, vol. 44, pp. 13–29, Taylor & Francis, 2017.

[4] E. Commission, "The european green deal," 2019.

[5] E.U.R. Federation, "ERF road statistics 2020," 2020.

[6] E. U. R. Federation, *Road Asset Management - An ERF Position Paper for Maintaining and Improving a Sustainable and Efficient Road Network*. Brussels, Belgium: European Union Road Federation, 2014.

[7] D. Balageas, C.-P. Fritzen, and A. Güemes, "Structural health monitoring," vol. 493, doi 10.1098/rsta.2006.1928, pp. 13–29, 2006.

[8] R. L. Lytton, *Backcalculation of pavement layer properties*. ASTM International West Conshohocken, Pennsylvania, 1989.

[9] H. L. Von Quintus, C. Rao, and L. H. Irwin, "Long-term pavement performance program determination of in-place elastic layer modulus: backcalculation methodology and procedures," tech. rep., United States. Federal Highway Administration. Office of Infrastructure , 2015.

[10] E. Horak, A. Hefer, and J. Maina, "Determination of pavement number for flexible pavements using FWD deflection bowl information," Southern African Transport Conference, 2015.

[11] S. W. Katicha, G. W. Flintsch, B. Ferne, and J. Bryce, "Limits of agreement method for comparing TSD and FWD measurements," *International Journal of Pavement Engineering*, vol. 15, no. 6, pp. 532–541, 2014.

[12] D. Kim, Y. Ji, and N. Z. Siddiki, "Evaluation of in-situ stiffness of subgrade by resilient and FWD modulus," 2010.

[13] D. Jansen, "Tsd evaluation in germany," in *Proceedings of the International Symposium Non-Destructive Testing in Civil Engineering*, pp. 700–708, 2015.

[14] B. Huang, M. Zhang, H. Gong, and P. Polaczyk, "Evaluation of traffic speed deflectometer for collecting network level pavement structural data in tennessee," tech. rep., Tennessee. Department of Transportation, 2022.

[15] M. Zhang, X. Jia, G. Fu, P. A. Polaczyk, Y. Ma, R. Xiao, and B. Huang, "Traffic speed deflectometer for network-level pavement management in Tennessee," *Transportation Research Record*, p. 03611981231197665, 2023.

[16] H. Ceylan, A. Guclu, E. Tutumluer, and M. R. Thompson, "Backcalculation of full-depth asphalt pavement layer moduli considering nonlinear stress-dependent subgrade behavior," *International Journal of Pavement Engineering*, vol. 6, no. 3, pp. 171–182, 2005.

[17] K. Gopalakrishnan, "Instantaneous pavement condition evaluation using non-destructive neuro-evolutionary approach," *Structure and Infrastructure Engineering*, vol. 8, no. 9, pp. 857–872, 2012.

[18] B. Ghorbani, A. Arulrajah, G. Narsilio, S. Horpibulsuk, and M. W. Bo, "Development of genetic-based models for predicting the resilient modulus of cohesive pavement subgrade soils," *Soils and Foundations*, vol. 60, no. 2, pp. 398–412, 2020.

[19] S. Fathi, M. Mehravar, and M. Rahman, "Development of fwd based hybrid back-analysis technique for railway track condition assessment," *Transportation Geotechnics*, vol. 38, p. 100894, 2023.

[20] F. Xiao, Q. Xiang, X. Hou, and S. N. Amirkhanian, "Utilization of traffic speed deflectometer for pavement structural evaluations," *Measurement*, vol. 178, p. 109326, 2021.

[21] M. Nasimifar, R. Kamalizadeh, and B. Heidary, "The available approaches for using traffic speed deflectometer data at network level pavement management system," *Measurement*, p. 111901, 2022.

[22] M. Zhang, R. Xiao, Y. Ma, X. Jiang, P. A. Polaczyk, and B. Huang, "Evaluating structural characteristics of asphalt pavements by using deflection slopes from traffic speed deflectometer," *Construction and Building Materials*, vol. 365, p. 130052, 2023.

[23] M. S. Lasalle, G. W. Flintsch, S. W. Katicha, A. S. Brand, and B. K. Diefenderfer, "A big-data-based approach towards concrete and composite pavement management and rehabilitation," 2022.

[24] L. Zhou, S. Pan, J. Wang, and A. V. Vasilakos, "Machine Learning on big data: Opportunities and challenges," *Neurocomputing*, vol. 237, pp. 350–361, 2017.

[25] N. Sholevar, A. Golroo, and S. R. Esfahani, "Machine Learning techniques for pavement condition evaluation," *Automation in Construction*, vol. 136, p. 104190, 2022.

[26] M. Wasimuddin, K. Elleithy, A.-S. Abuzneid, M. Faezipour, and O. Abuzaghleh, "Stages-based ECG signal analysis from traditional signal processing to Machine Learning approaches: A survey," *IEEE Access*, vol. 8, pp. 177782–177803, 2020.

[27] M. A. Elseifi and Z. U. Zihan, "Assessment of the traffic speed deflectometer in Louisiana for pavement structural evaluation," tech. rep., Louisiana Transportation Research Center, 2018.

[28] S. Katicha, G. Flintsch, and B. Diefenderfer, "Ten years of traffic speed deflectometer research in the United States: A review," *Transportation research record*, vol. 2676, no. 12, pp. 152–165, 2022.

[29] AFNOR, "NF P 98-086: Dimensionnement structural de chaussée routière, application aux chaussées neuves," Norme Française / French Standard NF P 98-121, AFNOR, 2019.

[30] Service of Technical Studies for Roads and Motorways (SETRA) and Central Laboratory of Bridges and Highways (LCPC), *Guide Technique, French Design Manual for Pavement Structures (English Version)*. Paris, France: SETRA, 1998.

[31] J. Krarup, S. Rasmussen, L. Aagaard, and P. G. Hjorth, "Output from the greenwood traffic speed deflectometer," in *Research into Practice: 22nd ARRB ConferenceARRB*, 2006.

[32] S. S. Park, A. Bobet, and T. E. Nantung, "Correlation between resilient modulus of soil, light weight deflectometer, and falling weight deflectometer FWD," 2018.

[33] S. R. Gunn *et al.*, "Support vector machines for classification and regression," *ISIS technical report*, vol. 14, no. 1, pp. 5–16, 1998.

[34] M. Tanveer, T. Rajani, R. Rastogi, Y.-H. Shao, and M. Ganaie, "Comprehensive review on twin support vector machines," *Annals of Operations Research*, pp. 1–46, 2022.

[35] D. Sulistyaningrum, S. Putri, B. Setiyono, E. Ahyudanari, and D. Oranova, "Classification of damaged road types using multiclass support vector machine (svm)," in *Journal of Physics: Conference Series*, vol. 1821, p. 012048, IOP Publishing, 2021.

[36] O. Chapelle, V. Vapnik, O. Bousquet, and S. Mukherjee, "Choosing multiple parameters for support vector machines," *Machine learning*, vol. 46, pp. 131–159, 2002.

[37] D. Anguita, S. Ridella, F. Rivieccio, and R. Zunino, "Automatic hyperparameter tuning for support vector machines," in *Artificial Neural Networks—ICANN 2002: International Conference Madrid, Spain, August 28–30, 2002 Proceedings 12*, pp. 1345–1350, Springer, 2002.

[38] "I-street project team systemic innovations for ecological and energy transitions in transport infrastructure." `https://www.editions-rgra.com/revue/957/nouvelles-mobilites/projet-route-du-futur-i-street`.

[39] SETRA (Service d'Études Techniques des Routes et Autoroutes), "Guide technique: Construction des chaussées neuves sur le réseau routier national," technical report, Mars 2003.

[40] D. D. B. Enterprise and I. I. S. T. E. Act, "This is a report of research and technology transfer activities carried out by the wisconsin department of transportation through the part ii research portion of the state planning and research program of the federal highway administration, us department of transportation. the report describes activities during federal fiscal year 2009, covering october 1, 2008, through september 30, 2009.,"

[41] W. F. Flora, G. P. Ong, and K. C. Sinha, "Development of a structural index as an integral part of the overall pavement quality in the INDOT PMS," 2010.

[42] PIARC, "Asset management for roads - an overview, https://www.piarc.org/ressources/publications/2/4545,06-09-vcd.pdf," 2005. Committee on Road Management (C6).

[43] R. Stubstad, R. Carvalho, R. Briggs, O. Selezneva, *et al.*, "Simplified techniques for evaluation and interpretation of pavement deflections for network-level analysis: Guide for assessment of pavement structure performance for pms applications," tech. rep., Turner-Fairbank Highway Research Center, 2012.

[44] G. R. Rada, S. Nazarian, B. A. Visintine, R. V. Siddharthan, S. Thyagarajan, *et al.*, "Pavement structural evaluation at the network level," tech. rep., United States. Federal Highway Administration. Office of Infrastructure . . . , 2016.

[45] G. W. Flintsch, B. Ferne, B. Diefenderfer, S. Katicha, J. Bryce, and S. Nell, "Evaluation of traffic-speed deflectometers," *Transportation research record*, vol. 2304, no. 1, pp. 37–46, 2012.

[46] K. D. Smith, J. E. Bruinsma, M. J. Wade, K. Chatti, J. Vandenbossche, H. T. Yu, *et al.*, "Using falling weight deflectometer data with mechanistic-empirical design and analysis," tech. rep., United States. Federal Highway Administration, 2017.

[47] L. M. Pierce, J. E. Bruinsma, K. D. Smith, M. J. Wade, K. Chatti, J. Vandenbossche, *et al.*, "Using falling weight deflectometer data with mechanistic-empirical design and analysis, volume iii: Guidelines for deflection testing, analysis, and interpretation," tech. rep., United States. Federal Highway Administration, 2017.

[48] T. S. Deflectometer, "Greenwood engineering, brondby, denmark."

[49] K. Worden and G. Manson, "The application of Machine Learning to Structural Health Monitoring," *Philosophical Transactions of the Royal Society A: Mathematical, Physical and Engineering Sciences*, vol. 365, no. 1851, pp. 515–537, 2007.

[50] SETRA-LCPC, *Conception et dimensionnement des structures de chaussée.* SETRA-LCPC, 1994.

[51] H. Di Benedetto, "J.f corté,matériaux routiers bitumineux, hermes sciences publications, traité mécanique et ingénierie des matériaux ," 2004.

[52] M. M. Hilal, "Prediction of permanent deformation models for asphalt pavements in hot climates," *University of Baghdad, Iraq*, 2011.

[53] L. Korkiala-Tanttu, "A new material model for permanent deformations in pavements," in *Proceedings of the international conferences on the bearing capacity of roads, railways and airfields*, 2005.

[54] SETRA, ed., *Pavement Monitoring and Reinforcement.* 2015. French guide, 260 pages.

[55] J. R. de Almeida, S. F. Brown, and N. H. Thorn, "A pavement linearity," *Nondestructive Testing of Pavements and Backcalculation of Moduli: Second Volume*, vol. 2, p. 218, 1994.

[56] J. Litzka, B. Leben, F. L. Torre, A. Weninger-Vycudil, M. d. L. Antunes, D. Kokot, G. Mladenovic, S. Brittain, and H. Viner, *The Way Forward for Pavement Performance Indicators Across Europe. COST Action 354: Performance Indicators for Road Pavements.* 2008.

[57] C. A. P. M. van Gurp, *Characterization of seasonal influences on asphalt pavements with the use of falling weight deflectometers.* 1995.

[58] C. Huet, *Etude par une méthode d'impédance du comportement viscoélastique des matériaux hydrocarbonés*. Ph.d. thesis, Université de Paris (France), 1963.

[59] G. Sayegh, *Contribution à l'étude des propriétés viscoélastiques des bitumes purs et des bétons bitumineux*. Ph.d. thesis, Faculté des Sciences de Paris (France), 1965.

[60] C.-J. Haecker, E. Garboczi, J. Bullard, R. Bohn, Z. Sun, S. P. Shah, and T. Voigt, "Modeling the linear elastic properties of portland cement paste," *Cement and Concrete Research*, vol. 35, no. 10, pp. 1948–1960, 2005.

[61] J. Atkinson, "Non-linear soil stiffness in routine design," *Géotechnique*, vol. 50, no. 5, pp. 487–508, 2000.

[62] H. D. Di Benedetto, B. Delaporte, and C. Sauzéat, "Three-dimensional linear behavior of bituminous materials: experiments and modeling," *International Journal of Geomechanics*, vol. 7, no. 2, pp. 149–157, 2007.

[63] X. Wang, H. Guo, B. Yang, X. Chang, C. Wan, and Z. Wang, "Aging characteristics of bitumen from different bituminous pavement structures in service," *Materials*, vol. 12, no. 3, p. 530, 2019.

[64] S. A. Romanoschi, *Characterization of pavement layer interfaces*. Louisiana State University and Agricultural & Mechanical College, 1999.

[65] P. Jaskula and D. Rys, "Effect of interlayer bonding quality of asphalt layers on pavement performance," in *IOP Conference Series: Materials Science and Engineering*, vol. 236, p. 012005, IOP Publishing, 2017.

[66] S. Fontul, *Structural evaluation of flexible pavements using non-destructive tests*. PhD thesis, Universidade de Coimbra (Portugal), 2004.

[67] C. A. Felippa, "Introduction to finite element methods," *University of Colorado*, vol. 885, 2004.

[68] J. Boussinesq, *Application des potentiels à l'étude de l'équilibre et du mouvement des corps élastiques*. Chauthier Villars, 1885.

[69] H. M. Westergaard, "Stresses in concrete pavements on elastic foundations," *Proceedings of the American Society of Civil Engineers*, vol. 51, no. 3, pp. 131–162, 1926.

[70] G. L. Hogg, "The elastic theory of pavement design," *Proceedings of the Institution of Civil Engineers*, vol. 19, no. 4, pp. 411–425, 1938.

[71] D. M. Burmister, "The theory of stresses and displacements in layered systems and applications of the design of airport runways," *Proceedings of the highways Research board*, vol. 23, pp. 126–148, 1943.

[72] C. Jeuffroy, "Étude des chaussées flexibles par analogie électrique," *Revue Générale des Routes*, vol. 34, pp. 5–17, 1955.

[73] J.-M. Roussel, C. Sauzéat, H. Di Benedetto, and M. Broutin, "Numerical simulation of falling/heavy weight deflectometer test considering linear viscoelastic behaviour in bituminous layers and inertia effects," *Road Materials and Pavement Design*, vol. 20, no. sup1, pp. S64–S78, 2019.

[74] Laboratoire Central des Ponts Et Chaussées, "ALIZé 2 Software," 2021.

[75] X. Q. Le, *Analysis and modelling of APT experiments based on optimized management of database of mechanical measurements*. Theses, École centrale de Nantes, Dec. 2022.

[76] J. E. Bruinsma, J. Vandenbossche, K. Chatti, K. D. Smith, *et al.*, "Using falling weight deflectometer data with mechanistic-empirical design and analysis, volume ii: Case study reports," tech. rep., United States. Federal Highway Administration, 2017.

[77] V. Le Boursicaud, *Nouvelles utilisations des mesures de bassins de déflexion pour caractériser l'état structurel des chaussées*. PhD thesis, École centrale de Nantes, 2018.

[78] "Infociments." www.Infociments.fr. Infociments est une plateforme d'information dédiée à la connaissance du ciment et de ses applications, proposée par les organisations professionnelles de l'industrie cimentière.

[79] E. Horak, "Benchmarking the structural condition of flexible pavements with deflection bowl parameters," *Journal of the South African Institution of Civil Engineering*, vol. 50, no. 2, pp. 2–9, 2008.

[80] J.-M. Simonin, J.-L. Geffard, and P. Hornych, "Performance of deflection measurement equipment and data interpretation in france," in *International Symposium Non-Destructive Testing in Civil Engineering (NDT-CE) September*, pp. 15–17, 2015.

[81] J. Simonin, V. Le Boursicaud, and P. Hornych, "Correction of deflection bowls measured by rolling devices using simple shape function," *Transportation Engineering*, vol. 3, p. 100050, 2021.

[82] Z. U. A. Zihan, *Evaluation of Traffic Speed Deflectometer for Pavement Structural Evaluation in Louisiana.* Louisiana State University and Agricultural & Mechanical College, 2019.

[83] M. Nasimifar, R. V. Siddharthan, G. R. Rada, and S. Nazarian, "Dynamic analyses of traffic speed deflection devices," *International Journal of Pavement Engineering*, vol. 18, no. 5, pp. 381–390, 2017.

[84] X. Jia, M. Woods, H. Gong, D. Zhu, W. Hu, and B. Huang, "Evaluation of influence of pavement data on measurement of deflection on asphalt surfaced pavements utilizing traffic speed deflection device," *Construction and Building Materials*, vol. 270, p. 121842, 2021.

[85] Cerema, "Essais croisés d'appareils innovants de déflexion pour déterminer la capacité portante des routes," 2022. Le Cerema a organisé une session d'essais croisés des matériels de déflexion à grande vitesse en Alsace en juin 2022, dans le cadre du projet national Durée de Vie Des Chaussées (DVDC) piloté par l'IREX.

[86] A. Skar, E. Levenberg, S. Andersen, and M. B. Andersen, "Analysis of a moving measurement platform based on line profile sensors for project-level pavement evaluation," *Road Materials and Pavement Design*, vol. 22, no. 9, pp. 2069–2085, 2021.

[87] S. Madsen and N. Pedersen, "Comparison of raptor measurements with falling weight deflectometer deflections using backcalculation," in *Eleventh International Conference on the Bearing Capacity of Roads, Railways and Airfields*, pp. 33–44, CRC Press, 2022.

[88] M. Stonecliffe-Jones, "Introduction to the dynatest raptor rolling wheel deflectometer," in *Proceedings of the ERPUG Conference*, (Copenhagen), Dynatest, 2017. Dynatest Director of Consulting.

[89] M. Scavone, S. W. Katicha, G. W. Flintsch, and E. Amarh, "On the tsd deflection velocity measurements: a revision to the current state of the art and discussion over its applicability for concrete pavement assessment," *International Journal of Pavement Engineering*, vol. 24, no. 2, p. 2138881, 2023.

[90] W. B. Muller and J. Roberts, "Revised approach to assessing traffic speed deflectometer data and field validation of deflection bowl predictions," *International journal of pavement engineering*, vol. 14, no. 4, pp. 388–402, 2013.

[91] B. W. Ferne, P. Langdale, N. Round, and R. Fairclough, "Development of a calibration procedure for the uk highways agency traffic-speed deflectometer," *Transportation research record*, vol. 2093, no. 1, pp. 111–117, 2009.

[92] K. Shen and H. Wang, "Impact of dynamic loading on pavement deflection measurements from traffic speed deflectometer," *Measurement*, vol. 217, p. 113086, 2023.

[93] S. Varma and M. Emin Kutay, "Backcalculation of viscoelastic and nonlinear flexible pavement layer properties from falling weight deflections," *International Journal of Pavement Engineering*, vol. 17, no. 5, pp. 388–402, 2016.

[94] R. V. Siddharthan, J. Yao, and P. E. Sebaaly, "Pavement strain from moving dynamic 3d load distribution," *Journal of Transportation Engineering*, vol. 124, no. 6, pp. 557–566, 1998.

[95] Z. U. Zihan, M. A. Elseifi, P. Icenogle, K. Gaspard, and Z. Zhang, "Mechanistic-based approach to utilize traffic speed deflectometer measurements in backcalculation analysis," *Transportation research record*, vol. 2674, no. 5, pp. 208–222, 2020.

[96] M. Nasimifar, S. Thyagarajan, and N. Sivaneswaran, "Backcalculation of flexible pavement layer moduli from traffic speed deflectometer data," *Transportation Research Record*, vol. 2641, no. 1, pp. 66–74, 2017.

[97] C. P. Nielsen, "Visco-elastic back-calculation of traffic speed deflectometer measurements," *Transportation research record*, vol. 2673, no. 12, pp. 439–448, 2019.

[98] C. Wu, H. Wang, J. Zhao, X. Jiang, and Y. Qiu, "Asphalt pavement modulus backcalculation using surface deflections under moving loads," *Computer-Aided Civil and Infrastructure Engineering*, vol. 35, no. 11, pp. 1246–1260, 2020.

[99] N. Andrew, "Machine learning," *Coursera. Available online: https://www. coursera. org/learn/machine-learning (accessed on 1 March 2019)*, 2016.

[100] Y. LeCun, Y. Bengio, and G. Hinton, "Deep learning," *nature*, vol. 521, no. 7553, pp. 436–444, 2015.

[101] I. El Naqa and M. J. Murphy, "What are machine and deep learning?," in *Machine and deep learning in oncology, medical physics and radiology*, pp. 3–15, Springer, 2022.

[102] F. Hoffmann, T. Bertram, R. Mikut, M. Reischl, and O. Nelles, "Benchmarking in classification and regression," *Wiley Interdisciplinary Reviews: Data Mining and Knowledge Discovery*, vol. 9, no. 5, p. e1318, 2019.

[103] S. Raschka, "Model evaluation, model selection, and algorithm selection in machine learning," *arXiv preprint arXiv:1811.12808*, 2018.

[104] C. Janiesch, P. Zschech, and K. Heinrich, "Machine learning and deep learning," *Electronic Markets*, vol. 31, no. 3, pp. 685–695, 2021.

[105] A. Zheng and A. Casari, *Feature engineering for Machine Learning: principles and techniques for data scientists*. " O'Reilly Media, Inc.", 2018.

[106] A. Amidi and S. Amidi, "Machine learning tips and tricks cheatsheet," *https://stanford. edu/˜ shervine/teaching/cs-229/cheatsheet-machine-learning-tips-and-tricks# classification-metrics*, 2020.

[107] N.-D. Hoang, "An artificial intelligence method for asphalt pavement pothole detection using least squares Ssupport Vector Machine and Neural Network with steerable filter-based feature extraction," *Advances in Civil Engineering*, vol. 2018, 2018.

[108] X. Xu, I. W. Tsang, and D. Xu, "Soft margin multiple kernel learning," *IEEE transactions on neural networks and learning systems*, vol. 24, no. 5, pp. 749–761, 2013.

[109] M. Svilar, I. Peško, and M. Šešlija, "Model for estimating the modulus of elasticity of asphalt layers using Machine Learning," *Applied Sciences*, vol. 12, no. 20, p. 10536, 2022.

[110] B. Mahesh, "Machine Learning algorithms-a review," *International Journal of Science and Research (IJSR).[Internet]*, vol. 9, no. 1, pp. 381–386, 2020.

[111] T. Ghalandari, L. Shi, F. Sadeghi-Khanegah, C. Vuye, *et al.*, "Utilizing artificial neural networks to predict the asphalt pavement profile temperature in western europe," *Case Studies in Construction Materials*, vol. 18, p. e02130, 2023.

[112] L. Breiman, "Random forests," *Machine learning*, vol. 45, pp. 5–32, 2001.

[113] A. Issa, H. Sammaneh, and K. Abaza, "Modeling pavement condition index using cascade architecture: classical and neural network methods," *Iranian Journal of Science and Technology, Transactions of Civil Engineering*, vol. 46, no. 1, pp. 483–495, 2022.

[114] L. Zhang, F. Yang, Y. D. Zhang, and Y. J. Zhu, "Road crack detection using deep convolutional neural network," in *2016 IEEE international conference on image processing (ICIP)*, pp. 3708–3712, IEEE, 2016.

[115] H. Nhat-Duc, Q.-L. Nguyen, and V.-D. Tran, "Automatic recognition of asphalt pavement cracks using metaheuristic optimized edge detection algorithms and Convolution Neural Networks CNN," *Automation in Construction*, vol. 94, pp. 203–213, 2018.

[116] X. Wang and Z. Hu, "Grid-based pavement crack analysis using Deep Learning," in *2017 4th International conference on transportation information and safety (ICTIS)*, pp. 917–924, IEEE, 2017.

[117] M. Eisenbach, R. Stricker, D. Seichter, K. Amende, K. Debes, M. Sesselmann, D. Ebersbach, U. Stoeckert, and H.-M. Gross, "How to get pavement distress detection ready for deep learning? a systematic approach," in *2017 international joint conference on neural networks (IJCNN)*, pp. 2039–2047, IEEE, 2017.

[118] S. Anand, S. Gupta, V. Darbari, and S. Kohli, "Crack-pot: Autonomous road crack and pothole detection," in *2018 Digital Image Computing: Techniques and Applications (DICTA)*, pp. 1–6, IEEE, 2018.

[119] S. Shah and C. Deshmukh, "Pothole and bump detection using convolution neural networks," in *2019 IEEE transportation electrification conference (ITEC-India)*, pp. 1–4, IEEE, 2019.

[120] J. Huyan, W. Li, S. Tighe, Z. Xu, and J. Zhai, "Cracku-net: A novel Deep Convolutional Neural Network for pixelwise pavement crack detection," *Structural Control and Health Monitoring*, vol. 27, no. 8, p. e2551. e2551 STC-19-0110.R2.

[121] S. L. H. Lau, E. K. P. Chong, X. Yang, and X. Wang, "Automated pavement crack segmentation using u-net-based convolutional neural network," *IEEE Access*, vol. 8, pp. 114892–114899, 2020.

[122] "Pavement crack detection and recognition using the architecture of segnet," *Journal of Industrial Information Integration*, vol. 18, p. 100144, 2020.

[123] L. Cui, Z. Qi, Z. Chen, F. Meng, and Y. Shi, "Pavement distress detection using random decision forests," in *Data Science: Second International Conference, ICDS 2015, Sydney, Australia, August 8-9, 2015, Proceedings 2*, pp. 95–102, Springer, 2015.

[124] Y. Shi, L. Cui, Z. Qi, F. Meng, and Z. Chen, "Automatic road crack detection using random structured forests," *IEEE Transactions on Intelligent Transportation Systems*, vol. 17, no. 12, pp. 3434–3445, 2016.

[125] S. Liaqat, K. Dashtipour, K. Arshad, K. Assaleh, and N. Ramzan, "A hybrid posture detection framework: Integrating machine learning and deep neural networks," *IEEE Sensors Journal*, vol. 21, no. 7, pp. 9515–9522, 2021.

[126] H. Zakeri, F. M. Nejad, and A. Fahimifar, "Image based techniques for crack detection, classification and quantification in asphalt pavement: a review," *Archives of Computational Methods in Engineering*, vol. 24, pp. 935–977, 2017.

[127] K. C. Wang and W. Gong, "Automated pavement distress survey: a review and a new direction," in *Pavement evaluation conference*, pp. 21–25, 2002.

[128] W. Song, Z. Zhang, B. Zhang, G. Jia, H. Zhu, and J. Zhang, "A benchmark dataset for multi-type pavement distress segmentation from CDD images in complex scenarios," *Remote Sensing*, vol. 15, no. 7, p. 1750, 2023.

[129] "Deep machine learning approach to develop a new asphalt pavement condition index," *Construction and Building Materials*, vol. 247, p. 118513, 2020.

[130] J.-F. Corté and M.-T. Goux, "Design of pavement structures: the french technical guide," *Transportation Research Record*, vol. 1539, no. 1, pp. 116–124, 1996.

[131] O. Elbagalati, M. Mousa, M. A. Elseifi, K. Gaspard, and Z. Zhang, "Development of a methodology to backcalculate pavement layer moduli using the traffic speed deflectometer," *Canadian Journal of Civil Engineering*, vol. 45, no. 5, pp. 377–385, 2018.

[132] A. Abdelmuhsen, J.-M. Simonin, F. Schmidt, D. Lievre, A. Cothenet, and A. Ihamouten, "On the variants of svm method for the estimation of soil elastic modulus from tsd model: Numerical parametric study," *Transportation Engineering*, vol. 13, p. 100187, 2023.

[133] A. Abdelmuhsen, J.-M. Simonin, F. Schmidt, A. Ihamouten, and D. Lièvre, "Database construction based upon numerical modelling of pavement deflection behaviour under the traffic speed deflectometer," in *25e Congrès Français de Mécanique*, 2022.

[134] Association Française de Normalisation (AFNOR), *Dimensionnement des structures routières, application aux chaussées neuves.* Paris, France: AFNOR, 2019.

[135] R. Ahlvin, Y. Chou, and R. Hutchinson, "The principle of superposition in pavement analysis," *Highway Research Record*, vol. 466, pp. 153–160, 1973.

[136] S. W. Katicha, G. Flintsch, J. Bryce, and B. Ferne, "Wavelet denoising of tsd deflection slope measurements for improved pavement structural evaluation," *Computer-Aided Civil and Infrastructure Engineering*, vol. 29, no. 6, pp. 399–415, 2014.

[137] R. Mondal, T. Pal, and P. Dey, "A hybrid regularized multilayer perceptron for input noise immunity," *IEEE Transactions on Artificial Intelligence*, 2023.

[138] X. Huang, "Stochastic resonance in a piecewise bistable energy harvesting model driven by harmonic excitation and additive gaussian white noise," *Applied Mathematical Modelling*, vol. 90, pp. 505–526, 2021.

[139] N. Ekbote, P. Dhanshetti, and S. Sakhrekar, "Techniques of exploratory data analysis,"

[140] H. Di Benedetto, F. Olard, C. Sauzéat, and B. Delaporte, "Linear viscoelastic behaviour of bituminous materials: From binders to mixes," *Road Materials and Pavement Design*, vol. 5, no. sup1, pp. 163–202, 2004.

[141] F. Pedregosa, G. Varoquaux, A. Gramfort, V. Michel, B. Thirion, O. Grisel, M. Blondel, P. Prettenhofer, R. Weiss, and V. Dubourg, "Scikit-learn: Machine Learning in Python," *the Journal of machine Learning research*, vol. 12, pp. 2825–2830, 2011.

[142] E. Bisong and E. Bisong, "Google colaboratory," *Building machine learning and deep learning models on google cloud platform: a comprehensive guide for beginners*, pp. 59–64, 2019.

[143] I. Syarif, A. Prugel-Bennett, and G. Wills, "SVM parameter optimization using grid search and genetic algorithm to improve classification performance," *TELKOMNIKA (Telecommunication Computing Electronics and Control)*, vol. 14, no. 4, pp. 1502–1509, 2016.

[144] "The pavement fatigue carrousel." Available online: https://lames.univ-gustave-eiffel.fr/en/equipments/the-pavement-fatigue-carrousel.

[145] Precision Transducers-Dynatest, "PAST-IIA Strain Gauges," 2021.

[146] N. Bahrani, J. Blanc, P. Hornych, and F. Menant, "Alternate method of pavement assessment using geophones and accelerometers for measuring the pavement response," *Infrastructures*, vol. 5, p. 25, 2020.

[147] M. Greenacre, P. J. Groenen, T. Hastie, A. I. d'Enza, A. Markos, and E. Tuzhilina, "Principal component analysis," *Nature Reviews Methods Primers*, vol. 2, no. 1, p. 100, 2022.

[148] S. Roweis, "EM algorithms for PCA and SPCA," *Advances in neural information processing systems*, vol. 10, 1997.

[149] Geospace Technology, "Geophone sensor." Orientation: Vertical. Model GS-ONE LF, `https://www.geometrics.com/wp-content/uploads/2021/05/GS-ONE-LF-4.5-2450-specs_Vert_147-00054_13-105-090D.pdf`.

[150] G. T. Reddy, M. P. K. Reddy, K. Lakshmanna, R. Kaluri, D. S. Rajput, G. Srivastava, and T. Baker, "Analysis of dimensionality reduction techniques on big data," *Ieee Access*, vol. 8, pp. 54776–54788, 2020.

[151] A. Maćkiewicz and W. Ratajczak, "Principal Components Analysis (PCA)," *Computers & Geosciences*, vol. 19, no. 3, pp. 303–342, 1993.

COLLEGE ED MATHEMATIQUES
DOCTORAL STIC
PAYS DE LA LOIRE

Nantes Université

Université Gustave Eiffel

LAMES
LABORATOIRE AUSCULTATION, MODÉLISATION, EXPÉRIMENTATION DES INFRASTRUCTURES DE TRANSPORT

Titre : Application de l'intelligence artificielle à l'exploitation des mesures de déflexion pour la caractérisation mécanique des structures de chaussées

Mot clés : Évaluation structurale, Modélisation du comportement mécanique des chaussées, Module d'élasticité, Déflectomètre à grande vitesse (TSD), Pente de déflexion, Apprentissage automatique (ML)

Résumé : Cette thèse présente un modèle et une méthodologie efficaces basés sur l'apprentissage automatique (ML) pour l'estimation du module d'élasticité des couches de chaussée (E_i). Cette approche novatrice utilise des mesures de pente de déflexion TSD (D_S) plutôt que la méthode classique de déflexion. Le modèle inverse développé dans le cadre de cette recherche repose sur des données issues de logiciels (Alizé-LCPC) reconnus par les praticiens et d'un simulateur expérimental externe, garantissant ainsi leur conformité aux conditions réelles. De plus, un processus de validation paramétrique avancé a été exécuté pour valider leur performance. Ce modèle surmonte non seulement les défis liés à l'estimation précise de E_i, mais mène également une analyse de sensibilité quantitative rigoureuse. Cette analyse examine systématiquement les impacts négatifs de quatre défis majeurs : la complexité des données TSD en haute dimension, l'influence du bruit de mesure, les variations de température, et les incertitudes de E_i des autres couches. Tout cela vise à souligner l'objectif principal : apporter des contributions précieuses au domaine de la mécanique des chaussées.

Title: Application of Artificial Intelligence in the Exploitation of Deflection Measurements for the Mechanical Characterization of Pavement Structures

Keywords: Bearing Capacity Assessment, Pavement Behavior Modeling, Pavement Elastic Modulus, Traffic Speed Deflectometer, Deflection Slope, Machine Learning

Abstract: This thesis presents an effective model and methodology based on machine learning (ML) for estimating the elastic modulus of pavement layers (E_i). This innovative approach uses deflection slope measurements from TSD (D_S) rather than the classical deflection method. The inverse model developed in this research is based on data from industry-recognized software (Alizé-LCPC) and an external experimental simulator, ensuring their conformity with real-world conditions. An advanced parametric validation process was also executed to validate the model performance. Moreover, a quantitative sensitivity analysis has been conducted to investigate the negative impacts of four major challenges: the complexity of high-dimensional TSD data, the influence of measurement noise, temperature variations, and uncertainties in E_i of other layers. All of this aims to underscore the primary objective: to make valuable contributions to the field of pavement mechanics.